NTNU
Det skapende universitet

Trykkpulsasjoner inne i et Francis løpehjul

Katarina Kloster

NTNU

Norwegian University
of Science and Technology

Department of Energy
and Process Engineering

EPT-M-2016-70

MASTER THESIS

for

Katarina Kloster

Spring 2016

Pressure pulsation inside a Francis turbine runner

Trykkpulsasjoner inne i et Francis løpehjul

Background

The average age of Norwegian hydro power plants are 45 year, and many show sign of fatigue and needs to be constantly maintained or refurbished. Additionally, some power plants in Norway has experienced failures on new Francis runners: Driva-, Sønnå-, Svartisen-, Hol 1-, Eriksdal-, Brokke- and Vinje Power Plant. The main problem is the formation of cracks in the turbine runner.

The main challenges for the numerical analysis of the Fluid-Structure Interaction (FSI) on high head Francis turbines originates in the natural frequency of the turbine runner and the fluid properties of the existing pressure oscillations.

Recently, researchers in the Waterpower Laboratory at the Norwegian University of Science and Technology, (NTNU) designed their own High head Francis turbine and published both geometry and model performance data in order to provide other researchers with a relevant case to work with and to promote the Francis-99 workshops. The Francis-99 workshops aim to determine the state of the art of high head Francis turbine simulations (flow and structure) under steady and transient operating conditions as well as promote their development and knowledge dissemination openly. This project will provide knowledge to understand how to carry out measurements of the stresses on the turbine runner blades, and it will be in close cooperation with Einar Agnalt. The final work will be delivered as a monolog and/or a paper with two authors.

Objectives

Analyze transient pressure measurements in a Francis turbine

The following tasks are to be considered:

1. Literature study
    a. Fatigue loads in high head Francis turbines
    b. Understand the nodal diameter of the Francis turbine runner
2. Software knowledge
    a. Data handling with Matlab and Labview
3. Laboratory work
    a. Carry out measurements for selected parts of the hill diagram of the Tokke turbine
    b. Install and calibrate the pressure sensors in the turbine
    c. Pressure pulsation measurements based on sensors installed in the draft tube cone, vanless space and in the runner in collaboration with Einar Agnalt
    d. Train gauge measurements in the runner in collaboration with Einar Agnalt
4. Carry out an FFT-analysis of the pressure and strain and correlate the results

Within 14 days of receiving the written text on the master thesis, the candidate shall submit a research plan for his project to the department.

When the thesis is evaluated, emphasis is put on processing of the results, and that they are presented in tabular and/or graphic form in a clear manner, and that they are analyzed carefully.

The thesis should be formulated as a research report with summary both in English and Norwegian, conclusion, literature references, table of contents etc. During the preparation of the text, the candidate should make an effort to produce a well-structured and easily readable report. In order to ease the evaluation of the thesis, it is important that the cross-references are correct. In the making of the report, strong emphasis should be placed on both a thorough discussion of the results and an orderly presentation.

The candidate is requested to initiate and keep close contact with his/her academic supervisor(s) throughout the working period. The candidate must follow the rules and regulations of NTNU as well as passive directions given by the Department of Energy and Process Engineering.

Risk assessment of the candidate's work shall be carried out according to the department's procedures. The risk assessment must be documented and included as part of the final report. Events related to the candidate's work adversely affecting the health, safety or security, must be documented and included as part of the final report. If the documentation on risk assessment represents a large number of pages, the full version is to be submitted electronically to the supervisor and an excerpt is included in the report.

Pursuant to "Regulations concerning the supplementary provisions to the technology study program/Master of Science" at NTNU §20, the Department reserves the permission to utilize all the results and data for teaching and research purposes as well as in future publications.
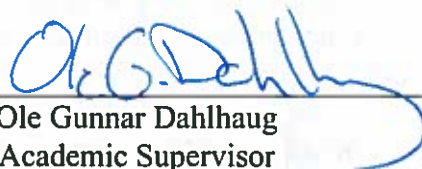
The final report is to be submitted digitally in DAIM. An executive summary of the thesis including title, student's name, supervisor's name, year, department name, and NTNU's logo and name, shall be submitted to the department as a separate pdf file. Based on an agreement with the supervisor, the final report and other material and documents may be given to the supervisor in digital format.

☒ Work to be done in lab (Waterpower lab, Fluids engineering lab, Thermal engineering lab)
☐ Field work

Department of Energy and Process Engineering, 25th January 2016

Olav Bolland
Department Head

Ole Gunnar Dahlhaug
Academic Supervisor

Co-Supervisors:
- Torbjørn K. Nielsen
- Pål-Tore S. Storli
- Carl Bergan

Preface

This Master thesis was written at the Waterpower Laboratory at NTNU, during the spring of 2016. The thesis has been conducted in relation to the Francis-99 workshops, and aims to measure and analyse the steady state and transient behaviour of the pressure pulsations inside the Francis-99 model runner. The thesis has been conducted in close cooperation with Einar Agnalt, and he should be considered a co-author of this thesis.

I would like to express my gratitude to Einar for enabling me to write this thesis. It would not have been possible without his hard work in the laboratory, and fruitful discussions during post processing of the measurement data. I would also like to thank Carl Werdelin Bergan for his patience and help during data analysis, and Bjørn Winter Solemslie for his valuable input to the uncertainty analysis. My supervisor, Ole Gunnar Dahlhaug, also deserves a big thank you for motivating me and believing in this project. Lastly, I would like to thank my fellow students at the laboratory for making my last year at NTNU a memorable one.

Katarina Kloster
Trondheim, 13.06.2016

ii

Abstract

In this thesis pressure and strain measurements have been conducted on the Francis-99 model runner at the Waterpower Laboratory at NTNU. The measurements have been performed using onboard pressure transducers mounted in the hub of the model runner, as well as flush mounted pressure transducers in the vaneless space and draft tube cone. Strain has been measured at the outlet of a runner blade using a single strain gauge. Steady state measurements were conducted in order to identify the frequencies present in the system, and to correlate the frequencies and amplitudes of the strain to the surrounding pressure measurements. Subsequently, transient measurements were carried out to investigate the amplitude development of the predominant frequencies in the runner during load variation. The conducted measurements have been analyzed using Fast Fourier Transform and Short-Time Fourier Transform in Matlab.

The measurements have been carried out under satisfactory laboratory conditions, with low uncertainties related to the onboard pressure measurements. The analysis show a close correlation between the observed frequencies on the strain gauge and the pressure oscillations in the model runner. The guide vane frequency is often observed to be the main source of vibration. However, it's second harmonic appear to be amplified in the strain gauge signal, due to the phase difference in the wake entering the surrounding hydraulic channels. The elastic fluctuation between the turbine and draft tube tank also appear to have a large relative amplitude in the strain gauge signal, and may cause additional fluctuating stresses in the runner. The absence of the synchronous component of the Rheinegans frequency in the strain gauge signal suggest the asynchronous component to be the predominant source of mechanical excitation caused by the Rheinegans frequency.

The transient amplitude development of the guide vane frequency in the model runner showed no sign of increased amplitudes due to the change in guide vane angle. Thus, the demonstrated development appear to not be adding to the fluctuating stresses on the turbine.

Sammendrag

I denne masteroppgaven har trykk- og strekklappmålinger vært gjennomført på Francis-99 løpehjulet, ved Vannkraftlaboratoriet på NTNU. Målingene ble gjennomført ved bruk av trykksensorer montert i bosset på løpehjulet, i tillegg til flush monterte sensorer i omdreiningshulrommet og sugerørskonusen. Strekk ble målt på en løpehjulsskovl ved bruk av én strekklapp. Steady state målinger ble gjennomført for å identifisere frekvensene i systemet og for å korrelere frekvensene og amplitudene på strekklappen til de omliggende trykkmålingene. Deretter ble transiente målinger gjennomført for å undersøke amplitudeforløpet til den mest dominerende frekvensen i løpehjulet ved lastvariasjon. De gjennomførte målingene ble analysert ved bruk av Fast Fourier Transformasjon og Short-Time Fourier Transformasjon i Matlab.

Målingene ble gjennomført under tilfredsstillende lab forhold, med lav usikkerhet relatert til trykkmålinene i løpehjulet. Analysen viser en tett korrelasjon mellom observerte frekvenser på strekklappen og trykkpulsasjonene i løpehjulet. Ledeskovlfrekvensen blir ofte observert som den største kilden til vibrasjon. Andre harmonien ser imidlertid ut til å forsterkes i strekklappsignalet på grunn av faseforskyvningen til vakene som går inn i de omliggende hydrauliske kanalene. Den elastiske bølgen mellom turbinen og sugerørstanken ser også ut til å ha en større relativ amplitude i strekklappsignalet, og kan potensielt foråsake ytterligere belastning på løpehjulet. Fraværet av den synkrone komponenten av Rheinegans frekvensen i strekklappmålingene antyder at den asynkrone komponenten er den dominerende kilden til mekanisk eksitasjon forårsaket av Rheinegans frekvensen.

Det transiente amplitudeforløpet til ledeskovlfrekvensen i løpehjulet viser ingen tegn til økning i amplitude som følge av endringen i ledeskovlsåpning. Dermed ser ikke amplitudeforløpet til ledeskovlsfrekvensen ut til å øke belastningen på turbinen.

Contents

x

List of Figures

List of Tables

Nomenclature

Abbreviations

BEP   Best Efficiency Point

DFT   Discrete Fourier Transform

FFT   Fast Fourier Transform

FSI   Fluid Structure Interaction

FSO   Full Scale Output

HL   High Load

PL   Part Load

RSI   Rotor-Stator-Interaction

RSS   Root-Sum-Square

NTNU   Norges Teknisk Naturvitenskaplige Universitet

Symbols

ρ Density

a Speed of sound

f_n Runner frequency

f_R Rheinegans frequency

f_s Sampling frequency

f_{bp} Blade passing frequency

f_{gv} Guide vane frequency

$f_{Nyquist}$ Nyquist frequency

K Bulk modulus

n Runner rotational speed [rpm]

z_{bp} Number of runner vanes

z_{gv} Number of guide vanes

1 | Introduction

1.1 Background

Historically, hydropower turbines were designed with the intention of running at the best efficiency point. However, since the energy act was implemented in the 1990s, the operating regime of the Norwegian turbines have changed and many of the turbines are operated with constant load variation. The induced dynamic pressure fluctuations exerts large stresses on the turbine components and ultimately increase the risk of fatigue failure. The desire for higher efficiencies and lower cost also result in low solidity and compact units which contribute to the increased stress in the runners. The recent breakdowns in high head Francis turbines add to the concern related to the reliability of the turbine runners. Thus, gaining a deeper knowledge of the pressure development in the turbine has become an important topic in the hydropower industry.

To facilitate further research on pressure pulsations inside Francis turbines, NTNU designed a modified model of the runner previously installed at the Tokke power plant. This runner has become the research object of the Francis-99 workshops, in which several aspects of Francis turbine operation is investigated. In relation to the second workshop, this thesis aims to measure and analyse the steady state and transient behaviour of the pressure pulsations in the Francis-99 model runner.

1.2 Objective

The objective of the current thesis is to conduct pressure and strain measurements on the Francis-99 model runner. Steady state measurements will be conducted in order to identify the frequencies present in the system, and to correlated the frequencies and amplitudes of the strain to the surrounding pressure measurements. Transient measurements are conducted to investigate the amplitude development of the predominant frequencies in the runner during load variation.

1.3 Previous work

Pressure pulsations in Francis turbines is a well researched field of study. However, few onboard pressure and strain measurements have been published, and available measurement reports from high head units are rare.

Most of the available experiments are done at the Laboratory for Hydraulic machines at Ecole Polytechnique Féderal de Lausanne, EPFL-IMHEF, where onboard model strain and pressure measurements have been performed in cooperation with Voith Simens [8], GE Energy Hydro [29] and Alstom [23]. The experiments focus on low head Francis units, and were conducted using miniature pressure transducers embedded in the model runner blades.

Similar measurements have also been conducted at the Waterpower Laboratory at NTNU. Kobro [19] conducted onboard pressure and strain measurements on a model and prototype in order to look for model-prototype and pressure-strain correlations. Trivedi, Cervantes Gandhi and Dahlhaug also performed extensive pressure measurements in conjunction with the Francis-99 workshops. Several master students at NTNU have also utilized onboard pressure and strain measurements in their work. Julie Hovland [13] and Ingeborg Bue [6] conducted measurements at steady state conditions, while Anders Tørklep considered the dynamic loads during start and stop procedures. However, the available results from the onboard measurements conducted at NTNU are limited, as the researchers experienced issues related to the durability of the embedded pressure transducers.

Cotu et al performed onboard strain measurements on a high head Francis prototype after major cracks were discovered on the outflow edge junction on several runner blades. The strain gauges were installed as part of a Root Cause Analysis. Lowys et al [20] also performed extensive onboard measurements on two low head prototype runners, due to cracks in several low head units. Favrel et al [2] used onboard pressure and strain measurements to determine the predominant source of mechanical excitation from the Rheinegans frequency. Bjørndal et al [25] conducted several onboard stress measurements on prototype runners to evaluate the dynamic forces on the runner structure, and discuss simple criteria that could be included in turbine condtracts to ensure the mechanical robustness of new runners.

In relation to the Hydrodyna collaborative research project, several onboard pressure measurements have also been conducted on reversible pump-turbines to investigate the RSI phenomena and fluid structure coupling with respect to influence on life span.

2 | Theory

2.1 Pressure pulsations in Francis turbines

A Francis turbine running at best efficiency point will normally be influenced by pressure oscillations caused by Rotor-Stator-Interaction (RSI) . However, running outside of BEP, additional phenomena such as vortex breakdown and flow separation at the inlet and outlet of the runner are also introduced. Pressure pulsations expose the system to fatigue loads and vibrations that can impose serious threats to the runner structure and possibly cause fatigue cracks. The magnitude of the pulsations introduced depend on the design of the machinery, operational patterns and the dynamic response of the system. In the following sections the dynamic pressure pulsations observed in Francis turbines will be presented.

2.1.1 Runner frequency

The runner frequency represent a single pulsation on a once per revolution basis in the runner [24]. Provided the rotational symmetry of the runner is maintained, the amplitude of this frequency is low. However, if there is damage to a runner blade, or the flow and/or runner is unbalanced, the amplitude of this frequency will increase. The runner frequency depend on the rotational speed of the runner, and is given by [11]:

$$f_n = \frac{n}{60} \quad [Hz] \tag{1}$$

2.1.2 Guide vane frequency

Pressure pulsations at the guide vane frequency occur when a given runner blade passes through the wake leaving the trailing edge of the guide vanes. Thus, the guide vane frequency may be expressed by [24]:

$$f_{gv} = f_n \cdot z_{gv} \cdot m \quad (m = 1, 2, 3, ...) \quad [Hz] \tag{2}$$

where m represents the various harmonics of the frequency.

The magnitude of the pressure pulse depend on the radial distance between the guide vanes and the runner inlet, as well as the inlet hight of the distributing unit

and the guide vane design [5]. As the radial distance between the guide vanes and the runner inlet is reduced with higher guide vane angles, the amplitude of the guide vane frequency is expected to be predominant at higher loads.

2.1.3   Blade passing frequency

Pressure pulsations at the blade passing frequency occur whenever the runner blades pass a given guide vane. The amplitude is predominant at stable operation, and is also influenced by the radial distance between the guide vanes and the runner blades [11]. The blade passing frequency is expected to be predominant in the vaneless space and is expressed by [24]:

$$f_{bp} = f_n \cdot z_{bp} \cdot k \quad (k = 1, 2, 3, ...) \quad [Hz] \tag{3}$$

where k represents the various harmonics of the frequency.

2.1.4   Rheingans frequency

The Rheinegans frequency, or the draft tube vortex frequency, is related to the draft tube pressure pulsations in Francis turbines. In the draft tube, the flow field is determined by the pressure and the velocity components of the flow exiting the runner. At best efficiency point (BEP), the flow is mostly parallel to the shaft axis and thus has no tangential velocity component and no swirl. However, at operation points outside of BEP, the direction of the outlet flow changes and a tangential velocity component is present. This tangential velocity component is the source of different flow phenomena in the draft tube. At part load (PL) the tangential velocity component is in the same direction as the rotating runner, and for certain loads a cavitated rotating vortex rope with a helical shape can be observed. At high load (HL) however, the tangential velocity component is in the opposite direction, resulting in a cavitated vortex core [19].

The Rheinegans frequency can be present for both part load and high load. However, the amplitude is usually strongest at 50-70% of BEP [18], as the vortex rope rotates closer to the draft tube wall causing stronger pressure pulses. These forces might cause vibrations in the system, and increase the risk of fatigue failure.

The frequency of the rotating vortex rope differs from unit to unit, and is reported to be in the range of

4

$$\frac{f_n}{3.6} \leq f_R \leq \frac{f_n}{3} \quad [Hz] \tag{4}$$

The induced pressure fluctuations in the draft tube cone may be decomposed into two different components [2]. The first component, known as the asynchronous component, corresponds to the rotation of the pressure pattern with the vortex core. However, the second, synchronous component is known to propagate upstream, into the hydraulic system, consequently acting like an excitation source for the system.

2.1.5 Frequency of the von Karman vortex shedding

von Karman vortex shedding is a known phenomenon in Francis turbines. The von Karman vortices form as part of a wake downstream of a bluff body located in a perpendicular flow, and are a result of flow separation. Usually vortex shedding can be observed at the trailing edge of the stay vanes, guide vanes and runner vanes. As a result of the vortex shedding, these components are subjected to a periodical reaction force pulsating with the frequency of the vortex filament detachment [24]. This phenomena can cause loud noise and vibrations that may influence the operation of the runner. The frequency of the von Karman vortex shedding is given by [5]

$$f_{vortex} = 190 \cdot \frac{B \cdot C}{100t + 0,56} \quad [Hz] \tag{5}$$

where B is the relative frequency, C is the velocity of the water, and t the thickness of the plate.

The frequency of the von Karman vortex can be difficult to accurately detect as the frequency is dependent on the operating condition and drift when the flow velocity change.

2.2 Elastic fluctuations

In addition to the pressure pulsations caused by the rotation of the runner, pressure pulsations may be introduced to the system by elastic fluctuations in the waterway. The oscillations are known as mass oscillations or water hammer oscillations, and are caused by system inequality. Typically the fluctuations are linked to changes in volume flow through the turbine. Any change in guide vane opening will cause a

5

dynamic pressure change in front of the turbine due to the retardation/acceleration of the water masses in the piping system. The introduced pressure pulse will propagate through the water at the speed of sound and reflect back at the nearest free water surface [22]. The period of the pressure wave depends on the speed of sound and the distance to the nearest free watersurface, and is given by [22]

$$T = \frac{4 \cdot L}{a} \quad [s] \tag{6}$$

The corresponding frequency of the pressure wave is thus

$$f = \frac{1}{T} = \frac{a}{4 \cdot L} \quad [Hz] \tag{7}$$

2.2.1   Speed of sound

The elastic fluctuations are closely related to the speed of sound. Sound is a mechanical wave that propagates in an elastic medium, and the speed of the propagation is directly dependent on the properties of the medium. For flow in an ideal, rigid pipe, the speed of sound is given by the Newton-Laplace equation [22]:

$$a = \sqrt{\frac{K}{\rho}} \quad [m/s] \tag{8}$$

where ρ is the water density and K the bulk modulus.

However, for flow in a pipe with elastic walls, the speed of sound in the fluid is influenced by the elasticity of the pipe wall and it's supporting points. Thus, the speed of sound becomes a function of the fluid and pipe properties. The speed of sound in an elastic pipe can be expressed in the following manner

$$a = \frac{1}{\sqrt{\rho(\frac{1}{K} + \frac{D}{E \cdot e})}} \tag{9}$$

where ρ is the fluid density, K is the Bulk modulus, D is pipe diameter, e is pipe thickness and E is Young's modulus.

2.3 Cyclic stresses and fatigue

During repeated load cycles, failure in structures may occur at stress levels considerably lower than the tensile or yield strength for a static load. Failure in structures subjected to repeated dynamic and fluctuating stresses is known as *fatigue*, and it normally occurs after a longer time period of repeated stress or strain. About 90% of all metallic failures are related to fatigue, causing it to be the single largest cause of failure in metals [16].

In high-cycle fatigue situations, material performance is usually characterized by an S-N curve, or a *Wöhler* curve. The Wöhler curve illustrates the relation between the stress amplitudes and the number of load cycles to failure for a given metal. The higher the magnitude of the stress, the smaller the number of cycles the material can sustain before failure. An illustration of a Wholer curve is provided in figure 1.
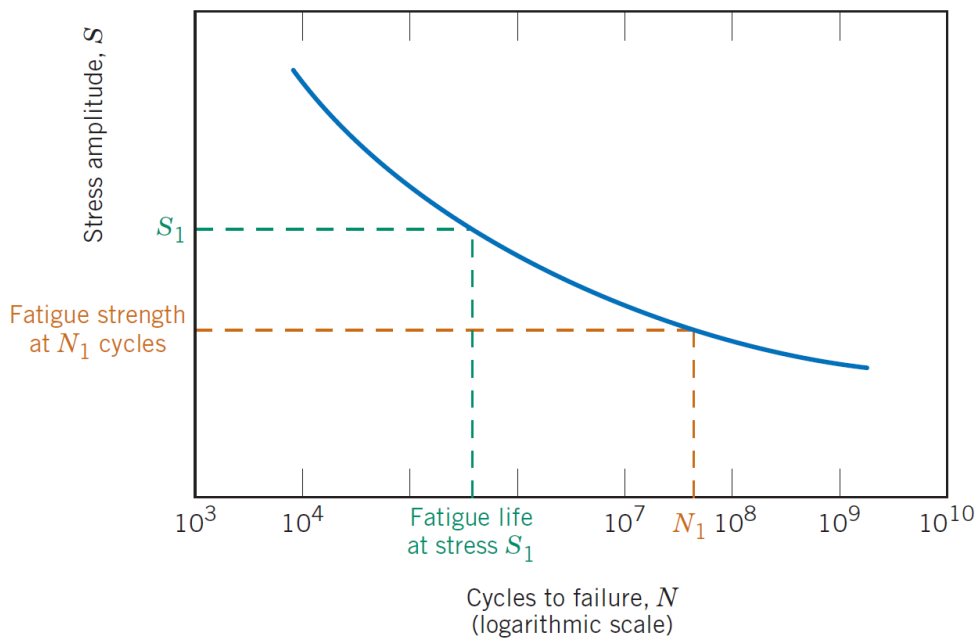

Figure 1: Example of a Wöhler curve [16]

An important parameter characterizing a materials fatigue behaviour is the materials *fatigue life*, providing the number of cycles to cause failure at a specific stress level. Thus, in terms of hydraulic machinery, the frequency and magnitude of the dynamic loads is key when it comes to runner life time.

2.4   Frequency analysis

Frequency analysis is a process of identifying the frequency and amplitude of a signal. When a signal is a pure sine wave, determining the frequency is a simple process. However, the general time-varying signal is more complex than a simple sine wave. Complicated waveforms can be represented by the sum of a set of sine and cosine waves of different frequencies and amplitudes. The method of determining these component frequencies and their assosiated amplitudes is known as spectral analysis [10].

2.4.1   Discrete sampling of time varying signals

When an analog signal is digitalized, the signal is converted to a series of numbers describing the course of the signal. As digital sampling of data is a discontinuous process and the data acquisition system only records data at discrete times with given time intervals, the information of the original signal between the time intervals are lost.

In order to reconstruct the original signal correctly, the choice of sampling rate is of great importance. Choosing an inadequate sampling rate, the sampled data may produce deceptive results and incorrect frequencies known as aliases. Aliases occur when the sampling rate is not high enough to reconstruct the original signal correctly, and are simply a product of the sampling process [10]. Figure 2 illustrate the aliased output signal due to undersampling of an analog signal. The reconstruction of this signal will produce spurious low-frequency signals that do not originate from the original signal [7]. In figure 3 however, the sampling rate is sufficiently high to capture the information and frequency components of the original analog signal.

Figure 2: Aliased signal due to undersampling [14]

Figure 3: Adequate sampling frequency [14]

2.4.2 Sampling rate theorem

The Nyquist-Shannon sampling theorem establishes a sufficient condition for a sample rate that permits a discrete sequence of samples to capture all the information from a continuous signal. The theorem states that the sampling rate must be grater than twice the highest frequency component in the original signal in order to reconstruct the original waveform correctly [10]. For a given sampling frequency, the maximum frequency that can be accurately represented without aliasing is known as the Nyquist frequency. The Nyquist frequency is given by [14]

$$f_{Nyquist} = \frac{f_s}{2} \quad [Hz] \tag{10}$$

2.4.3 Fast Fourier Transform

The technique most commonly used to spectrally decompose and analyse samples of time varying signals is the Fourier Transform. Fourier Transform is a generalization of Fourier series, using the complex exponential form to represent the sine and cosine expressions that constitute the signal. The Fourier transform does not require the signal to be periodic, and may be evaluated quickly using Fast Fourier Transform, (FFT). FFT is a mathematical algorithm that computes the Discrete Fourier Transform (DFT), defined by [10]

$$F(k\Delta f) = \sum_{n=0}^{N-1} f(n\Delta t) \cdot e^{-j(2\pi\Delta f)(n\Delta t)}, \quad k = 0, 1, 2, ..., N-1 \tag{11}$$

where N is the number of samples taken during a time period T.

The FFT algorithm has been developed to reduce the computational time of the DFT, by dividing the original DFT into several smaller DFTs [19]. For a time series with N samples, the number of operations required to complete the FFT is proportional to $Nlog_2N$.

Additional in-depth theory and mathematical derivation of the Fast Fourier Transform can be found in Wheeler and Ganji [10].

2.4.4 Spectral leakage and windowing

When a signal is processed by use of FFT, it implicitly assumes that the time series of length N repeats itself infinitely in a cyclic manner. In other words, the

9

transform interprets the starting point and the end point of the time series to be subsequent points. If the signal doesn't contain an integer number of cycles within the time series, there will be a discontinuity between the last sample and the first sample due to the cyclic continuation. The result is a spread of power in the frequency spectrum, into frequencies that are not present in the original signal. This is known as spectral leakage [10]. Noise, vibration and other disturbances may increase the spectral leakage in the frequency spectrum [12].

A common method to avoid spectral leakage is the use of a window function. A window function is a waveform that is applied to the sampled data to smooth the edges of the signal. The central part of the signal remains unaffected while the amplitude at the edges are gradually reduced to create a smoother transition. To attenuate the signal at the beginning and end of the sampling interval, the window function is superimposed on top of the time series prior to the application of FFT. This removes the discontinuity of the time series and decreases the spectral leakage into neighbouring frequencies [10].

There are several types of window functions. The most common window functions are Hamming, Hanning, Blackman and Flat-top [9]. Due to its simple but useful features, the Hanning window is often chosen. An illustration of the Hanning window and its application is given in figure 4.
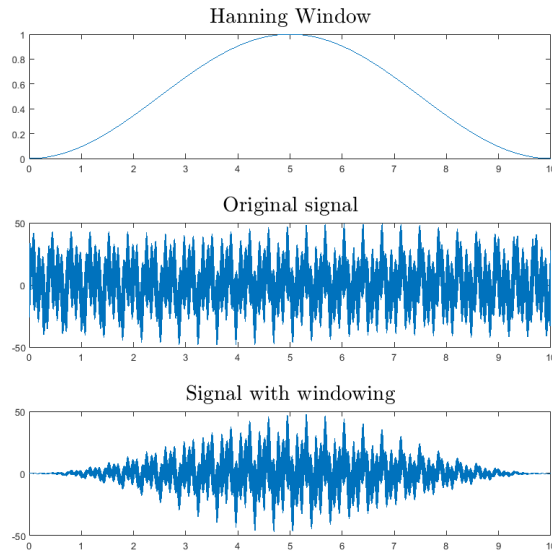

Figure 4: Illustration of the Hanning window

10

2.4.5 Overlap

When window functions are applied to a signal, the continuous data stream is split into several non-overlapping segments of length N prior to the FFT analysis. The subsequent segments of the signal are illustrated in figure 5.
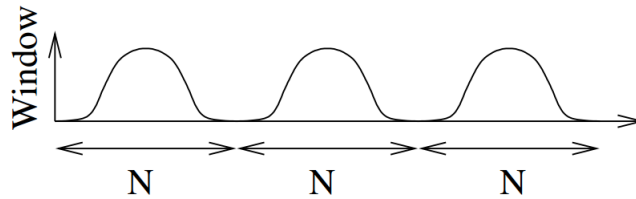

Figure 5: Segmented data stream with window function and no overlap [9]

Due to the smoothing edges of the window function, with values close to or equal to zero, a significant part of the data stream is effectively zeroed out in the analysis. This is not optimal as it is desirable to extract as much information as possible from the signal. However, by letting the segments overlap, as illustrated in figure 6, more of the information is included in the FFT analysis [9].
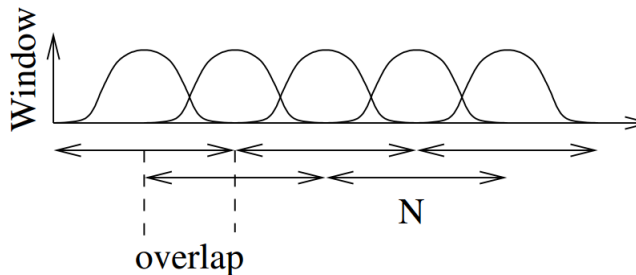
Figure 6: Segmented data stream with window function and overlap [9]

2.4.6 Harmonic Frequencies

When performing an FFT analysis, harmonic frequencies may prove to be present in the analysed signal. An harmonic frequency is defined as an integer multiple of the original frequency, and are usually generated in relation to certain predominant frequencies. The frequency of the original waveform is typically known as the fundamental frequency or the first harmonic frequency. Figure 7 illustrate the phenomenon with the fundamental frequency f and its subharmonics $2f$ and $3f$.

Figure 7: A fundamental frequency f, and its subharmonics 2f and 3f

3 | Experimental setup and intrumentation

3.1 Laboratory facilities

For the current experiments, the Francis test rig at the Waterpower Loboratory at NTNU has been utilized. The rig is according to IEC 60193 international standards [27], and consist of an upper reservoir, a pressure tank, a turbine and generator, and a draft tube tank. The flow in the rig is supplied by one or two pumps installed in the basement of the laboratory, providing up to 2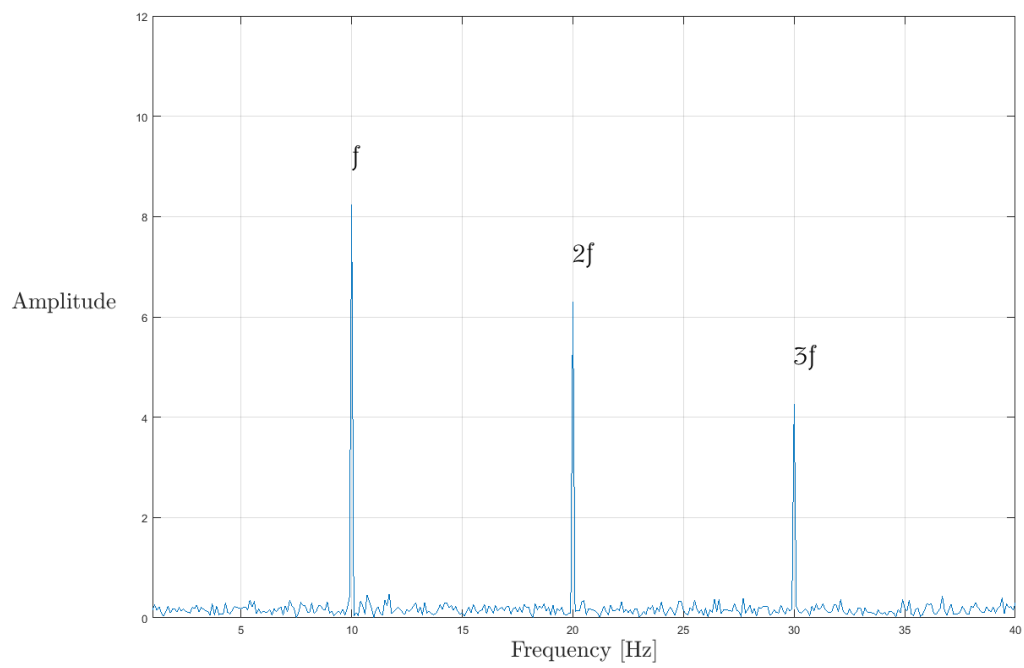*330kW of pumping power to the system. With the current setup the system can run either in open or closed loop, allowing the rig to run at numerous operating conditions. For the current experiments, the rig was run with open loop as this provides a free water surface and removes any instabilities or pressure pulsations in the flow that may be caused by the pumps. A complete sketch of the Francis test rig is provided in figure 8.
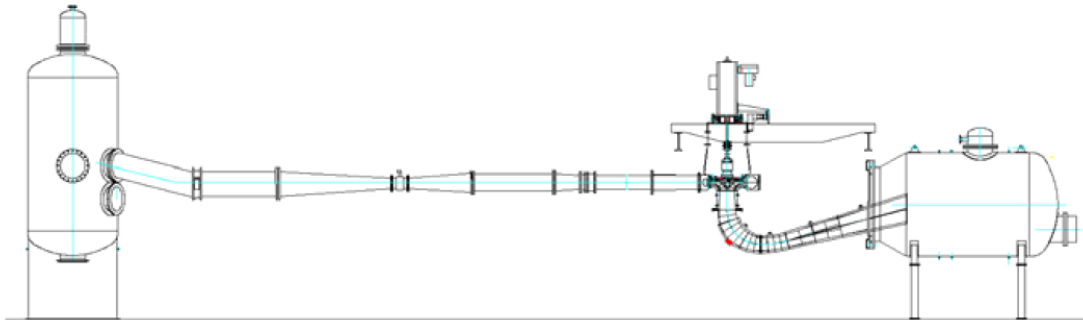
Figure 8: The Francis test rig [19]

3.2 The Francis-99 model runner

The model runner used during the current measurements is of splitter blade design with 15 + 15 runner blades. The runner is a modified model of the turbine previously installed at the Tokke power plant, and it was designed by NTNU to facilitate further research on pressure pulsations inside high head Francis turbines. The turbine has a speed number of $\Omega = 0{,}27$, and a distributing unit consisting

of 14 stay vanes and 28 guide vanes. The model runner has been part of several experiments previously conducted at the Waterpower Laboratory, including [12, 6, 3, 18, 19] and is the research object of the Francis-99 workshops.

Figure 9: The Francis-99 model runner

3.3   Measurement setup

3.3.1   Placement of pressure transducers

The previous experiments conducted on the Francis-99 model runner performed onboard pressure measurements using blade mounted pressure transducers [19]. However, due to the poor durability of the blade mounted sensors, it was decided to have the pressure transducers mounted in the hub for the current pressure measurements. Hub mounted sensors do not enable separate measurements on the pres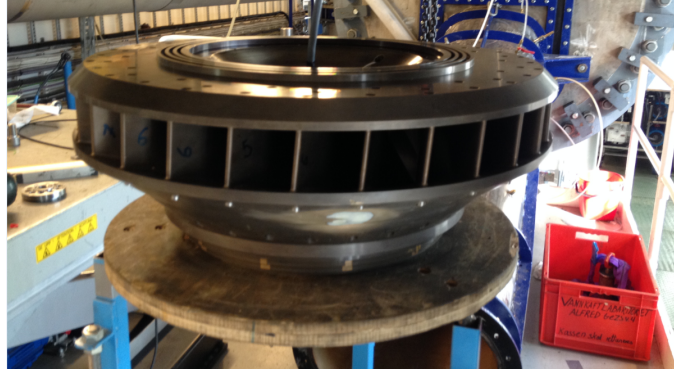sure and suction side of the runner blades, but allow the use of more robust and accurate sensors compared to the sensors mounted in the runner blade.

For the current experiment, five pressure transducers were mounted in the middle of two hydraulic channels in the model runner. To fully capture the propagation of the pressure pulses created by the RSI, one pressure transducer was placed close to the inlet and another close to the outlet of the runner. One sensor was also placed just upstream the splitter blade outlet and another just downstream in order to capture the effect of the change of channel cross section on the pressure pulse. A fifth sensor was mounted in the next equivalent hydraulic channel in order to identify the phase difference in the pressure pulses. Figure 10 illustrate the positions of the various hub mounted sensors. The described approach provide the ability to compare results with earlier measurements conducted by Kobro [19]

14

with blade mounted pressure transducers. The five pressure transducers were all flush mounted to facilitate direct measurement of the pressure.
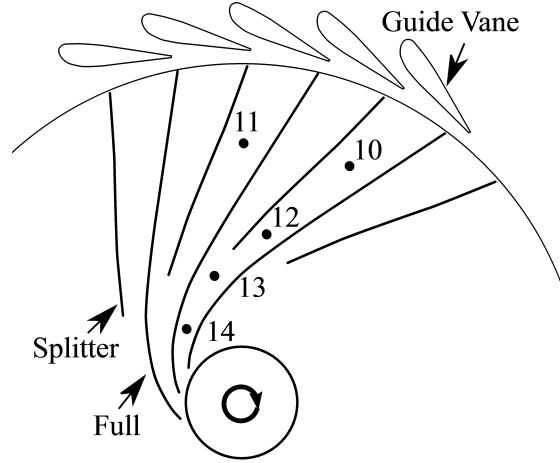

Figure 10: Positioning of the onboard pressure transducers. Schematic provided by Einar Agnalt.

Pressure transducers were also mounted in the stationary domain of the turbine. Two sensors were placed in the vaneless space and four in the draft tube cone. Note that the two sensors mounted in the vaneless space are positioned differently relative to the corresponding guide vane. See figure 11 for a schematic illustration. The draft tube pressure transducers are mounted in two horizontal planes, with 180 degree spacing between the sensors. PT30(5) and PT32(1) are mounted in the upper horizontal plane, and PT31(6) and PT33(4) are mounted in the lower plane. The numbers provided in the parenthesis correspond to the numbering of the sensors in the laboratory.

Adding to these pressure transducers are three sensors flush mounted to the penstock, inlet of spiral casing, and draft tube outlet. These pressure transducers were mounted to allow measurements of the speed of sound, as well as possible correlation between the pressure measurements upstream and downstream the runner and the rotating domain. A schematic of the placement of these sensors are given in figure 12. However, these sensors will not be the main target of investigation for the current thesis.
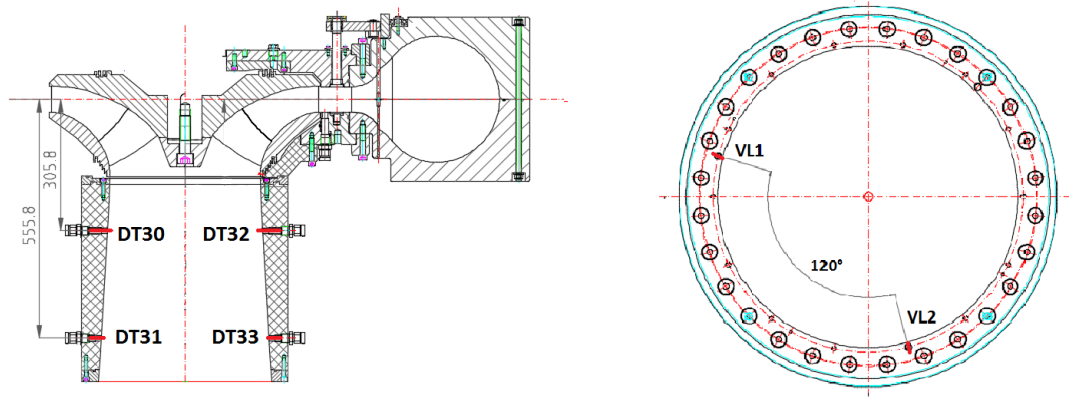
Figure 11: Position of the pressure transducers mounted in the vaneless space and draft tube cone.
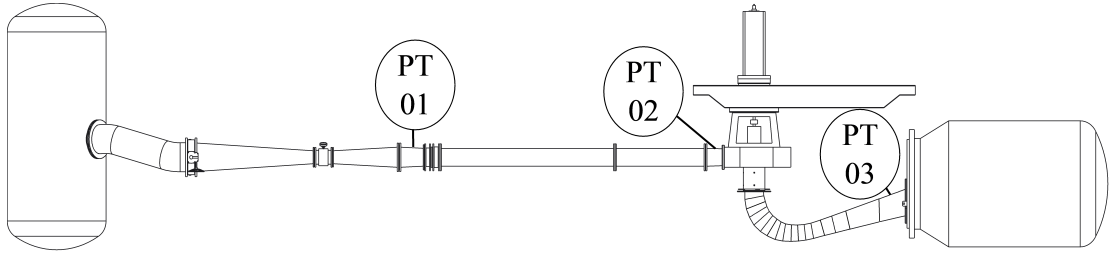
Figure 12: Pressure transducers mounted in the piping system

Table 1 provide an overview of the pressure transducers utilized in the measurements. Data sheets for Kulites XTM-190 series utilized for the onboard measurements can be found in appendix C.

Producer/Type	Quantity	Notation	Range [$bara$]	Placement
Kulite XTM-190SM	5	PT10-14	0 - 3,5	Onboard
Kulite HKM-375M	3	PT01-03	0 - 1,7	Pipeline
Kulite	2	PT20-21	0 - 10	Vaneless space
Kistler 701A	4	PT30-33	0 - 250	Draft tube

Table 1: Overview of pressure transducers utilized in the measurements

3.3.2 Placement of the strain gauge

The semiconductor strain gauge utilized in the measurements was attached at the outlet of a runner blade. Assuming a linear line between the fastening points of the blade to the hub and shroud, an assumed line of inflection was identified. The strain gauge was positioned on this line in order to capture the maximum strain about this axis. The assumed inflection line, and the placement of the strain gauge is shown in figure 13.

Figure 13: Placement of the strain gauge

The data sheet for the strain gauge used in the measurements is attached in appendix C.

3.3.3 Data acquisition system

To ensure simultaneous sampling of the rotating and stationary domain, a transmission system with slip ring was used. The slip ring is suitable for installation on a rotating shaft and allows transmission of an electrical signal from the rotating to the stationary domain. The electrical signal was transferred to a common eight slot chassis with an NI-9239 analog input module, equipped with an anti aliasing filter. To increase the signal to noise ratio, and utilize the resolution of the common cDAQ device, the signal was amplified prior to the transmission of the signal.

The dynamic pressure transducers mounted in the draft tube cone returns a signal in terms of electrostatic charge, pico-Coulomb (pC). Thus, a charge amplifier was needed to amplify and convert the signal to the desired volt to bar relation. The Kistler amplifiers were in turn connected to an NI-9239 analog input module on the common cDAQ device.

The piezoresistive bridge transducers mounted in the vaneless space and on the piping system have a full scale output (FSO) of 10mV/V. Thus, the pressure transducers were connected to an analog input bridge module, in order to obtain better resolution within the measuring range. The excitation voltage of the bridge module was set to 5 volts.

A complete overview of the hardware used in the data acquisition system is given in table 2.

Hardware	Quantity	Type
Slip ring	1	SRH80180-24S
Data acquisition chassis	1	NI-cDAQ-9178
Analog input module	5	NI-9239
Bridge analog input module	2	NI 9237
Charge meter	3	Kistler 5015A
Charge amplifier	1	Kistler 5011B

Table 2: Overview of hardware used for data acquisition

3.3.4 Calibration

All the measuring equipment needs to be calibrated prior to the measurements. The static pressure transducers mounted in the hub, as well as the pressure transducers in the vaneless space and on the piping system were calibrated using a dead weight manometer. Two dead weight testers of different range were used to allow for calibration of both low and high pressure ranges. The calibration of the static pressure transducers was conducted using the same data acquisition system planned for the experiment, in accordance with the IEC standards. An existing LabVIEW logging program was provided for recording and saving of data.

The flow, friction torque and generator torque, as well as the differential pressure transducer were also calibrated. The calibration was conducted according to the *Procedures for the Francis turbine test rig*, which is available in the laboratory. The dynamic pressure transducers mounted in the draft tube cone were not calibrated in the laboratory due to lack of dynamic calibration equipment. However, factory calibration data was used. The calibration reports for the various equipment is available in appendix D.

The strain gauge was calibrated by Einar Agnalt prior to the experiment. By use of the procedure presented in [4] he conducted a theoretical calibration of

the strain gauge. The output voltages with corresponding strain was plotted and fitted with a calibration curve. Due to the non linearity of the Wheatstone bridge, the calibration curve was created by use of a third degree function. Since the strain gauge has only been calibrated theoretically, it should be mentioned that the absolute values provided by the strain gauge measurements should be used with cation. However, for an FFT analysis identifying frequencies and relative amplitudes the strain gauge measurements should be adequate. The estimated uncertainty of the strain gauge calibration curve is 0.25%.

3.4   Expected frequencies

The frequencies expected to be found during the experiments on the Francis-99 model runner are summarized in table 3. The frequencies are calculated using the equations provided in section 2.1.

Frequency		[Hz]
Runner frequency	f_n	5.55
Guidevane frequency	f_{gv}	155.4
Blade passing frequency	f_{bp}	166.5
Rheinegans frequency	f_R	1.3875 - 2.775
Elastic fluctuation - Turbine to pressure tank	f_{e-TP}	15.37
Elastic fluctuation - Turbine to draft tube tank	f_{e-TD}	41.89

Table 3: Expected frequencies in the Francis-99 model runner

3.5   Sampling rate

To avoid faulty results, the sampling rate theorem suggest the use of a sampling rate that is at least the double of the highest expected frequency. However, the sampling rate is usually set higher for samples of discrete nature, as a higher sampling rate provide better data resolution which makes the spectral analysis more accurate.

According to the online data sheet for the NI 9239 module [21], the logging rates available for this particular module is given by equation

$$f_s = \frac{f_M \div 256}{n} \quad [Hz] \qquad n = integer[min1 \rightarrow max31] \tag{12}$$

where $f_M = $ 12,8 [MHz]. Thus, the choice of sampling rate is limited by the NI module. To ensure sufficient data resolution and minding the limitations of the NI module, the sampling rate for the current measurements were set to 5000Hz.

3.6   Running points

The running points for the experiment were set equal to the running points provided by the Francis-99 second workshop test case [1]. However, to reach the desired running points, the guide vane angle was increased slightly compared to the guide vane angles provided on the workshop's website. The altered guide vane angle may be do to inaccuracies in the mechanism measuring the guide vane angle, and thus, the actual angle at each operational point should be double checked. During the measurements, three steady state measurement series were conducted for every operational point, and ten for the transient measurement series between them. An additional ten measurement series were conducted for the transient measurements between BEP and HL in order to account for repeatability. The running points, as well as the applied guide vane angles are provided in table 4.

Parameter	PL	BEP	HL
n_{ED}	0.179	0.179	0.179
Q_{ED}	0.106	0.152	0.184
Guide vane angle	6.899	10.107	12.656

Table 4: Running points [1]

4 | Data Analysis

4.1 Steady state measurements

The raw data from the steady state measurements have been processed and analysed in Matlab. Matlab contains several advanced, built in functions that perform FFT and facilitate the use of overlapping windows. For the current analysis the Power Spectral Density (PSD) function and the pwelch function were considered. The two built in functions provided similar results. However, the PSD function proved to be less exposed to low frequency noise and showed more prominent frequencies in the lower frequency range. This corresponds to Kobros findings in [18]. Thus the PSD function was utilized for the spectral analysis of the steady state measurements.

The window function utilized for the analysis is the Hanning window. According to National Instruments [15], the Hanning window is well suited for signals containing a combination of sine waves, and it is widely used when analysing measurement series from Francis turbines. To clearly visualize the lower frequency range, the window length was set higher than the period of the lowest expected frequency. With a window length of 256*32 samples this corresponds to a frequency resolution of

$$\frac{Fs}{L} = \frac{5000}{256 * 32} = 0.61 \quad [Hz] \tag{13}$$

4.2 Transient measurements

The transient measurements series were analysed using Matlabs built in function, spectrogram. The spectrogram function use the Short-Time Fourier transform and determines the sinusoidal frequency content of local sections of the signal as it changes over time. In practice, this means the spectrogram function divides the full time signal into shorter segments of equal length and then computes the Fourier transform separately on each of the shorter segments. The spectrogram function returns a frequency, time and amplitude vector, allowing the amplitudes of a given frequency to be plotted against time.

The length of the shorter sections of the signal is of great importance when using the Short-Time Fourier transform, and should be closely considered. To ensure that the portion of the signal falling within the segment is close to stationary, the segment should be quite narrow. However, very narrow segments do not provide

sufficient frequency resolution to get a good localization of the frequencies in the frequency domain. Thus, choosing the length of the shorter segments is a constant trade-off between good frequency resolution and good time resolution. The concept is illustrated in figure 14.
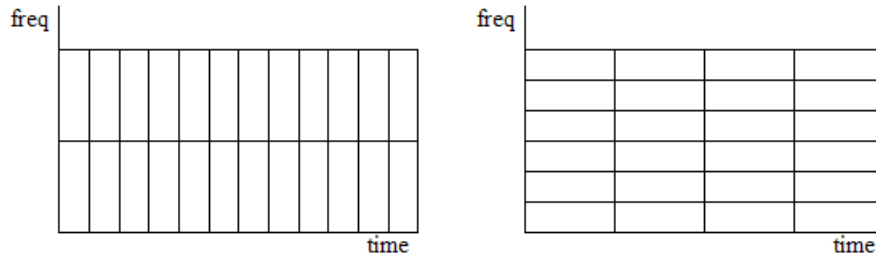

Figure 14: Short-Time Fourier Transform using different segment lengths. The illustration to the left has better time resolution, while the illustration to the right has better frequency resolution.

In the analysis of the transient measurement series the discrete signal was divided into 40 segments of equal length to ensure a reasonable balance between the time and frequency resolution. Subsequently, the Hanning window was applied to each segment, with an overlap of 50%.

5 | Analyzing uncertainty

To address the quality of the results obtained from the experiment, one should be able to evaluate the quality of the conducted measurements. When measuring a physical quantity there will always be a difference between the measured value and the true value of the quantity. Thus, it is important to determine and quantify the various sources of error when evaluating the quality of the measurement. Any measurement of a physical quantity has a related uncertainty which arise from various errors. This uncertainty is the range within which the true value of a measured quantity can be expected to lie [7]. According to the IEC60193 standard the probability for the given range should be set to a 95% confidence level.

The IEC60193 standard consider three types of errors:

- Spurious errors

- Random errors

- Systematic errors

Spurious errors typically arise from human errors or instrument malfunction. Such errors generally invalidate the measurement, and thus the corresponding measurement should be discarded to avoid incorporating the error in any statistical analysis.

Random errors are caused by small, independent influences which prevent the measuring instrument from delivering the same reading when measuring the same quantity of a physical property. The scatter of the readings observed during an experiment results from the combination of the random error arising from the instrumentation and the influence of the operating conditions. To reduce the random error it is important to repeat the measurements and ensure the repeatability of the measurement system. When the sample size is small, the uncertainty related to the random errors is estimated by means of the *Student's t distribution.*

Systematic errors have the same magnitude provided the conditions for the measurements remain the same. Thus, repeating measurements will not uncover the systematic errors. Systematic errors can be caused by poorly calibrated instruments, hysteresis or poor linearity of the measuring instrument. To identify the magnitude of the systematic errors, the complete measuring process needs to be analysed, including the calibration of the measuring instruments. Random errors during calibration of a measuring instrument becomes a systematic error in the

measurements and thus cation should be exercised when calibrating the measuring instrument.

In the uncertainty analysis conducted for the current experiment emphasis has been on establishing the uncertainty related to the measurements from the on-board pressure transducers.

5.0.1 Uncertainties from the calibration

During calibration of an instrument, different sources of error contribute to the uncertainty. The various errors are listed in table 5 and are defined by IEC [7]. X indicate the property measured by the instrument. Provided the uncertainties have the same probability distribution, they may be combined by the Root-Sum-Square method (RSS-method) . Using the RSS-method the total uncertainty related to the calibration of an instrument is expressed in the following manner:

$$f_{Xtot} = \sqrt{f_{Xa}^2 + f_{Xb}^2 + f_{Xc}^2 + f_{Xd}^2 + f_{Xe}^2 + f_{Xf}^2} \quad [\%] \tag{14}$$

Error	Description
$\pm f_{Xa}$	Systematic error of the primary calibration method
$\pm f_{Xb}$	Random error of the primary calibration method
$\pm f_{Xc}$	Systematic error (repeatability) of the secondary instrument
$\pm f_{Xd}$	Random error of the secondary instrument
$\pm f_{Xe}$	Physical phenomena and external influences
$\pm f_{Xf}$	Error in physical properties

Table 5: Component errors in the calibration of an instrument [26]

5.0.2 Systematic uncertainty in calibration

Every deadweight manometer comes with a documented uncertainty related to the pressure which is generated by the manometer. For the manometer used to calibrate the onboard pressure transducers the uncertainty is reported not to exceed ± 0.008 provided appropriate corrections in relation to gravity, air density and temperature has been made. As the onboard pressure transducers were calibrated using the same deadweight manometer, the systematic uncertainty from the calibration is equal for all the sensors. Since the density of air is low, any contribution

24

to the uncertainty from the height difference in the mounting of the sensors to the manometer is considered negligible ($f_{Pf} \approx 0$). Thus, the systematic uncertainty in the calibration of the onboard pressure transducers is set equal to

$$f_{Scal} = \sqrt{f_{Pa}^2 + f_{Pb}^2} = \pm 0.008 \quad [\%]$$

5.0.3   Random uncertainty in calibration

When calibrating a measuring instrument, several points showing the relation between the instruments output signal and the corresponding physical values are obtained. From these points a linear regression line is created. As the calibration points are not completely linear there is a specific uncertainty related to every calibration point. The random uncertainty related to the calibration of the onboard pressure transducers arise from these errors in the regression line. It also accounts for the instruments response to the pressures not included in the calibration. The random uncertainty from the regression line is represented by an uncertainty band with a 95% confidence interval, as illustrated in figure 15.
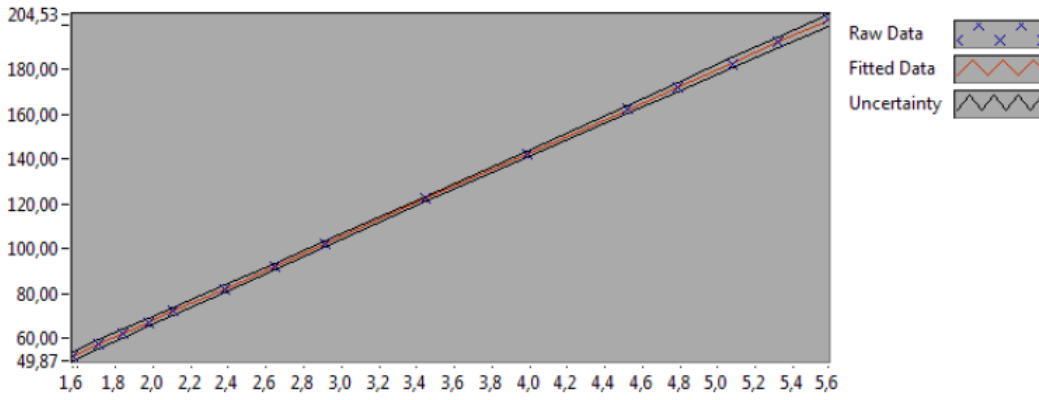

Figure 15: Regression line with uncertainty band

The random uncertainty in the calibration is the combined uncertainty of f_{Pc} and f_{Pd}, and it is denoted f_{Rcal}.

$$f_{Rcal} = \sqrt{f_{Pc}^2 + f_{Pd}^2} \tag{15}$$

5.0.4 Physical phenomena and external influences

Errors due to physical phenomena and external influences may originate from changes in temperature within the instrument. Prior to the calibration, the pressure transducers had been present in the laboratory for a few days. Thus, the sensors are thought to have reached thermal equilibrium with the surroundings prior to the calibration. Hence, f_{Pf} was considered negligible.

5.0.5 Total uncertainty

To obtain the maximum uncertainty f_{Ptot} for the measurements, the uncertainties described are combined. Using the RSS-method the total uncertainty for the measurements can be expressed in the following manner

$$f_{Ptot} = \sqrt{(f_{Scal})^2 + (f_{Rcal})^2} \tag{16}$$

where $fScal$ and $fRcal$ are the systematic and random uncertainty from the calibration.

Table 6 summarize the maximum uncertainties from the calibration obtained for the onboard pressure transducers used in the measurements.

Pressure Transducer	f_{Rcal} [%]	e_{Rcal} [kPa]
PT10	0.41	0.26
PT11	0.40	0.25
PT12	0.40	0.25
PT13	0.39	0.24
PT14	0.40	0.25

Table 6: Maximum random uncertainty from calibration of the onboard pressure transducers

6 | Experimental results and discussion

6.1 Steady state measurements

Three pressure transducers as well as the strain gauge have been chosen to visualize the frequencies present in the system during steady state operation. To highlight the relative change in amplitude for the different frequencies, the spectral analysis for the various operating points are grouped together in a waterfall diagram for every transducer. Note that all the amplitudes have been normalized with respect to the amplitude of the guide vane frequency at the inlet of the runner.

In any reference to waterfall diagrams for additional pressure transducers, see appendix A.

6.1.1 Onboard pressure transducer - PT11

Figure 16 present the waterfall diagram for PT11, mounted at the inlet of the model runner. The diagram show prominent amplitudes for the guide vane frequency at all three operating conditions, with increasing amplitudes for higher guide vane angles. This is in accordance with previous observations done by Kobro [19], and is consistent with the theory of the guide vane frequency's dependence on the radial distance between the runner and the guide vanes. The waterfall diagrams for the subsequent onboard pressure transducers also show the same trend. However, the amplitudes are reduced as one gets closer to the runner outlet.

A noteworthy observation from the waterfall diagram is the presence of the guide vane frequency's second harmonic (310Hz). According to Dörfler [24], only the effects of the guide vane frequency's fundamental frequency are normally observed in the runner. However, the exception arise when the runner has a mode shape with zero nodal diameters, and the whole circumference is excited with the same phase. In line with this reasoning, the model runner appears to have a vibration mode with zero nodal diameters. However, this assertion should be investigated further.

Another interesting observation is the presence of the blade passing frequency in the runner. This is an noteworthy discovery, as the blade passing frequency isn't expected to be present in the rotating domain. Also, in the measurements con-

ducted by Kobro [19], the blade passing frequency is found to not be present in the model runner. However, the diagram show increasing amplitudes for higher loads, which coincide with the theory of the blade passing frequency's dependence on the radial distance between the runner and guide vanes.
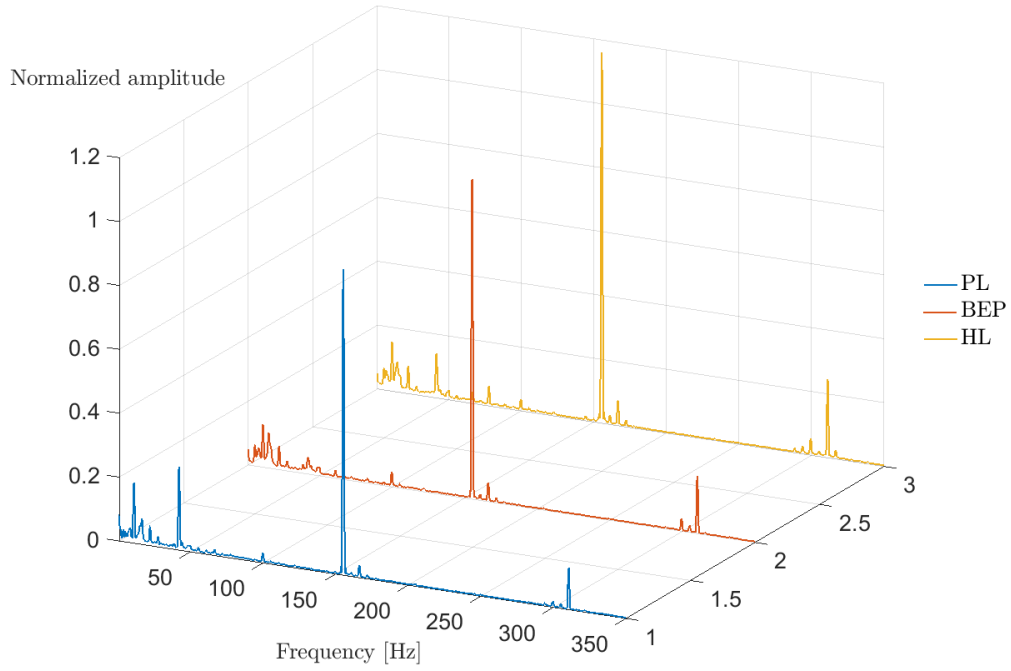

Figure 16: Spectral analysis of the pressure signal from PT11 at PL, BEP and HL

The waterfall diagrams for the onboard pressure transducers also show signs of the runner frequency, present at 5.55Hz. The amplitudes are very small, but increase in line with the increasing guide vane angle. In [19], Kobro also found the runner frequency to be present in the runner. Based on a CFD simulation conducted by Stückle [28], he suggested that the runner frequency occur due to higher flow velocities in the hydraulic channel by the spiral casing tongue. This would agree with the observation of increasing amplitudes during higher loads.

A possible second harmonic of the runner frequency (11Hz) is also present in the frequency spectra. However, the 11Hz peaks are considerably higher than the runner frequency, and thus the explanation of the 11Hz being a second harmonic seem less likely. On the other hand, the presence of the 11Hz frequency may be caused by some kind of unbalance in the model runner. Small peaks are also visible at

22Hz, which appear to be the second harmonic of the 11Hz.

Elastic fluctuations also appear to be present in the waterfall diagram. The elastic fluctuation between the turbine and draft tube tank (42Hz) is particularly prominent, with larger peaks at the off-design conditions. The 15Hz frequency corresponding to the elastic fluctuation between the turbine and pressure tank is also visible, with the largest amplitude at BEP.

As mentioned in section 2.1.4, the Rheinegans frequency may be decomposed into two different components. By definition, the synchronous component of the helical vortex rope does not depend on the reference frame of the pressure transducer. However, the asynchronous component is dependent on the reference frame of the transducer. When conducting measurements in the rotating domain, the asynchronous component of the Rheinegans frequency will be visible at approximately $\frac{2}{3}$ of the rotational frequency due to the change in reference frame. Thus the synchronous and asynchronous components of the Rheinegans frequency would be visible at 1.54-1.85Hz and 3.7Hz respectively in the rotating domain, provided the Rheinegans frequency is present in the runner. Considering the waterfall diagrams for the various onboard pressure transducers, the presence of the Rheinegans frequency is not obvious. However, frequencies of 1.7 and 3.87Hz are visible at part load for all the pressure transducers, with larger amplitudes for the sensors closer to the runner outlet. This corresponds to the findings of Favrel et al in [2]. Figure 17 show the waterfall diagram for pressure transducer PT14, highlighting the two components of the Rheinegans frequency.
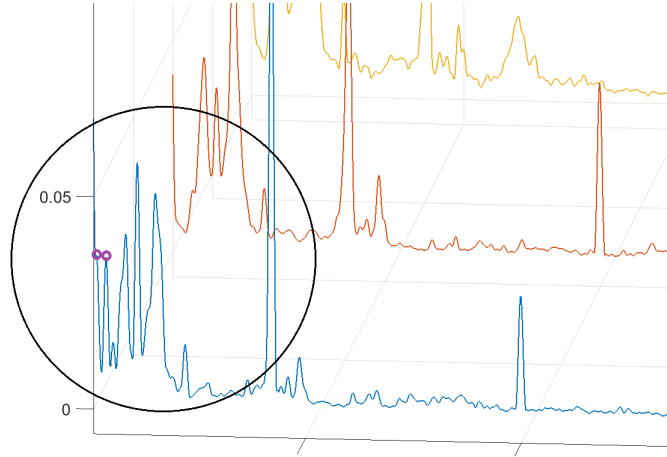

Figure 17: Presence of the two components of the Rheinegans frequency in the spectral analysis of the pressure signal from PT14

6.1.2 Vaneless space pressure transducer - VL2

Figure 18 present the waterfall diagram for VL2, mounted in the vaneless space. The diagram show prominent peaks at the blade passing frequency at all three operating conditions, as well as the half harmonic at 83Hz and second harmonic at 332Hz. This is to be expected as the blade passing frequency is thought to travel outward from the rotating domain, and coincide with results presented by Kobro [19] The amplitudes of the blade passing frequency appear to be increasing with the guide vane angle and the reduction of the radial distance between the runner inlet and the guide vanes. However, the spectral analysis of the pressure signal from VL1 show higher amplitudes for the off-design conditions compared to BEP. Thus, the position of the pressure transducers relative to the guide vanes appear to be of importance when considering the development of the amplitudes of the blade passing frequency.
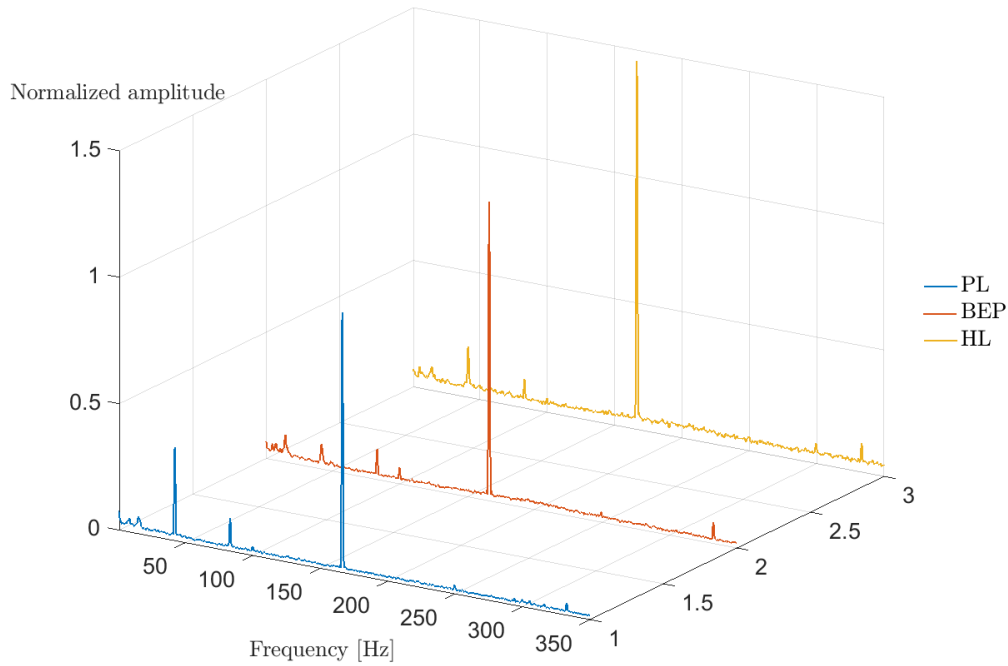
Figure 18: Spectral analysis of the pressure signal from VL2 at PL, BEP and HL

Elastic fluctuation also appear to be present in the measurements conducted in the vaneless space. The elastic fluctuation between the turbine and draft tube tank at 42Hz is clearly visible at all three operating points, with larger peaks at the off-design conditions. The 15Hz corresponding to the elastic fluctuation between

the turbine and pressure tank is also visible as small peaks in the lower frequency range.

6.1.3   Draft tube pressure transducer - DT33

Figure 19 present the waterfall diagram for the draft tube pressure transducer, PT33. The diagram show prominent peaks for the elastic fluctuation between the turbine and draft tube tank (42Hz), with the largest amplitude present at part load. The elastic fluctuation between the turbine and pressure tank (15Hz) and the half harmonic at 7.5Hz is also present.
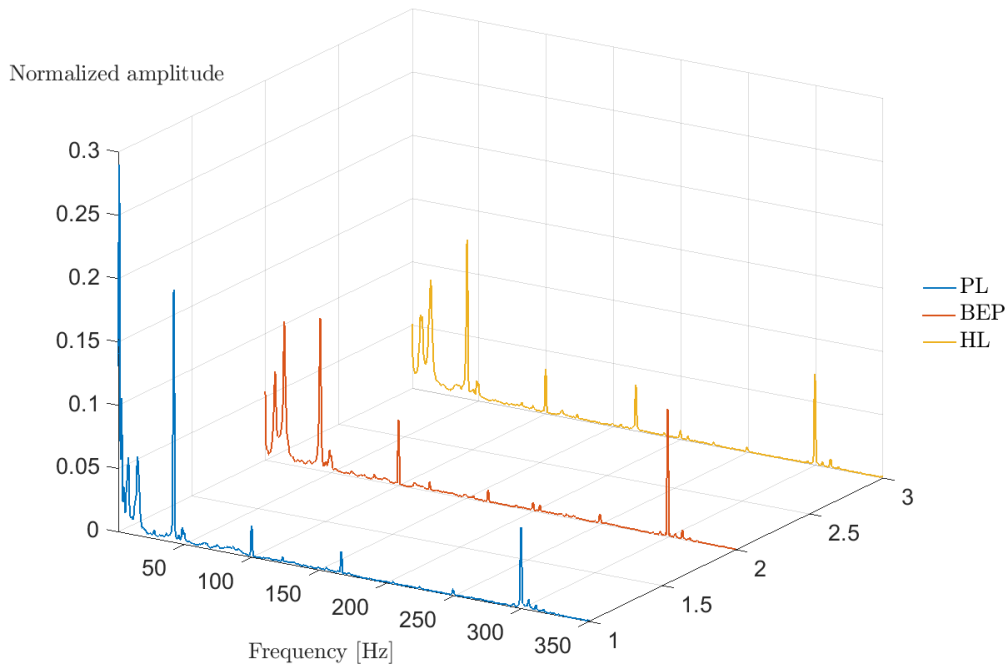

Figure 19: Spectral analysis of the pressure signal from DT33 at PL, BEP and HL

The waterfall diagram also show the presence of the Rheinegans frequency at part load. However, in the draft tube cone, the two components of the frequency can not be separated. The Rheinegans frequency appears in the range of 1.5-1.7Hz for the four pressure transducers mounted in the draft tube cone (See Appendix A for the remaining waterfall diagrams for the draft tube pressure transducers). However, there is a noteworthy change in the amplitude of the Rheinegans frequency

depending on the position of the pressure transducers. The transducers located in the same horizontal plane is expected to experience pulsations of the same magnitude, provided that the vortex rope rotates around the centerline of the draft tube. However, there is a large difference in the magnitude of the Rheinegans frequency captured by DT31 and DT33, which are located in the same horizontal plane. A slight difference in amplitudes on PT30 and PT32 in the upper horizontal plane can also be observed. A possible explanation of this is that the flow exiting the runner outlet is not symmetrical. In [19], Kobro describes a deviating flow pattern at the runner inlet due to the spiral casing tongue, with slightly higher velocities in this section. Entering the draft tube, this deviating flow pattern might effect the vortex rope so it does not rotate about the centerline of the draft tube, but around a line that is slightly tilted. This could explain why the amplitude of the Rheinegans frequency is higher on PT33 than PT31. An illustration of the described phenomena is given in figure 20. It should be noted that the amplitudes of the remaining frequencies appear to be in the same order of magnitude for all the pressure transducers mounted in the draft tube.
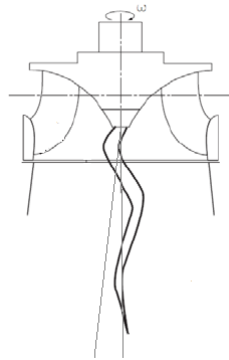
Figure 20: Tilted vortex rope

In the higher frequency range of the waterfall diagram, prominent peaks at 300Hz are visible. There is no obvious explanation to this frequency. However, Kobro [18] found the same frequency to be present in his measurements in the draft tube cone. He suggested that the frequency is a consequence of the rectifier converting alternating current to direct current, resulting in a frequency six times the grid frequency for a three phase alternating current. The hypothesis was later confirmed by measurements done on the generator in the laboratory, thus explaining the presence of the 300Hz frequency. It should be noted that the 300Hz have been present in the waterfall diagrams for the onboard pressure transducers and in the vaneless space as well. However, due to the scaling of the diagrams, the 300Hz frequency is more prominent in the waterfall diagrams of the draft tube pressure transducers.

32

6.1.4   Strain gauge

Figure 21 present the waterfall diagram for the strain gauge mounted at the runner outlet. The amplitudes have been normalized with respect to the BEP amplitude of the guide vane frequency. Note that the frequency range in the diagram has been expanded compared to previous diagrams to include amplitude peaks in the higher frequency range.
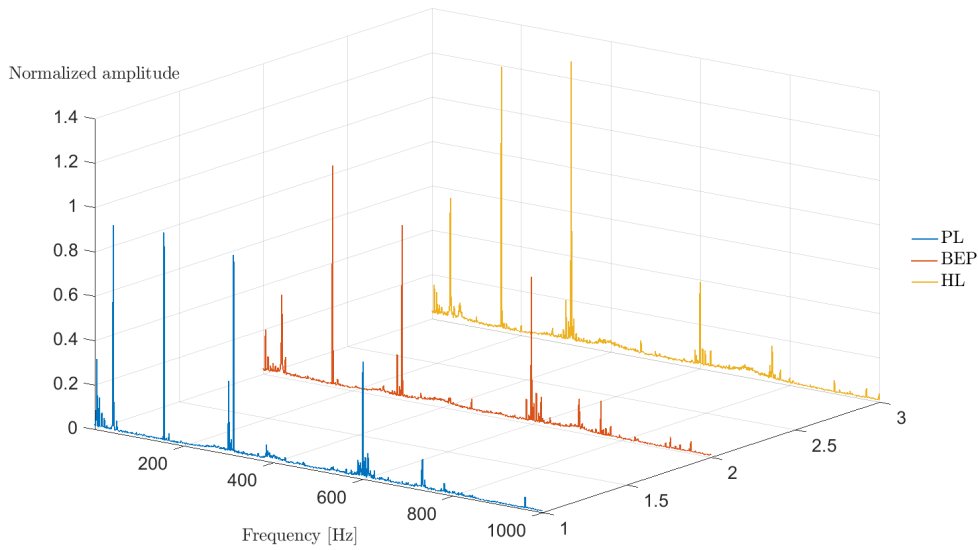

Figure 21: Spectral analysis of the Strain gauge signal at PL, BEP and HL

Strain gauges are sensitive to the mechanical behaviour of the material on which they are placed. Thus, by considering the waterfall diagram of the strain gauge, the different pressure pulsation's impact on the runner structure may be evaluated. In the lower frequency range of the diagram, several of the previously mentioned frequencies are present. Distinct amplitudes from the elastic fluctuations are visible at both 15Hz and 42Hz. The amplitude of the 42Hz is particularly noticeable as the peak appears to have a larger relative magnitude compared to the frequency spectra of the onboard pressure transducers. Also the runner frequency at 5.55Hz is present, with a larger relative amplitude.

A noteworthy observation from the strain gauge's waterfall diagram is the Rheinegans frequency. As the strain gauge is mounted in the rotating domain, both the synchronous and asynchronous component of the frequency can be observed.

33

However, only the asynchronous component at 3.87Hz appear to be present at part load in the frequency spectrum of the strain gauge. When Favel et al conducted similar measurements in [2], the synchronous component of the Rheinegans frequency was identified in the strain gauge measurements. However, the amplitude of the synchronous component appeared to be just 5% of the amplitude of the asynchronous component. The absence of the synchronous component in the current measurements could be due to the conducted FFT analysis. However, the qualitative result seem to correspond well with the findings of Favrel et al.

The waterfall diagram for the strain gauge also show prominent peaks for the guide vane frequency at 155Hz, with amplitudes increasing in accordance with higher guide vane angles. Also the second harmonic is noteworthy with amplitudes in the same order of magnitude as it's fundamental frequency. At high load the magnitude of the second harmonic is even larger than the amplitude of the guide vane frequency. This is unexpected, as the amplitudes of harmonic frequencies tend to be lower than the amplitude of the fundamental frequency. However, in [17], Agnalt et al provide a possible explanation of the phenomenon. He explains the amplification of the second harmonic on the strain gauge as a consequence of the phase difference of the pressure pulses entering the two consecutive hydraulic channels. With a phase difference between the two wakes, the pressure pulses may be amplified or dampened. Thus, the phase difference seem to have a dampening effect on the guide vane frequency, but an amplifying effect on its second harmonic.

The blade passing frequency is also present in the strain gauge signal. However, the amplitude of the frequency is very small compared to the other frequencies in the spectrum, and appear to be in the same relative order of magnitude as it was in the waterfall diagram of the onboard pressure transducers.

In the higher frequency range of the waterfall diagram, distinct peaks at 300Hz are visible, although with a higher relative magnitude than on the onboard pressure transducers. A possible second harmonic at 600Hz is also present. However, the 600Hz is considerably higher than the 300Hz at all three operational points, and thus this seem like an unsuitable explanation. The possibility of the 600Hz frequency originating from von karman vortex shedding was considered. However, as the frequency is constant for the various operating conditions, this seems less plausible. No other explenation for the 600Hz was found, and thus the origin of this frequency should be investigated further.

There are several frequencies in the 700-760Hz range present at the various load conditions. Prior to the mounting of the runner, the strain gauge was attached

34

to a runner blade and an exciting force was applied to the structure by use of a hammer. The resulting raw signal was investigated to provide a rough estimate of the natural frequency of the structure at 824Hz. Thus, considering the added mass effect,the frequencies in the 700-760Hz range could possibly correspond to one of the runners natural frequencies. However, for a natural frequency to be present in the frequency spectra, an excitation source is needed. No such excitation source has been identified. Thus, the explanation of these frequencies as natural frequencies seem insufficient, and hence they should be investigated further.

6.1.5 Considering amplitudes

The absolute value of the amplitudes from an FFT analysis have large uncertainties, and are best suited to consider the relative relation between the amplitudes of the different frequencies. Moreover, it does not provide the accumulated magnitude of the pressure peaks when the respective sinusoids are added together to recreate the pressure signal.

In order to get a better idea of the actual load the turbine is exposed to, the raw signal of the onboard pressure transducers at the different operation points have been investigated. By considering the standard deviation of the raw pressure signal, one can determine an estimate of the general amplitude of the pressure signal and the fatigue loads experienced by the turbine runner. The three steady state measurement series for every operating point have been considered, providing 3*97000 data points for the calculation. Figure 22 illustrate the procedure of the calculation. The plot show the raw pressure signal of the three measurement series for PT11, separated by black, dotted lines. The red line illustrates the mean pressure value, and the orange and green lines give one and two times the standard deviation respectively. For a normal distribution, 95% of the measured values will lie within two standard deviations of the mean value. Thus, the value of two times the standard deviation can be considered a valid estimate of the pressure amplitudes experienced by the model runner.
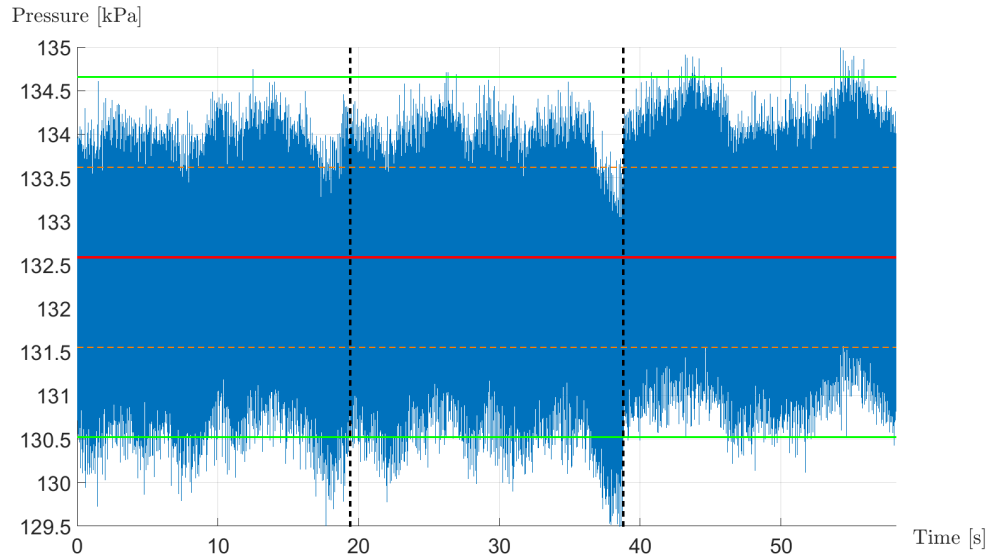
Figure 22: The three measurement series for PT11 at BEP, separated by black, dotted lines

In table 7 the mean and standard deviation of the pressure signal of each onboard pressure transducer is presented for every operating point. The value of two times the standard deviation is also presented, as this value provides the estimate of the pressure amplitudes experienced by the runner.

Pressure Transducer	mean_{PL} [kPa]	S_{PL} [kPa]	$2 \cdot S_{PL}$ [kPa]
PT10	131.9	$\pm$ 1.0	$\pm$ 2.0
PT11	129.9	$\pm$ 1.0	$\pm$ 2.0
PT12	110.2	$\pm$ 0.8	$\pm$ 1.6
PT13	106.6	$\pm$ 0.6	$\pm$ 1.3
PT14	103.5	$\pm$ 0.4	$\pm$ 0.8

Pressure Transducer	mean_{BEP} [kPa]	S_{BEP} [kPa]	$2 \cdot S_{BEP}$ [kPa]
PT10	134.6	$\pm$ 1.0	$\pm$ 2.1
PT11	132.6	$\pm$ 1.0	$\pm$ 2.1
PT12	112.8	$\pm$ 0.9	$\pm$ 1.7
PT13	108.3	$\pm$ 0.7	$\pm$ 1.4
PT14	103.6	$\pm$ 0.4	$\pm$ 0.9

Pressure Transducer	mean_{HL} [kPa]	S_{HL} [kPa]	$2 \cdot S_{HL}$ [kPa]
PT10	136.8	$\pm$ 1.2	$\pm$ 2.5
PT11	134.8	$\pm$ 1.2	$\pm$ 2.5
PT12	114.4	$\pm$ 1.1	$\pm$ 2.1
PT13	109.0	$\pm$ 0.9	$\pm$ 1.7
PT14	102.5	$\pm$ 0.6	$\pm$ 1.2

Table 7: Mean value, and standard deviation of the pressure signal from the various onboard pressure transducers, at PL, BEP and HL

Considering the values presented in table 7, one can observe pressure amplitudes in the range of $\pm$ 0.8-2.5 kPa depending on the operating point as well as the placement of the pressure transducer. The value of the $2 \cdot S_X$ amplitudes seem to be reduced throughout the hydraulic channel. The amplitudes also seem to increase for higher loads, which is logical considering f_{gv} predominance in the pressure signal and it's dependence on the radial distance between the runner and guide vanes. The observed trends are thus equivalent to the findings done in the previously presented spectral analysis.

6.2 Transient measurements

In the previous section, the predominance of the guide vane frequency in the model runner has been demonstrated. Thus, when considering the amplitude development of the pressures in the runner, the guide vane frequency has been selected for further study. Subsequently, the amplitude development of the guide vane frequency from all the onboard pressure transducers have been studied, for load variation between PL, BEP and HL. The transient amplitude development captured by the strain gauge has also been included for correlation of pressure and strain.

In the presented plots, the amplitudes have been normalized with respect to the highest amplitude present in the plot, in order to clearly visualize the dampening of the amplitudes throughout the hydraulic channel. The vertical, black, dotted lines in the plots represent the start and stop of the change in guide vane angle.

6.2.1 Amplitude development of the guide vane frequency

Between BEP and HL
In figure 23 the amplitude development of the guide vane frequency from BEP to HL is plotted for the five onboard pressure transducers.
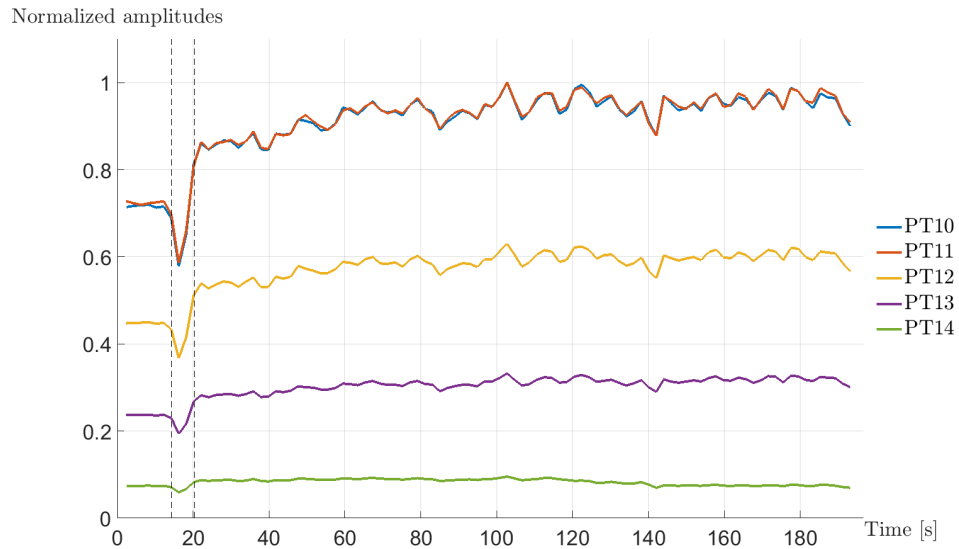
Figure 23: Amplitude development of the guide vane frequency from BEP to HL

The figure clearly show a dampening of the amplitudes throughout the hydraulic channel, from PT11 at the inlet of the runner to PT14 at the outlet. In the figure, the dampening of the amplitudes appear to be proportional to the distance between the onboard pressure transducers. However, in the results presented by Kobro [19], a significant reduction of the amplitudes between the two sensors located prior to- and after the splitter blade in the runner is described. The sudden dampening of the amplitude is explained as an effect of the mixing of the flow from the two neighbouring channels by the splitter blade. However, this additional dampening does not seem to appear in the current results. It should be mentioned that the current experimental setup deviate from the experimental setup used by Kobro. This may be a reason for the deviating results.

Another interesting observation from figure 23 is the transient development of the guide vane frequency amplitude. The figure clearly illustrates how the amplitude changes from a lower value at BEP to a higher value at HL. This is in accordance with the results previously presented (section 6.1.1), and coincide with the theory of the amplitude's dependence on the radial distance between the runner inlet and the guide vanes. However, during the change in guide vane angle, the plot show a sudden drop in amplitude for all the onboard sensors prior to the expected build up.

A possible explanation to this, may be found by considering the cause of the pressure pulse generating the amplitudes. At steady state, the wake from the guide vanes causing the pressure pulses may be illustrated by figure 24. However, during a change in guide vane angle, the trailing edge of the guide vane is moved, disrupting the flow field and the wake leaving the trailing edge. Thus, the wake causing the pressure pulsations is weakened during the transition phase, and the amplitude of the guide vane frequency drop. As the guide vane angle begin to stabilize, the wake will become more distinct and the amplitude will tend towards it's steady state value.
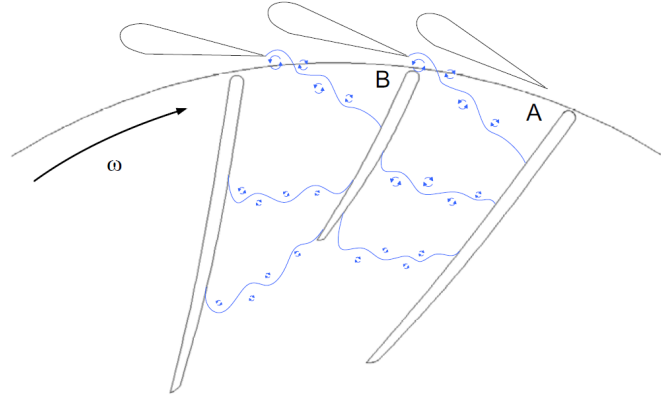
Figure 24: Guide vane wake travelling through the hydraulic channel [19]

In order to verify the transient development of the guide vane frequency amplitude, the raw signal was investigated. To visualize the actual amplitudes, a fitting curve was created and subtracted from the original signal to remove the static pressure from the signal. Subsequently, the remaining signal was filtered using a bandpass filter in order to highlight the amplitude of the guide vane frequency. Figure 25 illustrate the described approach and show the resulting amplitude development for the guide vane frequency from BEP to HL for pressure transducer PT10.
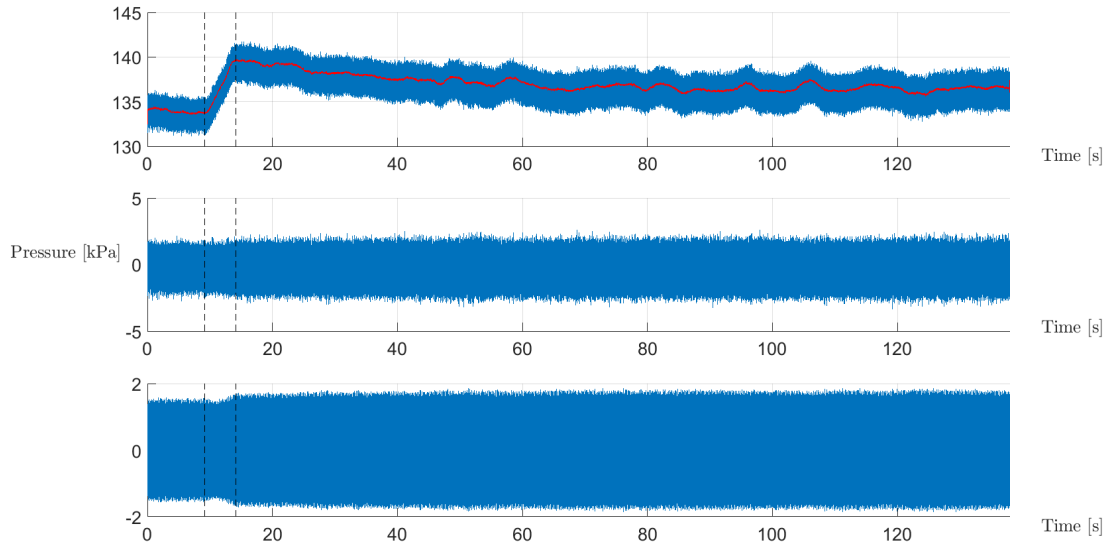
Figure 25: Raw pressure signal from PT10 at BEP to HL

Looking closely at the amplitude development between the black, dotted lines, one can observe a reduction in amplitude during the change in guide vane angle. Thus, the results obtained using the Short-Time Fourier transform coincide with the measured physical signal.

Figure 26 provide the equivalent amplitude development of the guide vane frequency from HL to BEP. The figure show a reversed amplitude development compared to the transient development from BEP to HL, with higher amplitudes at HL and lower amplitudes at BEP. This seems logical, as one would expect the amplitude to return to the same value for a given operating point. The previously discussed drop in amplitude is also present during the change in guide vane opening.
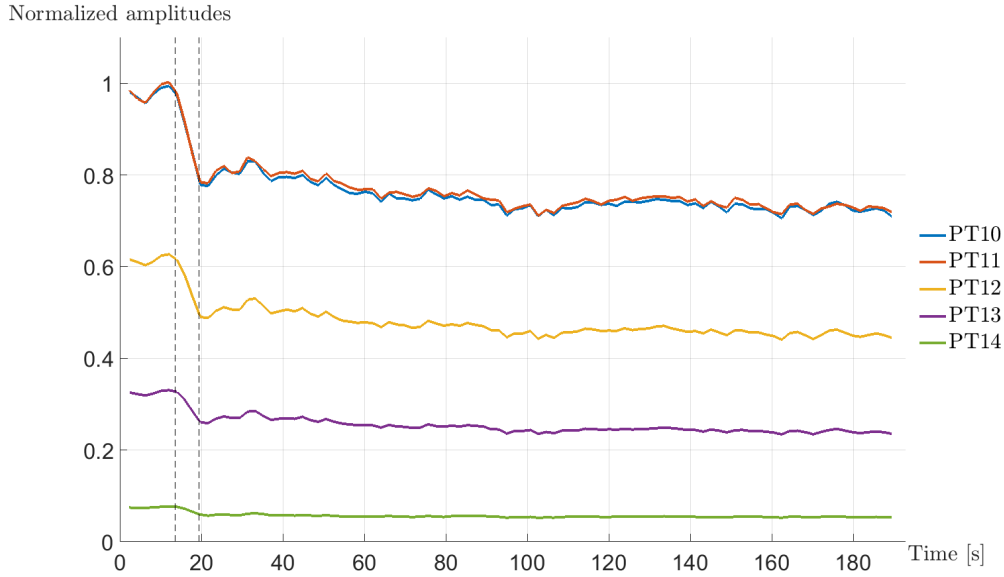
Figure 26: Amplitude development of the guide vane frequency from HL to BEP

Between BEP and PL

Given the transient development of the amplitude between BEP and HL, one would expect to find the same qualitative development between PL and BEP. However, the amplitude plots for the amplitude development between PL and BEP deviate from the expected development. In figure 27 the amplitude development of the guide vane frequency from PL to BEP is plotted. The figure clearly illustrate how the amplitudes change from a lower value at PL to a higher value at BEP in accordance with theory previously presented. The drop in amplitude during the change in guide vane opening is also present. However, the noteworthy change appears just after the guide vane angle has reached it's target value, when the amplitudes drop significantly. The sudden change in amplitude is captured by all the onboard pressure transducers, and it repeats itself in the 10 measurement series conducted between PL and BEP. It is also present when the raw signal is filtered and plotted like described previously (see figure 28). Thus, the change in amplitude seems to be related to something physical. However, a possible cause of the sudden amplitude drop has not been identified, and thus this phenomena should be investigated further.
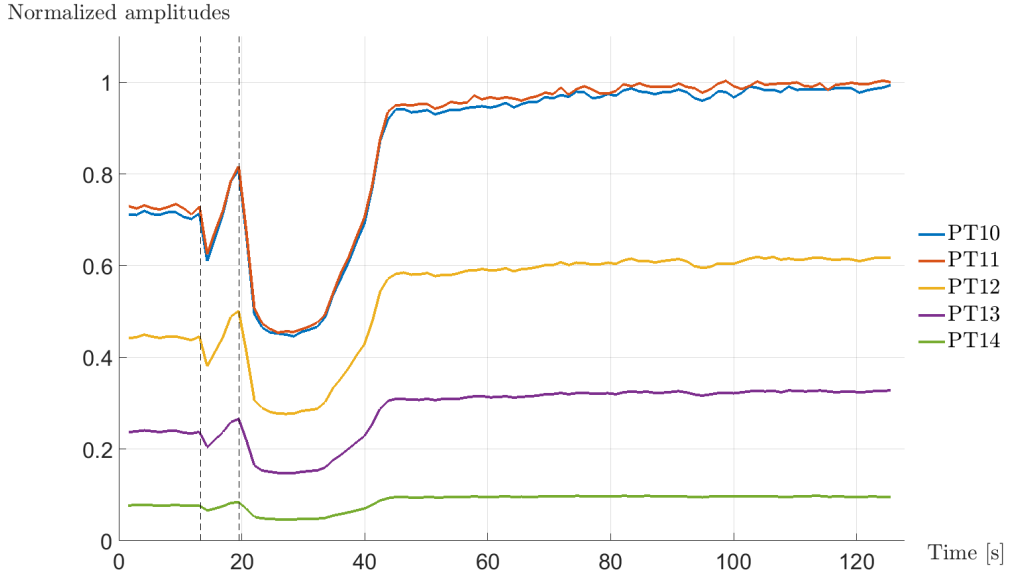
Figure 27: Amplitude development of the guide vane frequency from PL to BEP
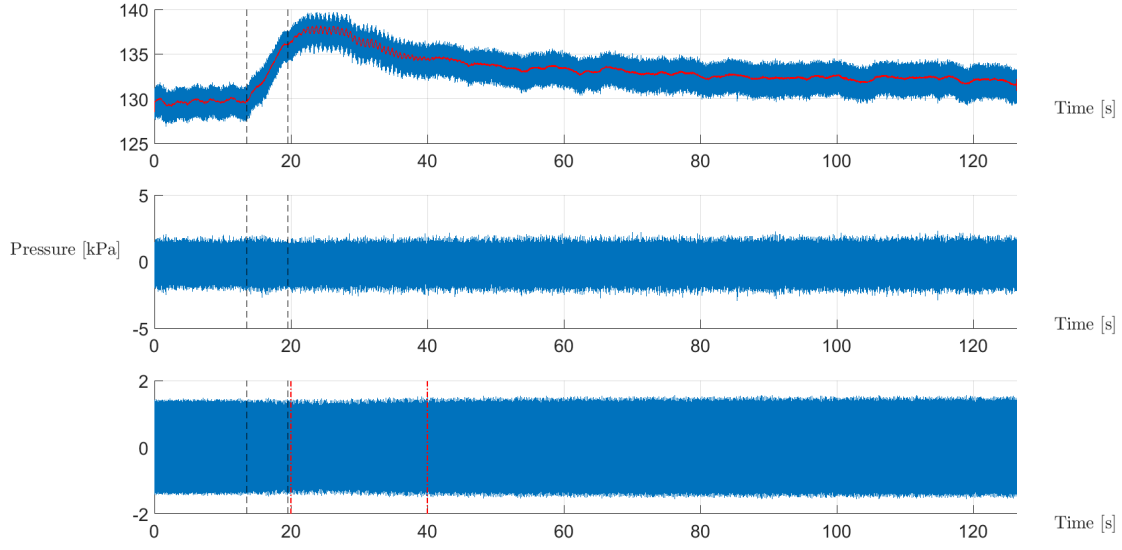
Figure 28: Raw signal from PT11 at PL to BEP
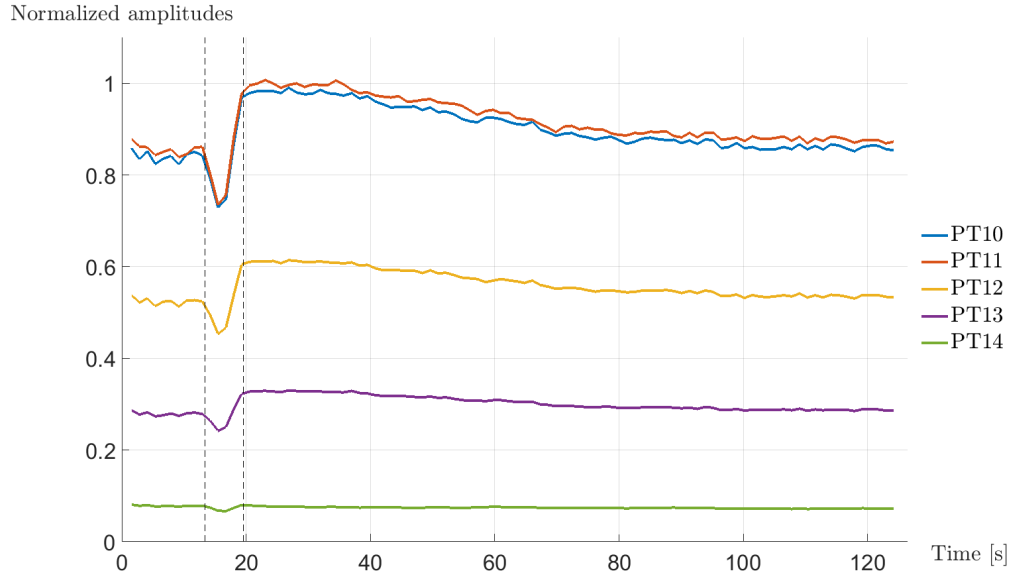
Figure 29: Amplitude development of the guide vane frequency from BEP to PL

Figure 29 show the equivalent amplitude development of the guide vane frequency from BEP to PL. The figure illustrate the same amplitude drop during the change in guide vane opening, as has been observed for the preceding transient measure-

ments. However, the steady state amplitude at BEP appears to be lower than the amplitudes at PL. This is not in accordance with the theory of the amplitude's dependence on the radial distance between the runner and guide vanes, and deviates from the results from the steady state measurements. Running between BEP and PL, one would also expect the amplitude to return to the same value for a given operating point. Comparing figure 29 to figure 27, this does not appear to be the case. In order to better visualize and compare the amplitudes prior to- and after the change in guide vane angle, the amplitude from PL to BEP and BEP to PL have been plotted in the same diagram. They have also been normalized using the same value, to facilitate the comparison. The plot is presented in figure 30.
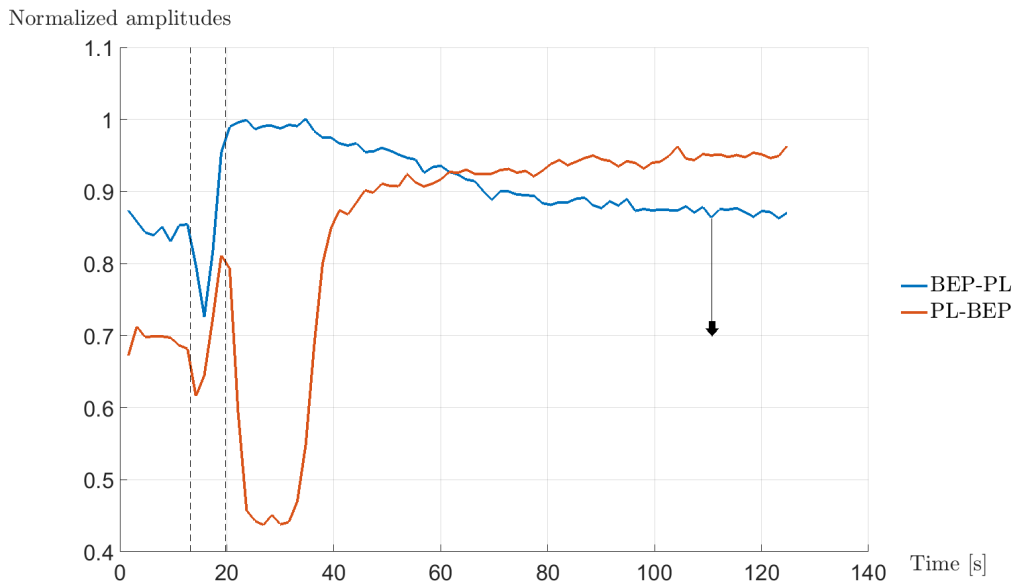
Figure 30: Amplitude development of the guide vane frequency between PL and BEP

Considering figure 30, one can observe the level of the amplitudes prior to- and after a change in guide vane opening between PL and BEP. The figure show the expected difference in amplitude prior to the change in guide vane opening, with a larger amplitude value at BEP and a lower value at PL. However, after the change, the blue line representing the amplitude development between BEP and PL stabilize at a level significantly higher than the starting point of the red curve, representing the development from PL to BEP. This seems odd as the measurements were conducted in repeating cycles. Measuring the pressure from PL to BEP, the subsequent measurement series was done from BEP to PL. This cycle

was repeated 10 times. Thus, one would expect the amplitudes to return to the same value for each operational point. One possible explanation for the large deviation in the amplitude values is that the amplitudes need more than the given time to stabilize to it's steady state value. However, the blue curve seems to be levelling off and show no sign to be dropping further down. Also, when running the experiment, there was not a lot of additional time between the end of one measurment series (PL-BEP) and the next (BEP-PL). Thus, this does not seem like a sufficient explanation for the deviating amplitude values.

Strain Gauge

In figure 31, the amplitude development from BEP to HL is plotted for the strain gauge, as well as the onboard pressure transducers. To facilitate comparison of the various curves, each of the curves have been normalized with respect to its highest value. The figure show good agreement between the pressure amplitudes captured by the onboard pressure transducers, and the strain felt by the strain gauge. This seems reasonable as the vibration of the runner is expected to reflect the frequency and magnitude of the pressure pulses in the system. Similar plots have been made for the amplitude development between PL and BEP and from HL and BEP, showing the same trend. These plots are presented in appendix B.2.
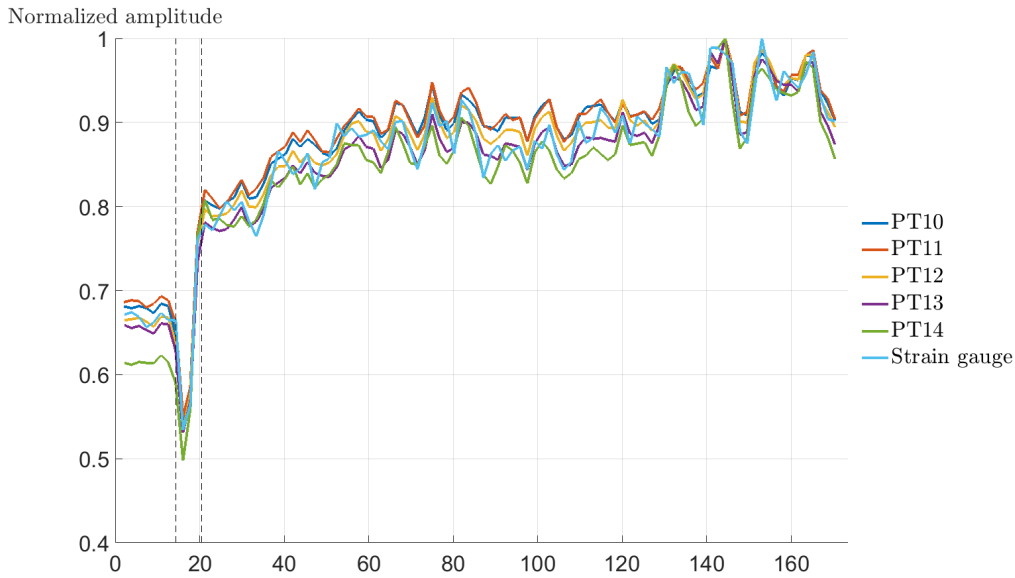
Figure 31: Comparison of the amplitude development of the guide vane frequency on the Strain Gauge and onboard pressure transducers - from BEP to HL

6.2.2 Repeatability of the transient measurements

To account for the repeatability of the conducted measurements, the measurement series from BEP to PL was repeated 20 times. Subsequently, the amplitude development of the guide vane frequency for the 20 measurement series was plotted for comparison. Figure 32 present the result. The figure show good agreement between the various measurement series, with subsequent curves following the same path. Thus, the repeatability of the conducted measurements seem to be good.
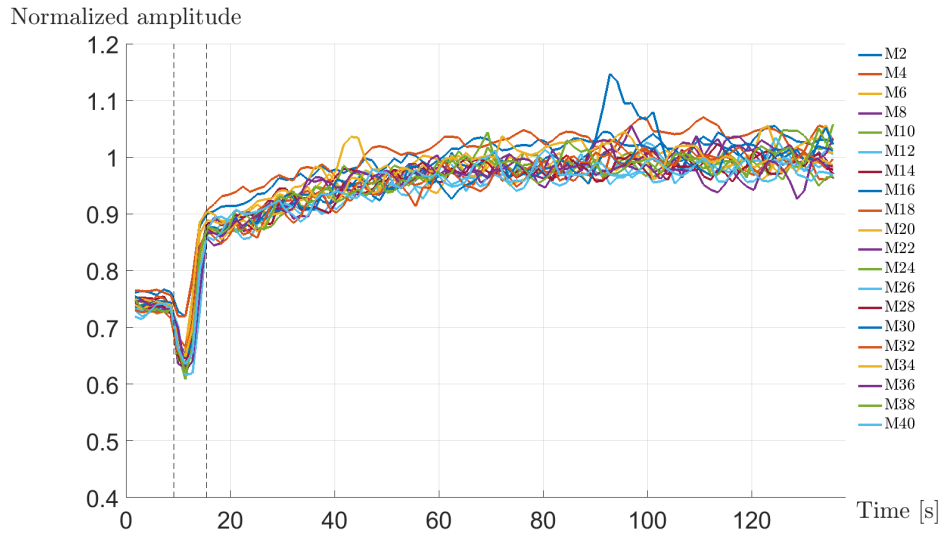
Figure 32: Amplitude development (PT11) from BEP to HL for the various measurement series

7 | Conclusion

Onboard pressure and strain measurements have been successfully carried out on the Francis-99 model runner at the Waterpower Laboratory at NTNU. The measurements were carried out under satisfactory laboratory conditions, with relatively low uncertainties related to the onboard pressure measurements. FFT analysis of the steady state measurements revealed the presence of several frequencies caused by dynamic pressure pulsations. However, elastic fluctuations were also observed in the system.

The predominant frequencies observed throughout the system are consistent with previous experiments conducted on high head Francis turbines. The guide vane frequency appears to be the predominant frequency inside the runner, with increasing amplitudes for higher guide vane angles. The blade passing frequency is identified as the predominant frequency in the vaneless space, and the Rheinegans frequency is clearly visible in the draft tube cone during part load operation.

The analysis also show a close correlation between the observed vibration frequencies on the strain gauge and the pressure oscillations in the model runner. The guide vane frequency is often observed to be the main source of vibration. However, the guide vane frequency's second harmonic appear to be amplified in the strain gauge signal, due to the phase difference in the pressure pulses entering the surrounding hydraulic channels. Also the elastic fluctuation downstream the runner have a large relative amplitude in the strain gauge signal, and appear to generate fluctuating stresses and potential fatigue damage in the runner. Due to the absence of the synchronous component of the Rheinegans frequency in the strain gauge signal, the asynchronous component appear to be the predominant source of mechanical excitation caused by the Rheinegans frequency.

The transient amplitude development of the guide vane frequency in the model runner showed no sign of increased amplitudes due to the change in guide vane angle. Thus, the demonstrated development appear to not be adding to the fluctuating stresses on the turbine. The transient amplitude development illustrated an even dampening of the amplitudes throughout the hydraulic channel.

8 | Further work

- Measurements with the current experimental setup should be repeated with additional strain gauges. This will provide a more comprehensive view of the fluctuating stresses on the runner. A rosett setup of the strain gauges is a possibility in order to capture the multi-directional loadings on the runner blades. This would also be beneficial for potential FSI simulations.

- The natural frequencies and vibration modes of the model runner should be investigated to account for the presence of the guide vane frequency's second harmonic in the runner.

- Measures to reduce the stiffness of the model runner should be evaluated. The strain gauge used in the current setup permits the measurement of strain in the model runner. However, to imitate the behaviour of the prototype a reduced stiffness would be preferable to bring out the equivalent vibration modes in the model runner.

- The transient measurements should be repeated in order to verify the presented transient results. The study could also be extended to include the amplitude development of other predominant frequencies in the runner, such as the guide vane frequency's second harmonic.

References

[1] Francis-99 second workshop test case. NTNU. `https://www.ntnu.edu/nvks/test-case`.

[2] Arthur Favel Christian Landry Anders Muller Fransic Avellan. Analysis of the part load helical vortex rope of a francis turbine using onboard sensors. *Physics Conference series*, Descember 2015.

[3] Carl Werdeling Bergan. *Transient LDV-measurements in the draft tube of a high head Francis turbine*. NTNU, 2014.

[4] K.Kalita N. Das P.K Boruah and U. Sarma. Design and uncertainty evaluation of a strain measurement system. 2015.

[5] Hermod Brekke. A review on oscillatory problems in francis turbines, 2010.

[6] Ingeborg Lassen Bue. *Pressure pulsations and stress in a high head turbine - comparison between model and geometrically similar prototype*. NTNU, 2013.

[7] International Electrotechnical Commision. *IEC 60193: Hydraulic turbines, storage pumps and pump turbines - Model acceotance tests*. 1999.

[8] J.H Gummer F. Avellan, S. Etter and U. Seidel. Dynamic pressure measurements on a model turbine runner and their use in preventing runner fatigue failure. 2000.

[9] A. Rudiger G. Heinzel and R. Shilling. Spectrum and spectral density estimation by discrete fourier transform, including a comprehensive list of window functions and some new flat-top windows. `https://holometer.fnal.gov/GH_FFT.pdf`, 2012.

[10] Anthony J. Wheeler & Ahmad R. Ganji. *Introduction to Engineering Experimentation*. 3 edition, 2010.

[11] Jan Otto Haugen. Laboratoriet - typiske frekvenser i strømningsmaskiner, 1994.

[12] Kari Haugen. *Trykkpulsasjoner i Francisturbiner*. NTNU, 2007.

[13] Julie Marie Hovland. *Pressure pulsations and stress in a high head Francis model turbine*. 2013.

[14] National Instruments. `http://www.ni.com/white-paper/5509/en/`. Online; accessed 5-May-2016.

[15] National Instruments. `http://www.ni.com/white-paper/4844/en/`. Online; accessed 27-May-2016.

[16] Wiliam D. Callister Jr. *Materials Science and Engineering - An Introduction.* 7 edition, 2007.

[17] Einar Agnalt Katarina Kloster and Ole Gunnar Dahlhaug. Analysis of on-board pressure pulsations and it's influence on blade loading in a high head francis turbine. 2016. Unpublished.

[18] Einar Kobro. *Trykkpulsasjoner i Francisturbiner.* NTNU, 2006.

[19] Einar Kobro. *Measurement of Pressure Pulsations in Francis Turbines.* PhD thesis, NTNU, 2010.

[20] P.Y. Lowys J.L Deniau E. Gaudin P. Leroy and M. Djatout. On-board model runner dynamic measurements. 2006.

[21] National Instruments. *Datasheet: NI 9239*, 2014. `http://www.ni.com/datasheet/pdf/en/ds-199`.

[22] Torbjørn Nielsen. *Dynamisk dimensjonering av vannkraftverk.* SINTEF, 1990.

[23] S. Natal P. Lowys F. Parquet M. Couston M. Farhat and F. Avellan. Onboard measurments of pressure and strain fluctuations in a model of low head francis turbine. part 1: Instrumentation. 2002.

[24] Mirjam Sick & André Coutu Peter Dorfler. *Flow-Inducedc Pulsation and Vibration in Hydroelectric Machinery.* 2013.

[25] Halvard Bjørndal Andre P. Reynaud and Anders L. Holo. Mechanical robustness of francis runners, requirements to reduce the risk of cracks in blades. 2011.

[26] Bjørn Winther Solemslie. *Optimalisering av ringledning for Peltonturbin.* 2010.

[27] Pål Tore Selbo Storli. *Modelltest av Francis turbin i vannkraftlaboratoriet ved NTNU.* 2006.

[28] A Stuckle. *CFD-Analysis of the Stay Vanes in a High Head Francis turbine.* 2007.

[29] B. Nennemann T.C. Vu and M. Farhat. Cfd prediction of unsteady wicket gate - runner interaction in francis turbines: A new standard hydraulic design procedure. 2005.

Appendices

A | Results - Steady state measurements

A.1 Onboard pressure transducers
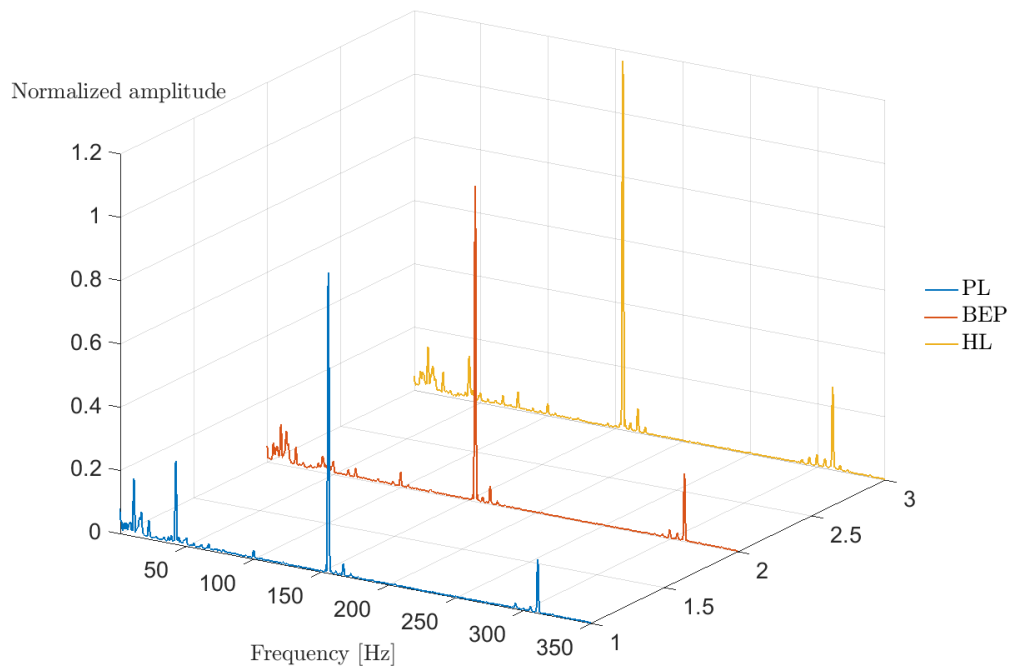
Figure 33: Spectral analysis - PT10
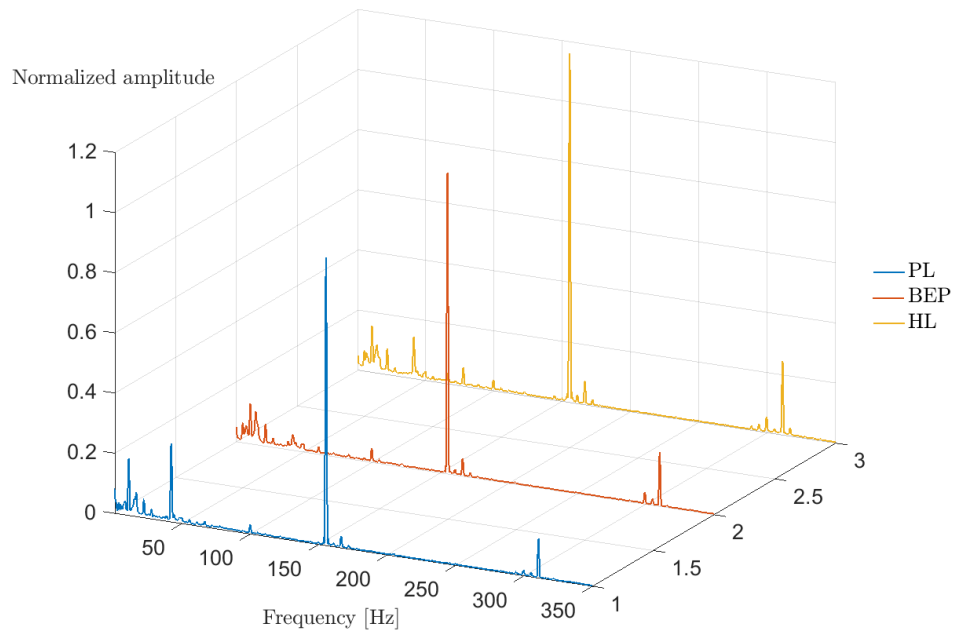
Figure 34: Spectral analysis - PT11
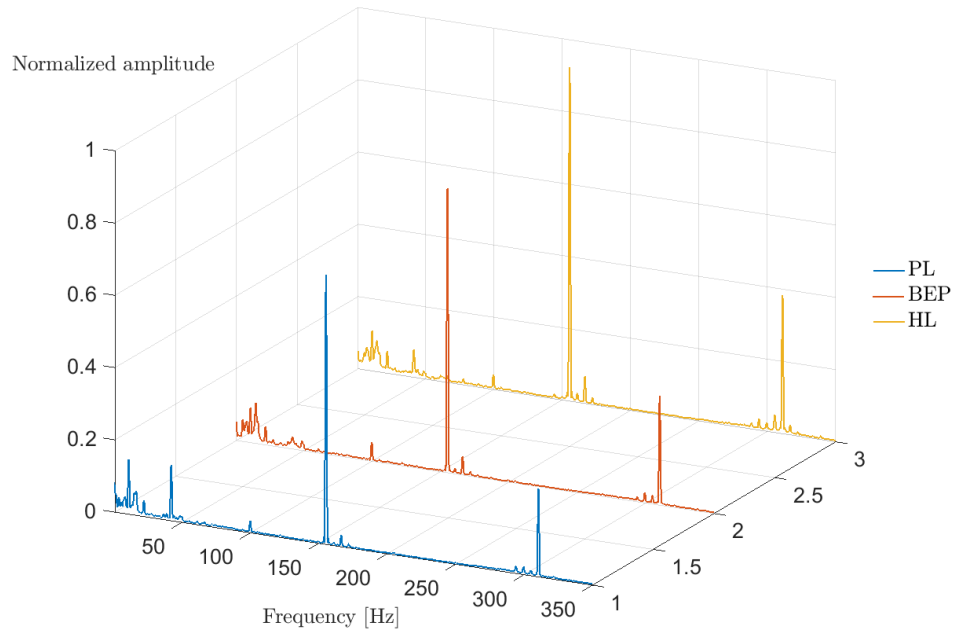
Figure 35: Spectral analysis - PT12

II
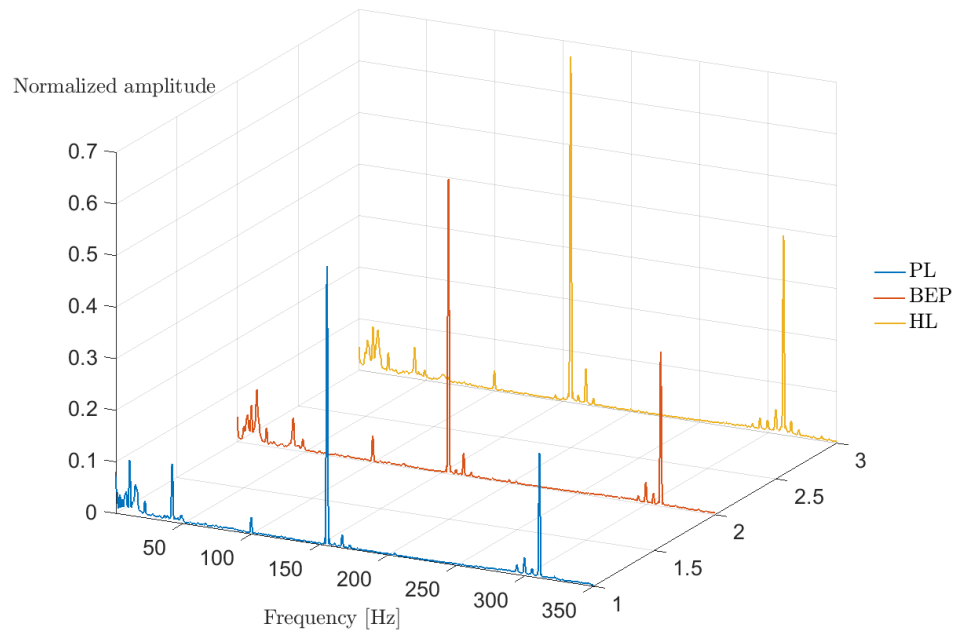
Figure 36: Spectral analysis - PT13
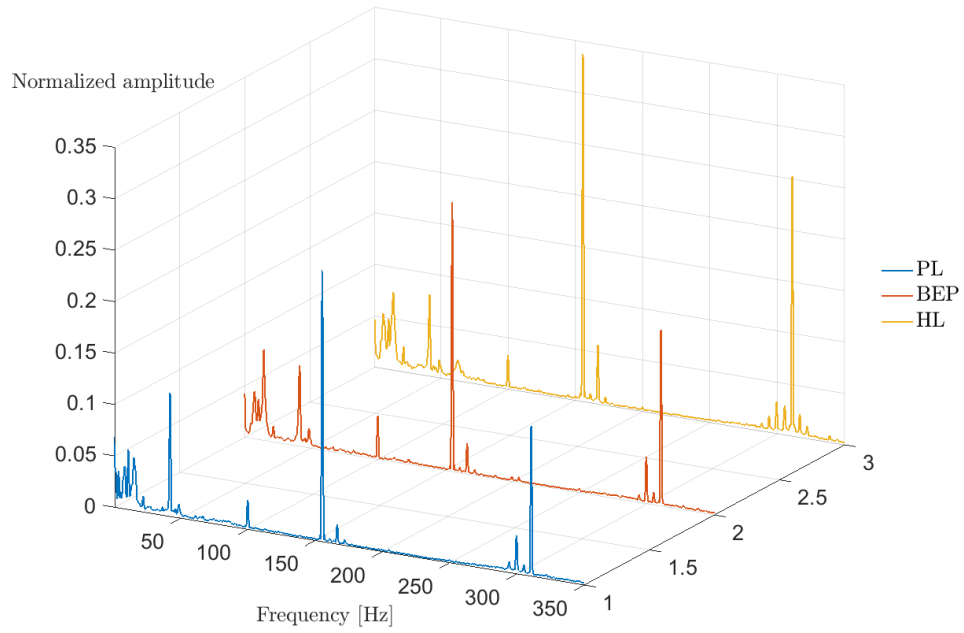
Figure 37: Spectral analysis - PT14

A.2 Vaneless space
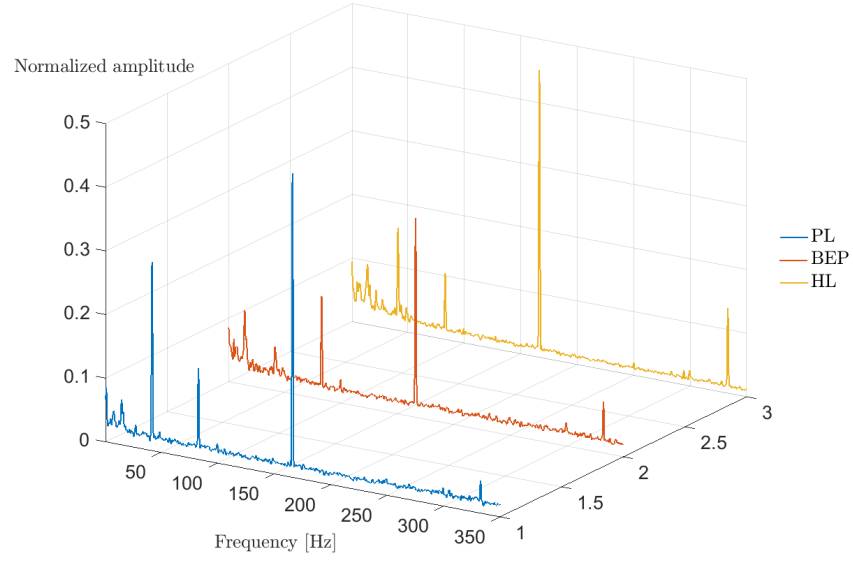
Figure 38: Spectral analysis - VL1
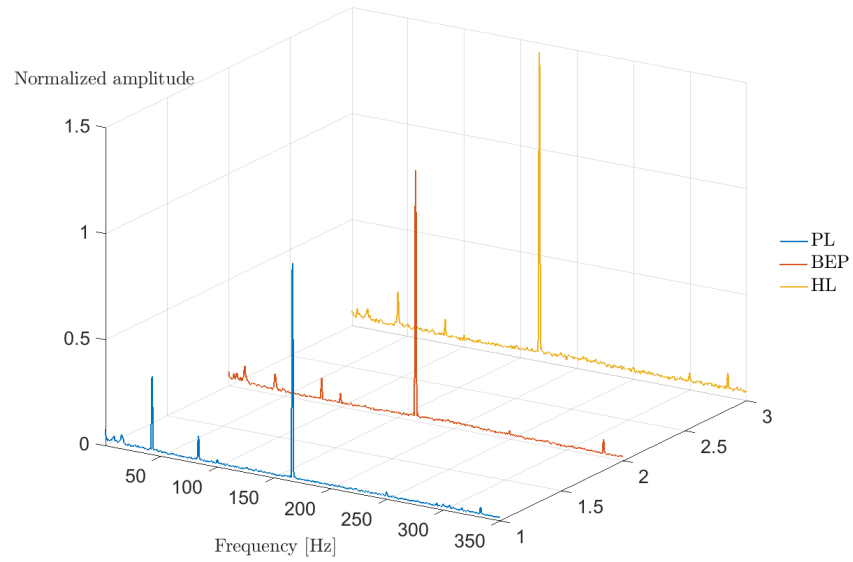
Figure 39: Spectral analysis - VL2

A.3 Draft tube
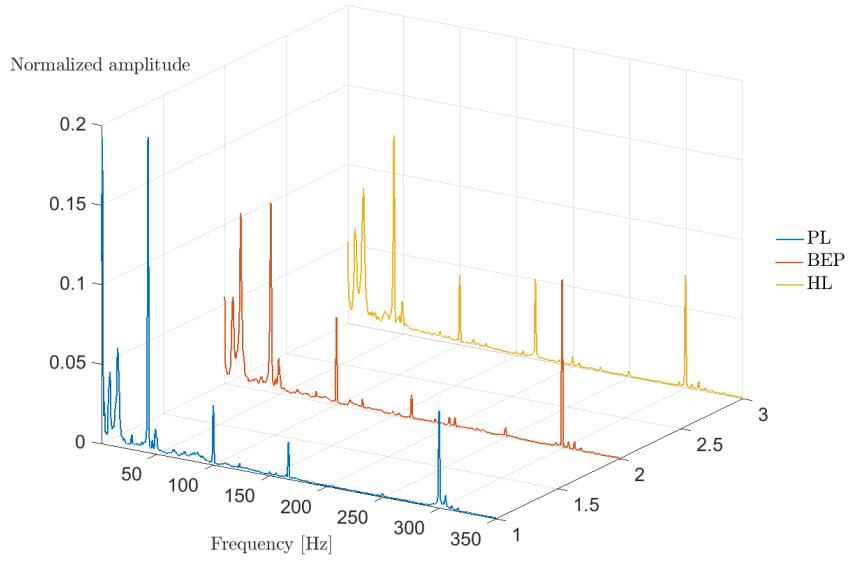
Figure 40: Spectral analysis - DT30 (5)
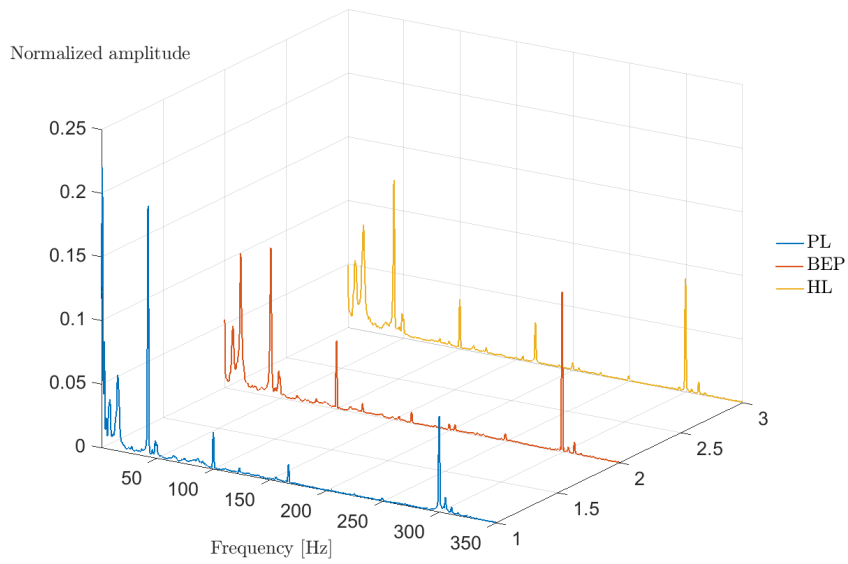
Figure 41: Spectral analysis - DT31 (1)
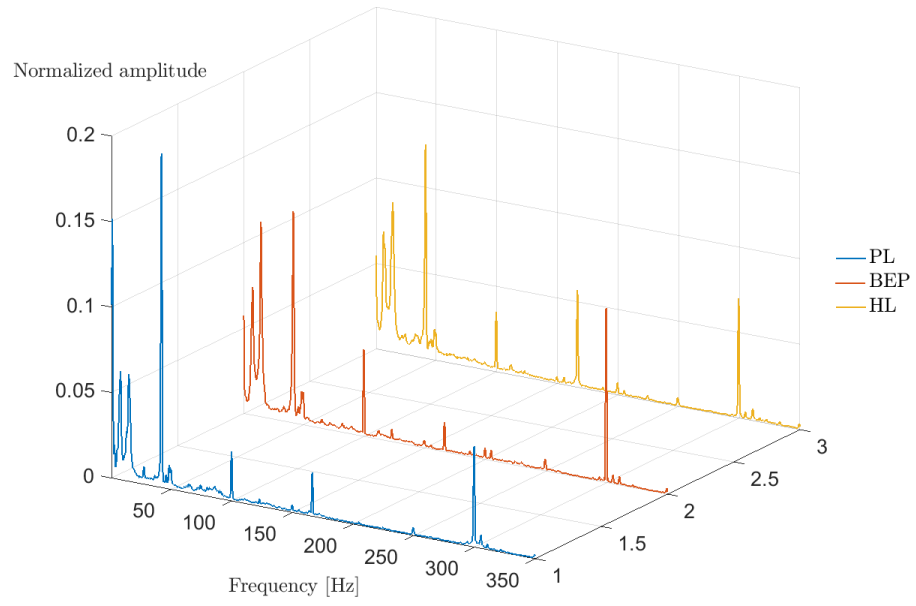
Figure 42: Spectral analysis - DT32 (6)
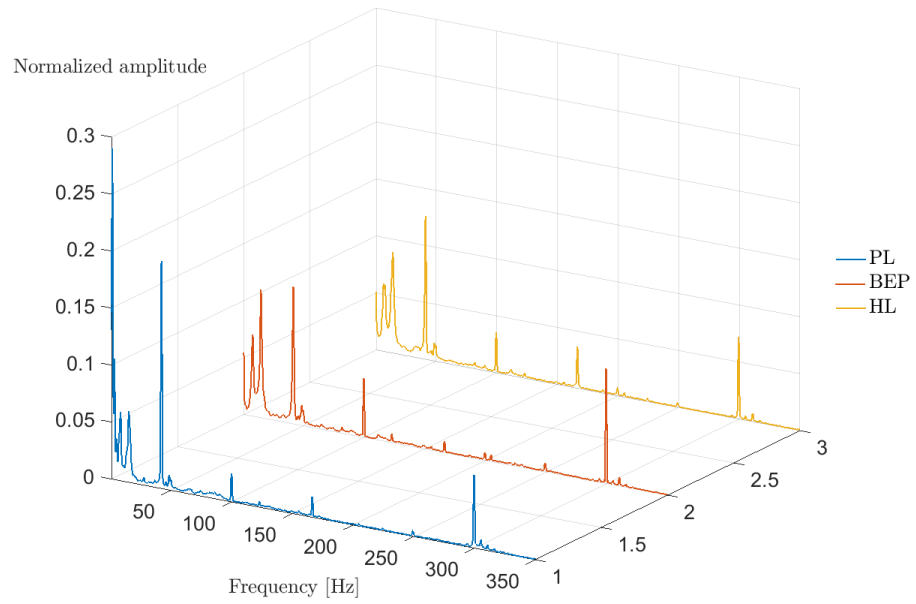
Figure 43: Spectral analysis - DT33 (4)

A.4 Pipeline
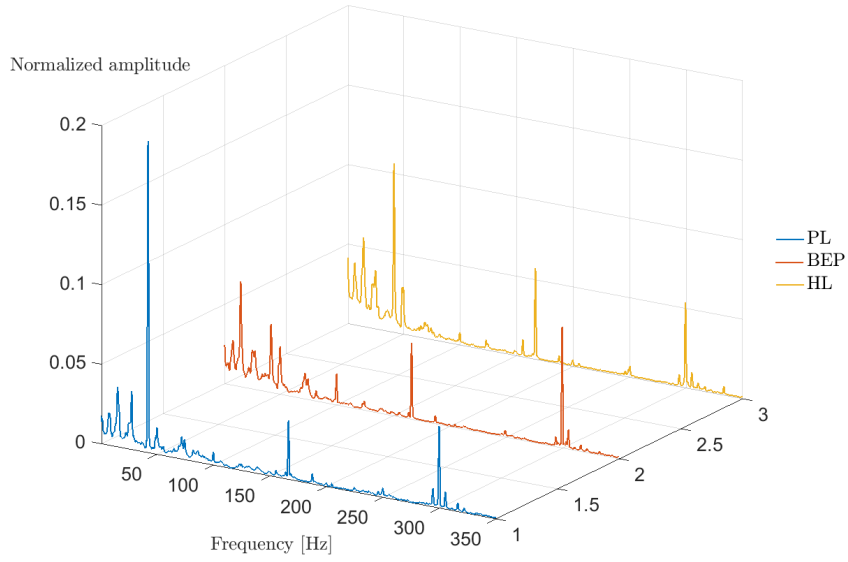
Figure 44: Spectral analysis - PT01
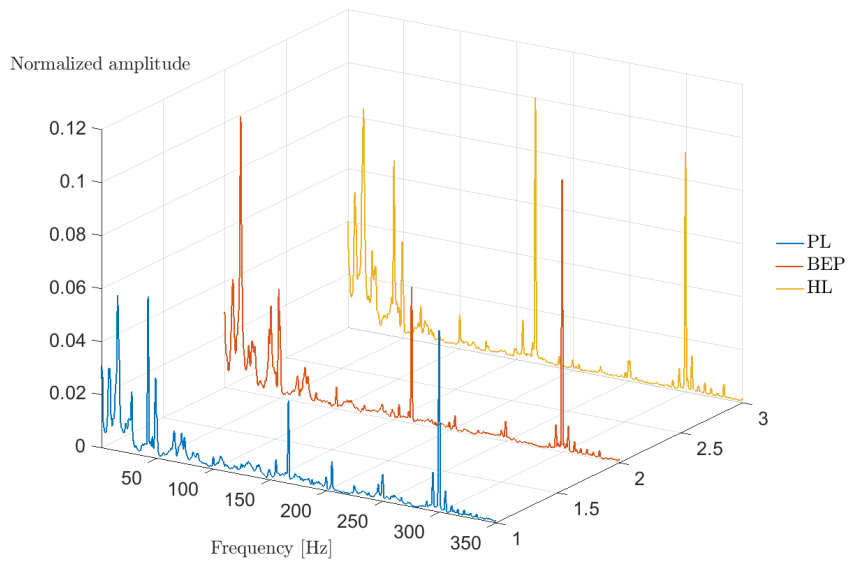
Figure 45: Spectral analysis - PT02
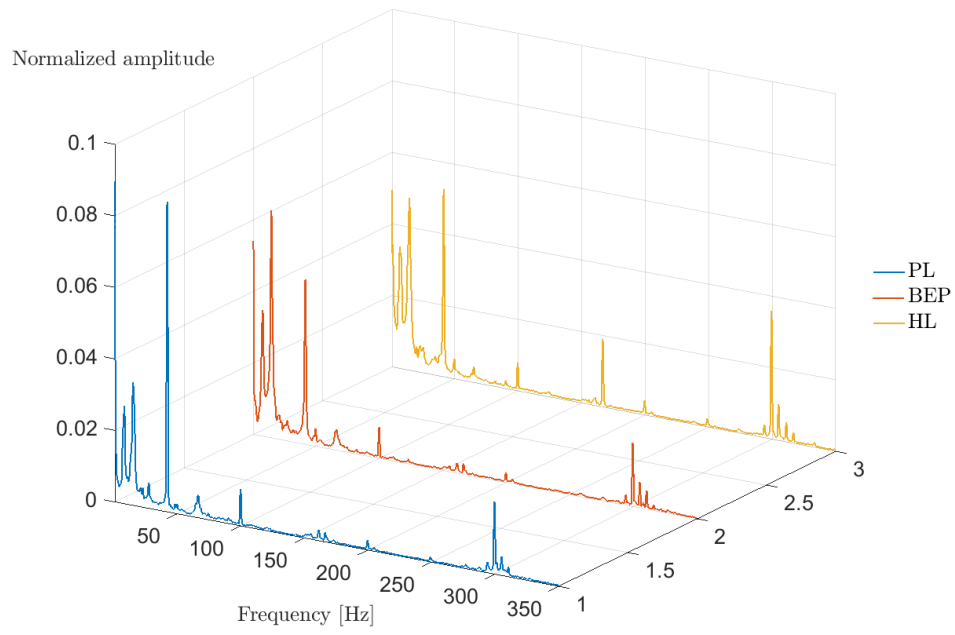
Figure 46: Spectral analysis - PT03

VIII

B | Results - Amplitude development transient measurements

B.1 Onboard pressure transducers
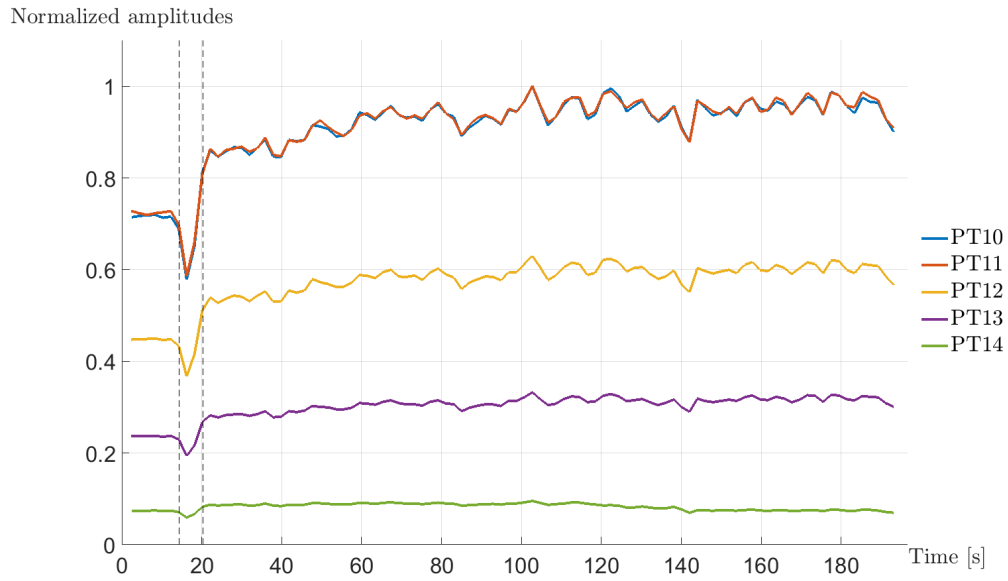
Figure 47: Amplitude development of the guide vane frequency from BEP to HL
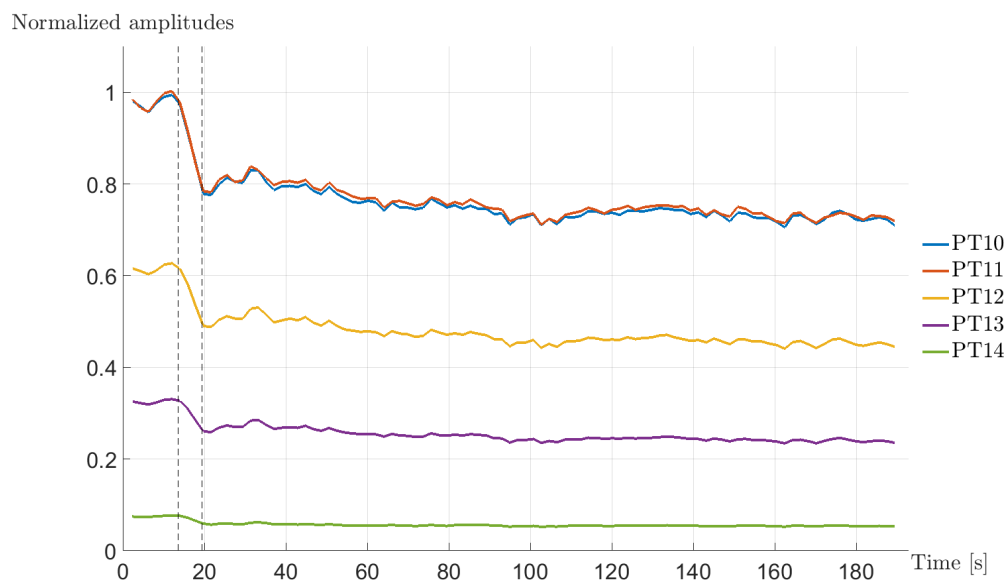
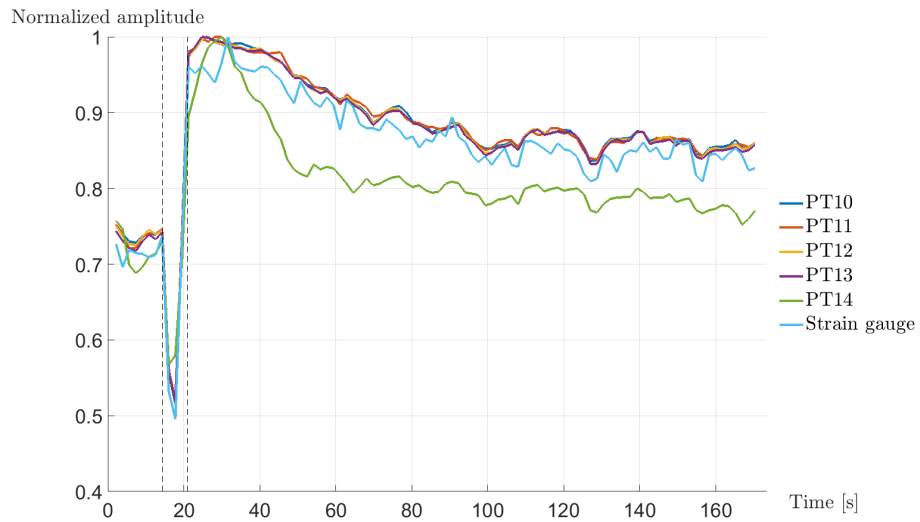Figure 48: Amplitude development of the guide vane frequency from HL to BEP
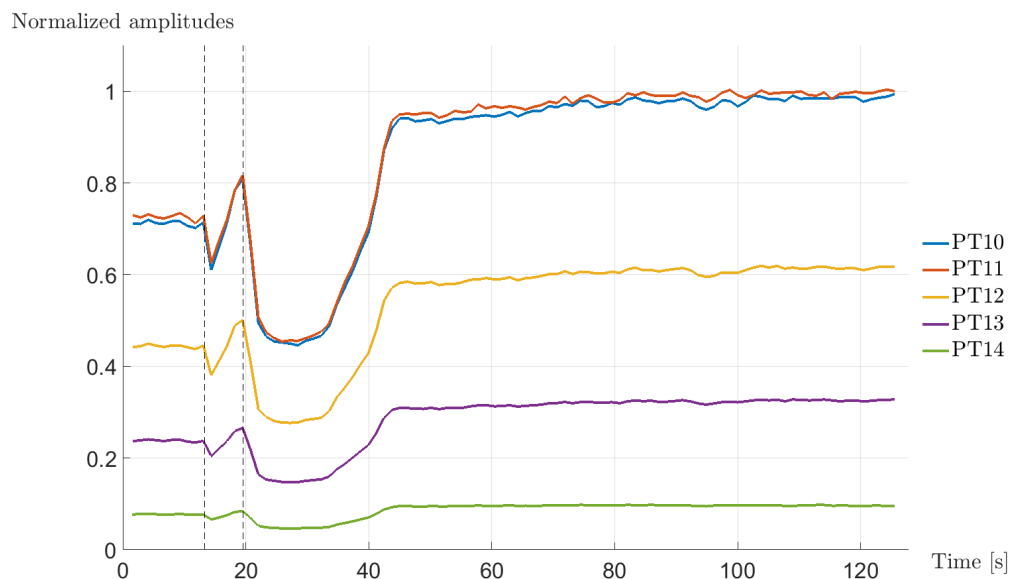
Figure 49: Amplitude development of the guide vane frequency from PL to BEP

X
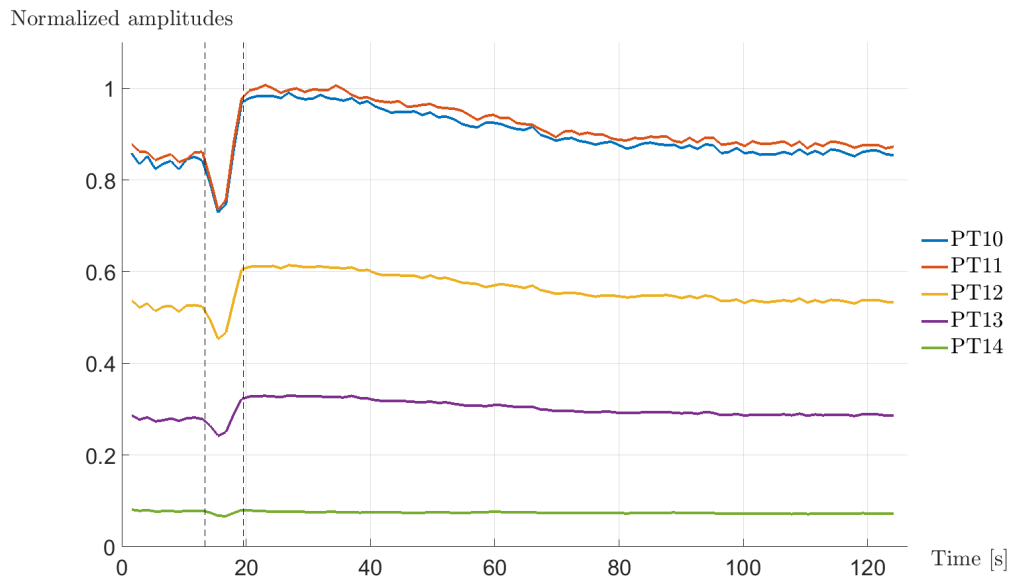
Figure 50: Amplitude development of the guide vane frequency from BEP to PL

XII

B.2 Strain gauge and onboard pressure transducers
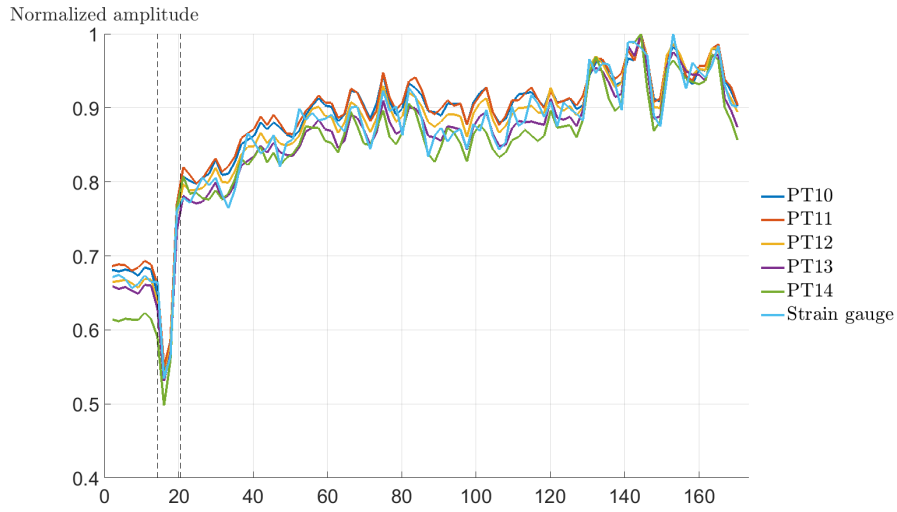
Figure 51: Normalized amplitude development of the guide vane frequency from BEP to HL
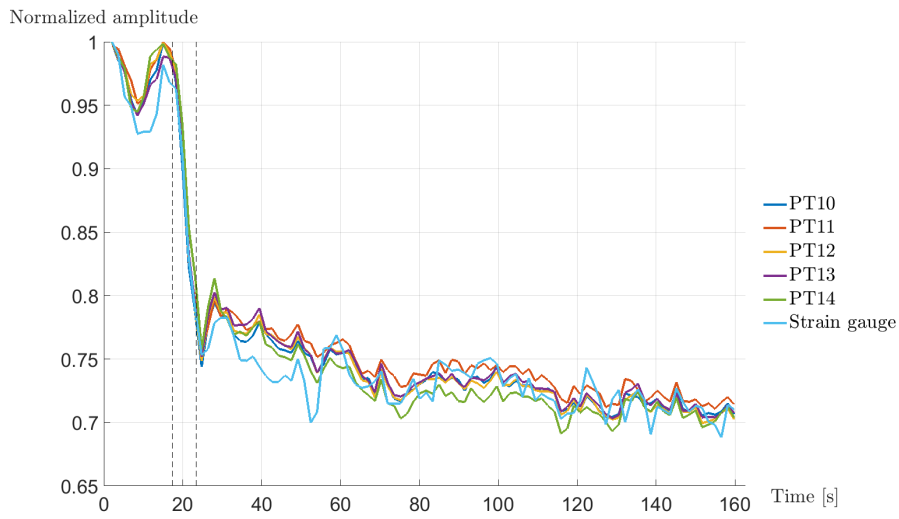
Figure 52: Normalized amplitude development of the guide vane frequency from HL to BEP
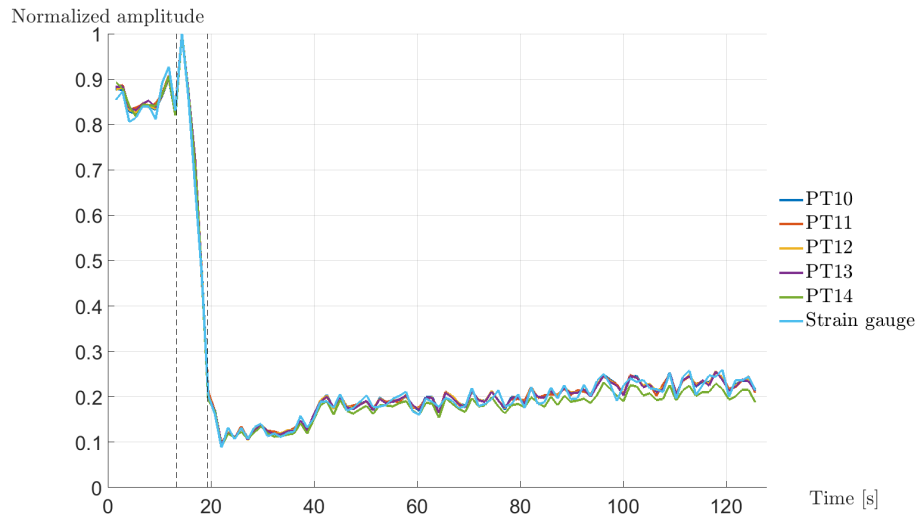
Figure 53: Normalized amplitude development of the guide vane frequency from PL to BEP

Figure 54: Normalized amplitude development of the guide vane frequency from BEp to PL

XIV

C | Data sheets

MINIATURE RUGGEDIZED PRESSURE TRANSDUCER
XTM-190 (M) SERIES

- Excellent Stability
- High Natural Frequency
- Inorganically Bonded Sensor
- Robust Construction

The XTM-190 miniature pressure transducer utilizes a metal diaphragm as a force collector with a Piezoresistive Sensor as its sensing element. With the threaded body, hexagonal head and o-ring seal, the XTM-190 is easy to mount and simple to apply. The small size and flush diaphragm permit direct installation of the transducer in the wall of pressure containers, tubes, pipes, etc., eliminating the need for costly, space consuming hardware. Differential versions of all ranges up to 500 psi are available. The reference pressure source should be dry, noncorrosive gas. Absolute and sealed versions of the XTM-190 have a reference vacuum sealed in the transducer.
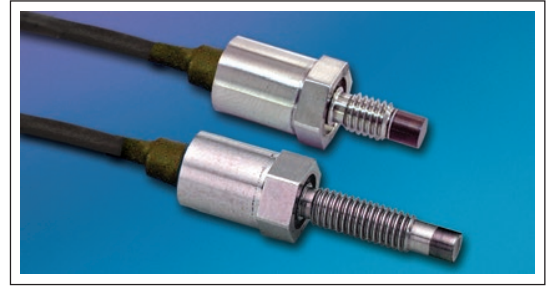
Kulite recommends the KSC-2 signal conditioner to maximize the measurement capability of the XTM-190 transducer.

OPTIONAL CONNECTOR VERSION

.630 (16.0)

KEYWAY DETAIL

CONNECTOR, CMR-S1-E-04P OR EQUIVALENT

ORDER AS: XTM-100-190(M)

NOT AVAILABLE ON GAGE OR DIFFERENTIAL UNIT

CABLE STRAIN RELIEF

PRESSURE REFERENCE TUBE .030 X 1" LONG (.76 X 25.4) FOR GAGE & DIFFERENTIAL UNITS

.190 (4.8)   .56 (14.2)   "L"   3/8 HEX (9.5)

.17 (4.3)

THREAD "T"

.148 NOM. (3.8)

SILICONE O – RING .176 I.D. X .040 C.S. (4.5 I.D. X 1.0 C.S.)

PRESSURE SENSITIVE AREA

4 COND. # 30 AWG SHIELDED CABLE 36" (914) LONG

*LENGTH MUST BE STATED ON P.O. AT TIME OF ORDER PLACEMENT.

P/N*	"T"	"L"	
190	10-32 UNF-2A	.437	11.1 mm
190(M)	M5 x .8	.437	11.1 mm
190	10-32 UNF-2A	.745	18.9 mm
190(M)	M5 x .8	.745	18.9 mm

FUNCTION		
WIRING COLOR		CONNECTOR PIN
RED	+ INPUT	1
WHITE	- OUTPUT	2
BLACK	- INPUT	3
GREEN	+ OUTPUT	4

INPUT	Pressure Range	1.7 25	3.5 50	7 100	17 250	35 500	70 1000	170 2500	350 BAR 5000 PSI
	Operational Mode	Absolute, Gage, Differential	Absolute, Gage, Sealed Gage, Differential			Absolute, Sealed Gage			
	Over Pressure	3.5 50	7 100	14 200	35 500	70 1000	140 2000	210 3000	420 BAR 6000 PSI
	Burst Pressure	3 Times Rated Pressure to a Maximum of 6500 PSI (450 BAR)							
	Pressure Media	Any Liquid or Gas Compatible With 17-4 PH or 15-5 Stainless Steel (All Media May Not Be Suitable With O-Ring Supplied)							
	Rated Electrical Excitation	10 VDC/AC							
	Maximum Electrical Excitation	12 VDC/AC							
	Input Impedance	650 Ohms (Min.)							
OUTPUT	Output Impedance	1000 Ohms (Nom.)							
	Full Scale Output (FSO)	75 mV (Nom.)							
	Residual Unbalance	± 5 mV (Typ.)							
	Combined Non-Linearity, Hysteresis and Repeatability	±1% FSO BFSL (Typ.)							
	Resolution	Infinitesimal							
	Natural Frequency (KHz) (Typ.)	75	95	125	210	290	410	560	930
	Acceleration Sensitivity % FS/g Perpendicular	2.3×10^{-3}	1.4×10^{-3}	9.6×10^{-4}	6.2×10^{-4}	4.3×10^{-4}	3.0×10^{-4}	2.1×10^{-4}	1.3×10^{-4}
	Insulation Resistance	100 Megohm Min. @ 50 VDC							
ENVIRONMENTAL	Operating Temperature Range	-20°F to +350°F (-29°C to +175°C)							
	Compensated Temperature Range	80°F to 180°F (25°C to 80°C) Any 100°F Range Within The Operating Range on Request							
	Thermal Zero Shift	± 2% FS/100°F (Typ.)							
	Thermal Sensitivity Shift	± 2% /100°F (Typ.)							
	Linear Vibration	10-2,000 Hz Sine, 20g. (Max.)							
PHYSICAL	Electrical Connection	4 Conductor 30 AWG Shielded Cable 36" Long							
	Weight	8 Grams (Nom.) Excluding Cable							
	Pressure Sensing Principle	Inorganically Bonded Piezoresistive Sensor							
	Mounting Torque	15 Inch-Pounds (Max.) 1.7 Nm							

kulite®

STRAIN GAGE SERIES

When compared to conventional metallic wire and foil gages, Kulite semiconductor gages offer some significant advantages:

- Higher Sensitivity
- Smaller Sizes
- Higher Resistance
- Higher Fatigue Life
- Lower Hysteresis
- Lower Non-linearity
- Increased Temperature Envelope

The semiconductor strain gage may be thought of as a strain sensitive resistor. Generally when bonded to a stressed member, its resistance changes as a function of applied strain. This characteristic makes it useful in the fields of stress analysis, physical measurements, testing, transducer and instrumentation manufacture. Additionally, the latest Silicon-On-Insulator (SOI) technology enables the fabrication of the high temperature strain gages with enhanced performance characteristics. These gages, as well as all other silicon based strain gages, are easily optimized for specific customer applications and have been found by customers to be truly superior to their foil gage counterparts.
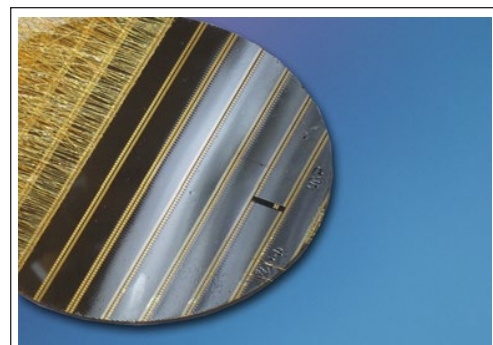
For further information, please download our *Strain Gage Manual.*

Kulite recommends the KSC-2 signal conditioner to maximize the measurement capability of the Strain Gage Series.

GAGE TYPES

FIG. B1 A-TYPE

FIG. B2 U-TYPE

FIG. E1 S/A-TYPE

FIG. E2 S/U-TYPE

GAGE GEOMETRY
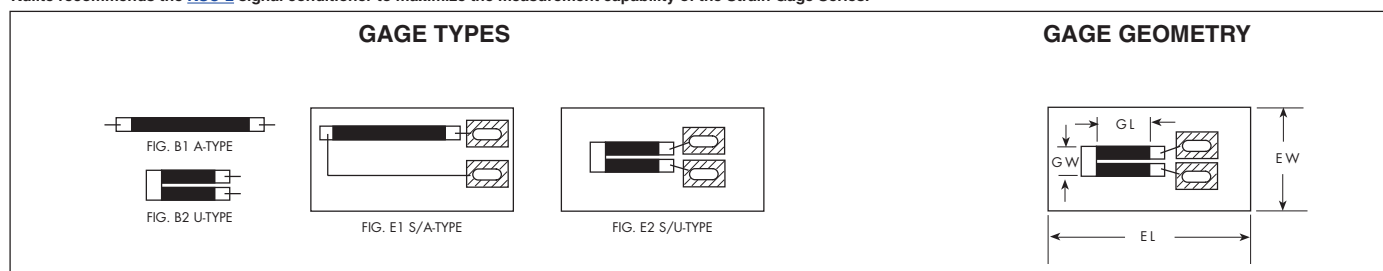
STRAIN GAGE CHARACTERISTICS AND SELECTION TABLE

GAGE DOPING CODE	GAGE CHARACTERISTICS		PART NUMBER	FIGURE	(GL) EFFECTIVE LENGTH ±5%	(GW) GAGE WIDTH ±5%	(EL) ENCAPSULATION LENGTH ±10%	(EW) ENCAPSULATION WIDTH ±10%
C	G.F. TCR TCGF Linearity	+ 100 + 4% - 6% ± 0.2%	ACP-15-150 ACP-30-150 ACP-120-300 UCP-120-090 S/ACP-120-300 S/UCP-120-090	B1 B1 B1 B2 E1 E2	.100 .100 .250 .060 .250 .060	.020 .010 .009 .020 .009 .020	.500 .280	.210 .140
D	G.F. TCR TCGF Linearity	+ 115 + 3% - 8% ± 0.2%	ADP-250-220 ADP-350-300 UDP-350-175 S/ADP-350-300 S/UDP-350-175	B1 B1 B2 E1 E2	.186 .250 .140 .250 .140	.009 .010 .016 .010 .020	.500 .350	.210 .140
E	G.F. TCR TCGF Linearity	+ 130 + 6% - 10% ± 0.2%	AEP-350-220 AEP-500-300 UEP-350-060 UEP-350-090 S/AEP-500-300 S/UEP-350-090	B1 B1 B2 B2 E1 E2	.170 .250 .030 .060 .250 .060	.009 .010 .020 .020 .010 .020	.500 .280	.210 .140
F	G.F. TCR TCGF Linearity	+ 140 + 10% - 11% ± 0.2%	AFP-500-090 AFP-350-090 UFP-750-090 S/AFP-500-090 S/UFP-750-090	B1 B1 B2 E1 E2	.060 .060 .060 .060 .060	.010 .010 .020 .010 .020	.280 .280	.140 .140
G	G.F. TCR TCGF Linearity	+ 155 + 18% - 13% ± 0.2%	AGP-350-090 AGP-500-090 AGP-1000-300 UGP-1000-060 UGP-1000-090 S/AGP-1000-300 S/UGP-1000-090	B1 B1 B1 B2 B2 E1 E2	.060 .060 .250 .030 .065 .250 .060	.010 .010 .010 .020 .020 .010 .020	.500 .280	.210 .140
H	G.F. TCR TCGF Linearity	+ 175 + 45% - 23% ± 0.2%	AHP-10000-220 AHP-10000-300 UHP-5000-060 S/AHP-10000-220 S/AHP-10000-300 S/UHP-5000-060	B1 B1 B2 E1 E1 E2	.170 .250 .030 .170 .250 .030	.009 .009 .020 .009 .009 .020	.250 .500 .250	.150 .210 .140

Nominal Gage Resistance (Ω) Indicated in Red

Note: Dimensions are in inches. All dimensions nominal. (C)

XVIII

D | Calibration reports

CALIBRATION REPORT

CALIBRATION PROPERTIES
Calibrated by: Katarina Kloster
Type/Producer: Kulite XTM-190SM
SN: 8317-1-201
Range: 0-3,5bar a
Unit: kPa

CALIBRATION SOURCE PROPERTIES
Type/Producer: Pressurements deadweight tester P3023-6-P
SN: 66611
Uncertainty [%]: 0,008

POLY FIT EQUATION:
$Y = -6{,}79035476E{+}0X^0 + 37{,}37745937E{+}0X^1$

CALIBRATION SUMARY:
Max Uncertainty   : 0,412824 [%]
Max Uncertainty   : 0,255793 [kPa]
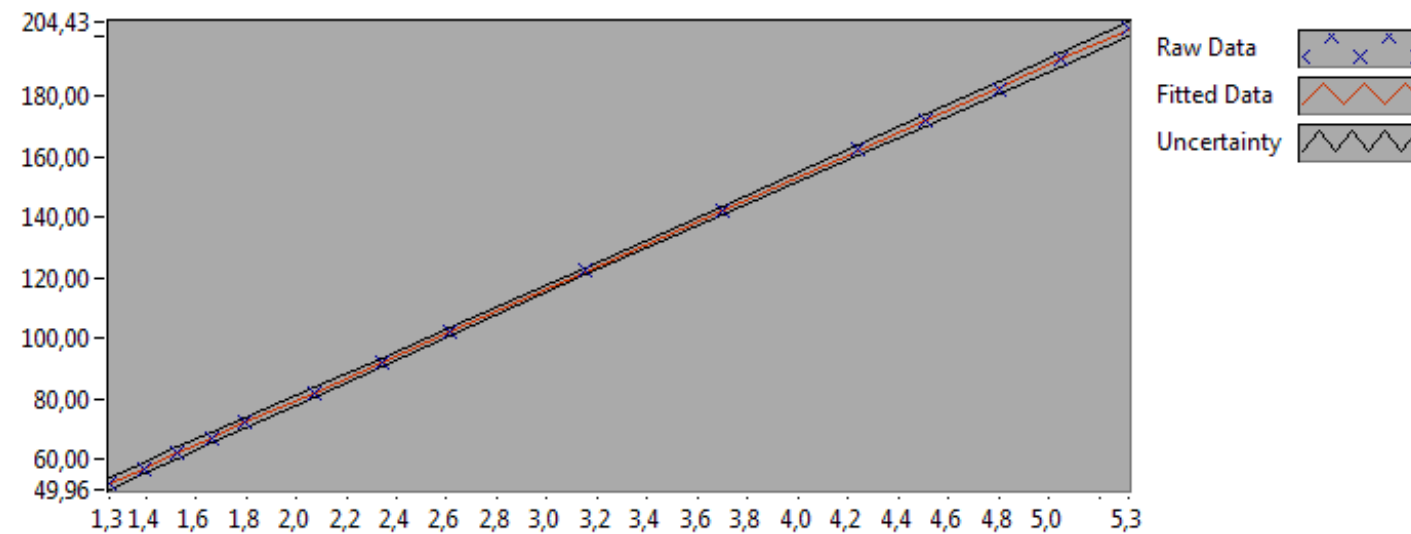RSQ   : 0,999978
Calibration points : 15
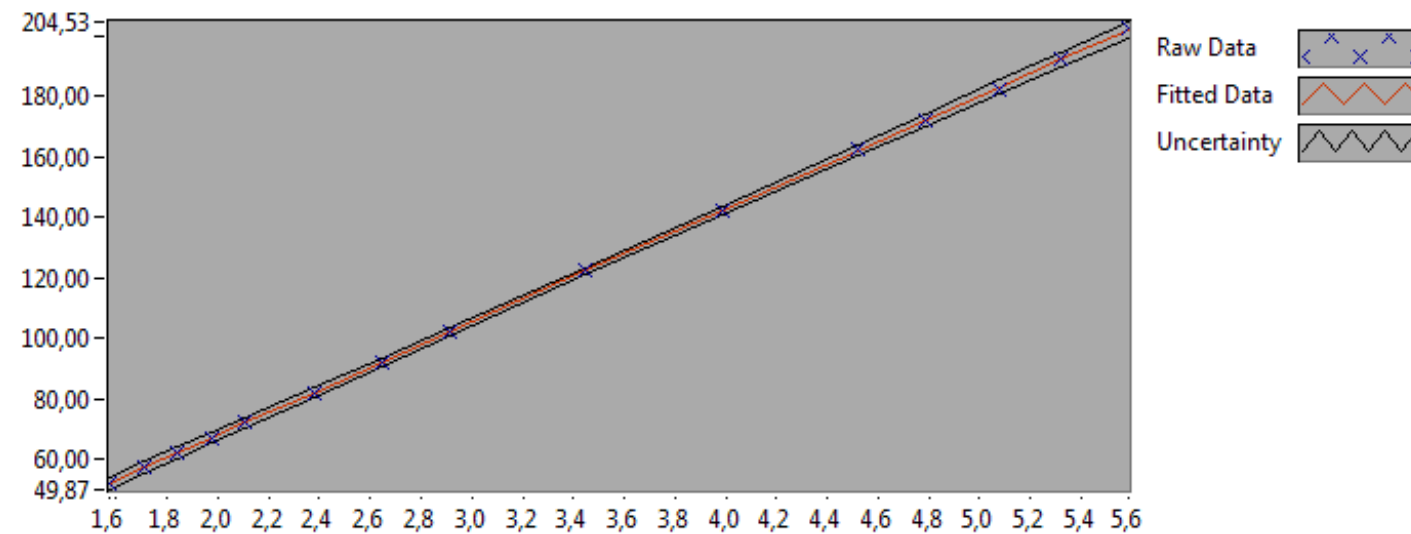
Figure 1 : Calibration chart (The uncertainty band is multiplied by 10)

Katarina Kloster

CALIBRATION VALUES

Value [kPa]	Voltage [V]	Best Poly Fit [kPa]	Deviation [kPa]	Uncertainty [%]	Uncertainty [kPa]
52,024465	1,573476	52,022183	0,002281	0,412824	0,214769
57,032018	1,707366	57,026649	0,005369	0,359201	0,204860
62,039572	1,841416	62,037098	0,002473	0,314763	0,195277
67,047125	1,975587	67,052056	-0,004930	0,277559	0,186095
72,054679	2,109498	72,057322	-0,002643	0,246191	0,177392
82,069786	2,377531	82,075730	-0,005944	0,196966	0,161649
92,084893	2,645303	92,084357	0,000536	0,161537	0,148751
102,100000	2,913199	102,097618	0,002382	0,136593	0,139461
122,130214	3,448776	122,116143	0,014071	0,110093	0,134457
142,160428	3,983703	142,110359	0,050069	0,104357	0,148355
162,190643	4,517960	162,079517	0,111125	0,109034	0,176843
172,205750	4,784111	172,027565	0,178184	0,113004	0,194600
182,220857	5,079663	183,074541	-0,853684	0,118517	0,215962
192,235964	5,318855	192,014942	0,221022	0,121911	0,234357
202,251071	5,585231	201,971383	0,279688	0,126473	0,255793

COMMENTS:

The uncertainty is calculated with 95% confidence. The uncertainty includes the randomness in the calibrated instrument during the calibration, systematic uncertainty in the instrument or property which the instrument under calibration is compared with (dead weight manometer, calibrated weights etc.), and due to regression analysis to fit the calibration points to a linear calibration equation.The calculated uncertainty can be used as the total systematic uncertianty of the calibrated instrument with the given calibration equation.

CALIBRATION REPORT

CALIBRATION PROPERTIES
Calibrated by: Katarina Kloster
Type/Producer: Kulite XTM-190SM
SN: 8317-1-202
Range: 0-3,5 bar a
Unit: kPa

CALIBRATION SOURCE PROPERTIES
Type/Producer: Pressurements deadweight tester P3223-1
SN: 66256
Uncertainty [%]: 0,01

POLY FIT EQUATION:
Y= + 5,63531073E+0X^0 + 36,92939840E+0X^1

CALIBRATION SUMARY:
Max Uncertainty   : 0,397652 [%]
Max Uncertainty   : 0,246463 [kPa]
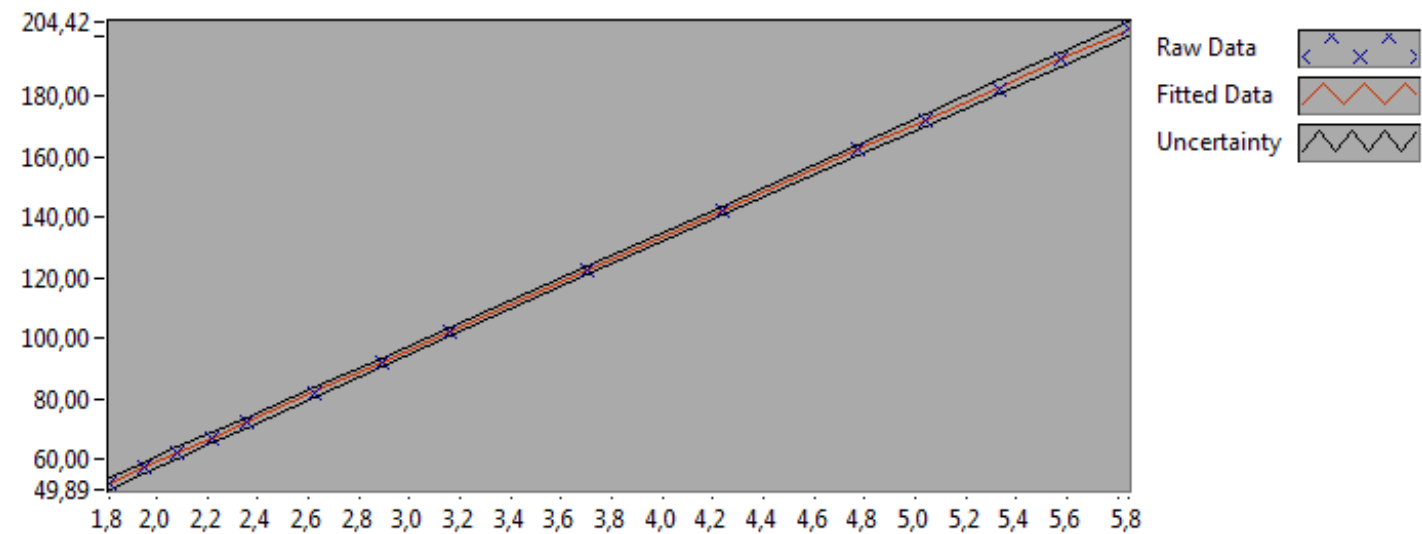RSQ   : 0,999979
Calibration points : 15

Figure 1 : Calibration chart (The uncertainty band is multiplied by 10)

Katarina Kloster

CALIBRATION VALUES

Value [kPa]	Voltage [V]	Best Poly Fit [kPa]	Deviation [kPa]	Uncertainty [%]	Uncertainty [kPa]
52,024465	1,256370	52,032286	-0,007822	0,397652	0,206876
57,032018	1,391836	57,034973	-0,002955	0,346012	0,197338
62,039572	1,527381	62,040570	-0,000998	0,303218	0,188115
67,047125	1,662928	67,046244	0,000881	0,267408	0,179289
72,054679	1,798475	72,051911	0,002768	0,237190	0,170906
82,069786	2,069613	82,064873	0,004913	0,189777	0,155750
92,084893	2,340708	92,076251	0,008641	0,155644	0,143324
102,100000	2,611900	102,091213	0,008787	0,131613	0,134377
122,130214	3,154053	122,112587	0,017627	0,106088	0,129565
142,160428	3,695751	142,117161	0,043267	0,100571	0,142972
162,190643	4,236547	162,088431	0,102212	0,105101	0,170464
172,205750	4,506808	172,069010	0,136739	0,108910	0,187550
182,220857	4,803963	183,042758	-0,821901	0,114162	0,208028
192,235964	5,046814	192,011100	0,224864	0,117468	0,225815
202,251071	5,316436	201,968094	0,282976	0,121860	0,246463

COMMENTS:

The uncertainty is calculated with 95% confidence. The uncertainty includes the randomness in the calibrated instrument during the calibration, systematic uncertainty in the instrument or property which the instrument under calibration is compared with (dead weight manometer, calibrated weights etc.), and due to regression analysis to fit the calibration points to a linear calibration equation. The calculated uncertainty can be used as the total systematic uncertianty of the calibrated instrument with the given calibration equation.

CALIBRATION REPORT

CALIBRATION PROPERTIES
Calibrated by: Katarina Kloster
Type/Producer: Kulite XTM-190SM
SN: 8317-1-203
Range: 0-3,5 bar a
Unit: kPa

CALIBRATION SOURCE PROPERTIES
Type/Producer: Pressurements deadweight tester P3223-1
SN: 66256
Uncertainty [%]: 0,01

POLY FIT EQUATION:
$Y= -15,59293487E+0X^0 + 37,22867417E+0X^1$

CALIBRATION SUMARY:
Max Uncertainty   : 0,398919 [%]
Max Uncertainty   : 0,247063 [kPa]
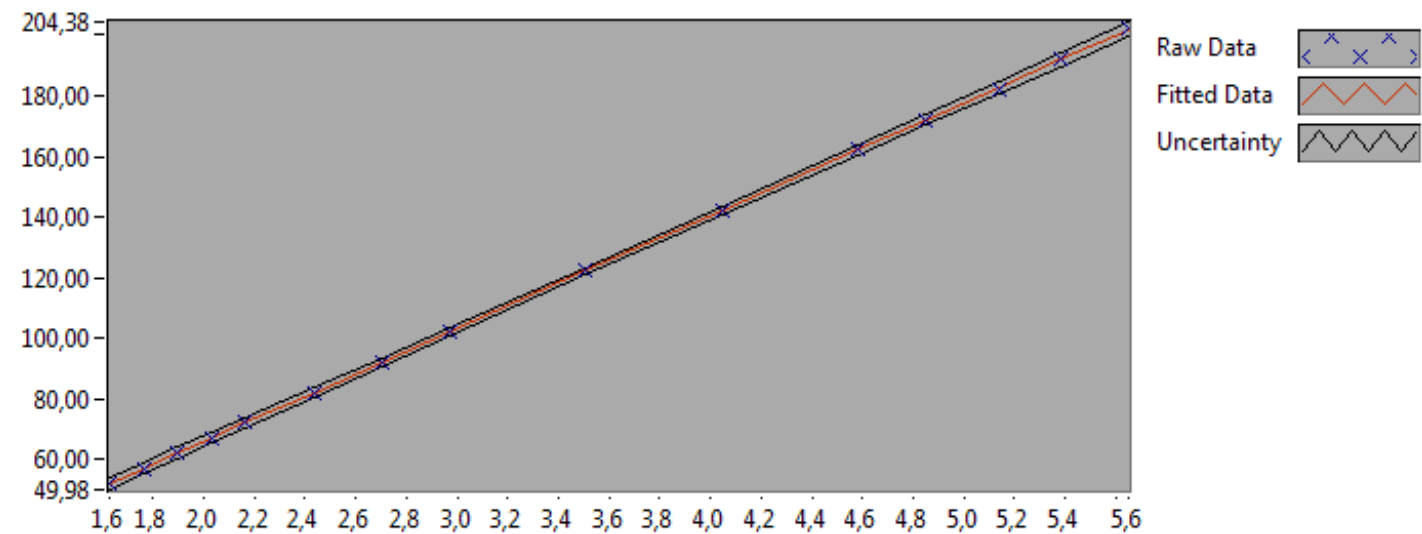RSQ   : 0,999979
Calibration points : 15

Figure 1 : Calibration chart (The uncertainty band is multiplied by 10)

Katarina Kloster

CALIBRATION VALUES

Value [kPa]	Voltage [V]	Best Poly Fit [kPa]	Deviation [kPa]	Uncertainty [%]	Uncertainty [kPa]
52,024465	1,814818	51,970319	0,054146	0,398919	0,207535
57,032018	1,950244	57,012067	0,019951	0,346983	0,197892
62,039572	2,085131	62,033734	0,005838	0,304028	0,188618
67,047125	2,219728	67,044592	0,002533	0,268106	0,179757
72,054679	2,354344	72,056172	-0,001493	0,237794	0,171342
82,069786	2,623907	82,091649	-0,021863	0,190226	0,156118
92,084893	2,893109	92,113675	-0,028782	0,156004	0,143656
102,100000	3,161908	102,120721	-0,020721	0,131935	0,134706
122,130214	3,699622	122,139075	-0,008861	0,106367	0,129906
142,160428	4,236823	142,138375	0,022054	0,100845	0,143362
162,190643	4,773052	162,101471	0,089172	0,105357	0,170880
172,205750	5,040319	172,051455	0,154295	0,109149	0,187961
182,220857	5,335225	183,030432	-0,809576	0,114433	0,208520
192,235964	5,575989	191,993727	0,242237	0,117751	0,226360
202,251071	5,843424	201,950000	0,301071	0,122156	0,247063

COMMENTS:

The uncertainty is calculated with 95% confidence. The uncertainty includes the randomness in the calibrated instrument during the calibration, systematic uncertainty in the instrument or property which the instrument under calibration is compared with (dead weight manometer, calibrated weights etc.), and due to regression analysis to fit the calibration points to a linear calibration equation.The calculated uncertainty can be used as the total systematic uncertianty of the calibrated instrument with the given calibration equation.

CALIBRATION REPORT

CALIBRATION PROPERTIES
Calibrated by: Katarina Kloster
Type/Producer: Kulite XTM-190SM
SN: 8317-1-204
Range: 0-3,5bar a
Unit: kPa

CALIBRATION SOURCE PROPERTIES
Type/Producer: Pressurements deadweight tester P3223-1
SN: 66256
Uncertainty [%]: 0,01

POLY FIT EQUATION:
Y= -8,69549532E+0X^0 + 37,28439544E+0X^1

CALIBRATION SUMARY:
Max Uncertainty   : 0,390050 [%]
Max Uncertainty   : 0,241706 [kPa]
RSQ   : 0,999980
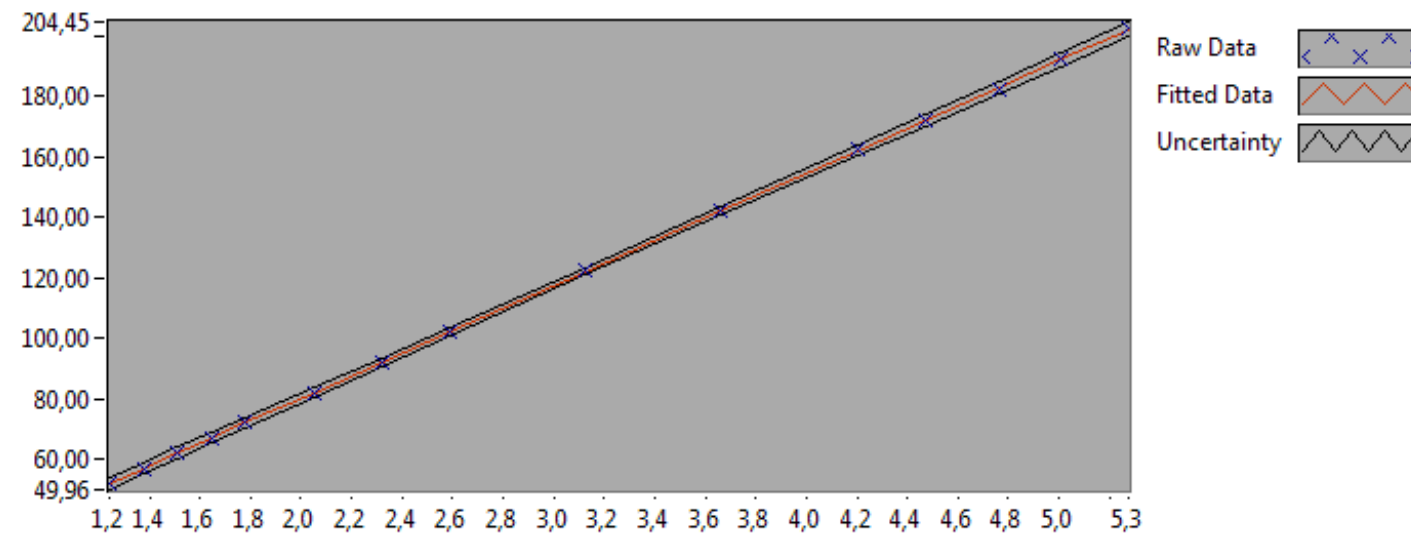Calibration points : 15

Figure 1 : Calibration chart (The uncertainty band is multiplied by 10)

Katarina Kloster

CALIBRATION VALUES

Value [kPa]	Voltage [V]	Best Poly Fit [kPa]	Deviation [kPa]	Uncertainty [%]	Uncertainty [kPa]
52,024465	1,628072	52,006172	0,018293	0,390050	0,202922
57,032018	1,762727	57,026725	0,005293	0,339339	0,193532
62,039572	1,897090	62,036351	0,003221	0,297364	0,184483
67,047125	2,031375	67,043106	0,004019	0,262243	0,175826
72,054679	2,165738	72,052747	0,001932	0,232601	0,167600
82,069786	2,434635	82,078403	-0,008617	0,186090	0,152724
92,084893	2,703210	92,092051	-0,007158	0,152624	0,140544
102,100000	2,971733	102,103759	-0,003759	0,129071	0,131782
122,130214	3,508752	122,126199	0,004015	0,104054	0,127082
142,160428	4,044996	142,119741	0,040688	0,098644	0,140233
162,190643	4,580491	162,085326	0,105317	0,103065	0,167162
172,205750	4,848974	172,095584	0,110166	0,106921	0,184124
182,220857	5,142000	183,020852	-0,799995	0,111955	0,204006
192,235964	5,382836	192,000301	0,235662	0,115197	0,221450
202,251071	5,649968	201,960148	0,290923	0,119508	0,241706

COMMENTS:

_____

The uncertainty is calculated with 95% confidence. The uncertainty includes the randomness in the calibrated instrument during the calibration, systematic uncertainty in the instrument or property which the instrument under calibration is compared with (dead weight manometer, calibrated weights etc.), and due to regression analysis to fit the calibration points to a linear calibration equation.The calculated uncertainty can be used as the total systematic uncertianty of the calibrated instrument with the given calibration equation.

CALIBRATION REPORT

CALIBRATION PROPERTIES
Calibrated by: Katarina Kloster
Type/Producer: Kulite XTM-190SM
SN: 8317-1-205
Range: 0-3,5 bar a
Unit: kPa

CALIBRATION SOURCE PROPERTIES
Type/Producer: Pressurements deadweight tester P3223-1
SN: 66256
Uncertainty [%]: 0,01

POLY FIT EQUATION:
$Y = +5{,}87661454E{+}0X^0 + 37{,}17518896E{+}0X^1$

CALIBRATION SUMARY:
Max Uncertainty   : 0,397164 [%]
Max Uncertainty   : 0,246198 [kPa]
RSQ   : 0,999979
Calibration points : 15

Figure 1 : Calibration chart (The uncertainty band is multiplied by 10)

Katarina Kloster

CALIBRATION VALUES

Value [kPa]	Voltage [V]	Best Poly Fit [kPa]	Deviation [kPa]	Uncertainty [%]	Uncertainty [kPa]
52,024465	1,241435	52,027208	-0,002744	0,397164	0,206623
57,032018	1,376092	57,033111	-0,001093	0,345577	0,197090
62,039572	1,510832	62,042062	-0,002491	0,302827	0,187873
67,047125	1,645553	67,050344	-0,003219	0,267057	0,179054
72,054679	1,780273	72,058608	-0,003929	0,236873	0,170678
82,069786	2,049690	82,074230	-0,004445	0,189520	0,155539
92,084893	2,318990	92,085523	-0,000630	0,155435	0,143132
102,100000	2,588248	102,095209	0,004791	0,131444	0,134204
122,130214	3,126414	122,101637	0,028577	0,105952	0,129399
142,160428	3,664240	142,095420	0,065008	0,100428	0,142769
162,190643	4,201565	162,070604	0,120038	0,104951	0,170221
172,205750	4,470140	172,054923	0,150827	0,108760	0,187292
182,220857	4,765781	183,045421	-0,824565	0,114021	0,207770
192,235964	5,007269	192,022798	0,213165	0,117331	0,225553
202,251071	5,275393	201,990363	0,260708	0,121729	0,246198

COMMENTS:

The uncertainty is calculated with 95% confidence. The uncertainty includes the randomness in the calibrated instrument during the calibration, systematic uncertainty in the instrument or property which the instrument under calibration is compared with (dead weight manometer, calibrated weights etc.), and due to regression analysis to fit the calibration points to a linear calibration equation.The calculated uncertainty can be used as the total systematic uncertianty of the calibrated instrument with the given calibration equation.

CALIBRATION REPORT

CALIBRATION PROPERTIES
Calibrated by: Katarina Kloster
Type/Producer: Kulite
SN: V4537-34
Range: 0-10 bar a
Unit: kPa

CALIBRATION SOURCE PROPERTIES
Type/Producer: Pressurements deadweight tester P3023-6-P
SN: 66611
Uncertainty [%]: 0,008

POLY FIT EQUATION:
Y= + 98,86246121E+0X^0 -70,35007630E+3X^1

CALIBRATION SUMARY:
Max Uncertainty   : 0,039565 [%]
Max Uncertainty   : 0,029554 [kPa]
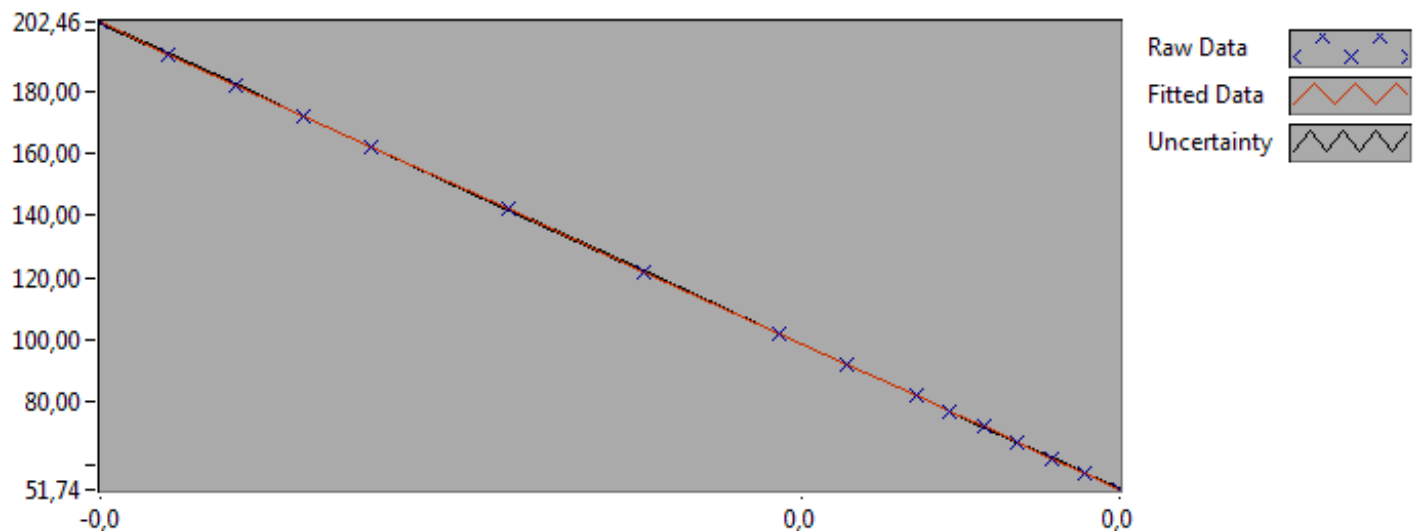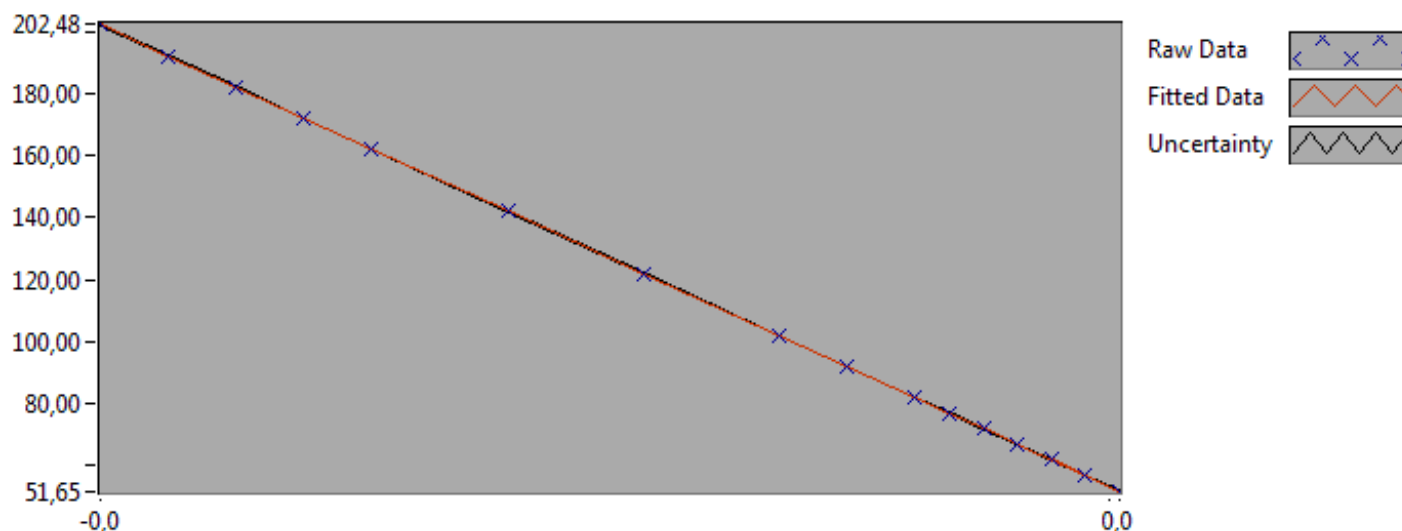RSQ   : 1,000000
Calibration points : 16

Figure 1 : Calibration chart (The uncertainty band is multiplied by 10)

Katarina Kloster

CALIBRATION VALUES

Value [kPa]	Voltage [V]	Best Poly Fit [kPa]	Deviation [kPa]	Uncertainty [%]	Uncertainty [kPa]
51,954465	0,000667	51,945614	0,008851	0,039565	0,020556
56,962018	0,000596	56,961839	0,000179	0,034545	0,019677
61,969572	0,000525	61,963083	0,006489	0,030565	0,018941
66,977125	0,000453	66,976076	0,001049	0,027085	0,018141
71,984679	0,000382	71,985625	-0,000946	0,024602	0,017709
76,992232	0,000311	76,994447	-0,002215	0,023104	0,017788
81,999786	0,000240	81,999547	0,000239	0,020736	0,017004
92,014893	0,000097	92,016276	-0,001383	0,017514	0,016115
102,030000	-0,000045	102,031898	-0,001898	0,015502	0,015816
122,060214	-0,000330	122,071054	-0,010840	0,013133	0,016030
142,090428	-0,000615	142,099123	-0,008695	0,013976	0,019858
162,120643	-0,000899	162,128092	-0,007450	0,015579	0,025257
172,135750	-0,001042	172,139068	-0,003318	0,013677	0,023543
182,150857	-0,001184	182,149320	0,001536	0,013885	0,025292
192,165964	-0,001326	192,159500	0,006464	0,014314	0,027506
202,181071	-0,001468	202,169133	0,011937	0,014618	0,029554

COMMENTS:

The uncertainty is calculated with 95% confidence. The uncertainty includes the randomness in the calibrated instrument during the calibration, systematic uncertainty in the instrument or property which the instrument under calibration is compared with (dead weight manometer, calibrated weights etc.), and due to regression analysis to fit the calibration points to a linear calibration equation.The calculated uncertainty can be used as the total systematic uncertianty of the calibrated instrument with the given calibration equation.

CALIBRATION REPORT

CALIBRATION PROPERTIES
Calibrated by: Einar Agnalt and Katarina Kloster
Type/Producer: Kulite
SN: V4537-33
Range: 0-10 bar a
Unit: kPa

CALIBRATION SOURCE PROPERTIES
Type/Producer: Pressurements deadweight tester P3023-6-P
SN: 66611
Uncertainty [%]: 0,008

POLY FIT EQUATION:
Y= + 53,37801232E+0X^0 -77,26353937E+3X^1

CALIBRATION SUMARY:
Max Uncertainty   : 0,052726 [%]
Max Uncertainty   : 0,030448 [kPa]
RSQ   : 1,000000
Calibration points : 16

Figure 1 : Calibration chart (The uncertainty band is multiplied by 10)

Einar Agnalt

CALIBRATION VALUES

Value [kPa]	Voltage [V]	Best Poly Fit [kPa]	Deviation [kPa]	Uncertainty [%]	Uncertainty [kPa]
51,954465	0,000019	51,919861	0,034604	0,052726	0,027393
61,969572	-0,000111	61,942501	0,027070	0,031512	0,019528
56,962018	-0,000047	56,971794	-0,009776	0,037707	0,021479
66,977125	-0,000176	66,967565	0,009560	0,027897	0,018685
71,984679	-0,000241	71,996309	-0,011631	0,024981	0,017983
76,992232	-0,000306	77,016601	-0,024369	0,022538	0,017353
81,999786	-0,000371	82,016920	-0,017134	0,020525	0,016831
92,014893	-0,000500	92,024780	-0,009887	0,017451	0,016058
102,030000	-0,000630	102,024453	0,005547	0,015408	0,015721
122,060214	-0,000889	122,077012	-0,016797	0,013541	0,016528
142,090428	-0,001148	142,099463	-0,009035	0,014582	0,020720
162,120643	-0,001407	162,121678	-0,001035	0,013619	0,022079
172,135750	-0,001537	172,134553	0,001196	0,013961	0,024033
182,150857	-0,001667	182,147625	0,003231	0,014328	0,026098
192,165964	-0,001796	192,154310	0,011654	0,014900	0,028633
202,181071	-0,001926	202,174270	0,006801	0,015060	0,030448

COMMENTS:

The uncertainty is calculated with 95% confidence. The uncertainty includes the randomness in the calibrated instrument during the calibration, systematic uncertainty in the instrument or property which the instrument under calibration is compared with (dead weight manometer, calibrated weights etc.), and due to regression analysis to fit the calibration points to a linear calibration equation.The calculated uncertainty can be used as the total systematic uncertianty of the calibrated instrument with the given calibration equation.

CALIBRATION REPORT

CALIBRATION PROPERTIES
Calibrated by: Katarina Kloster and Ingebjørg Valkvæ
Type/Producer: Kulite HKM-375M
SN: 8240-4-887
Range: 0-1.7 bar a
Unit: kPa

CALIBRATION SOURCE PROPERTIES
Type/Producer: Pressurements deadweight tester P3023-6-P
SN: 66611
Uncertainty [%]: 0,008

POLY FIT EQUATION:
Y= -4.25163513E+0X^0 + 22.85839685E+3X^1

CALIBRATION SUMARY:
Max Uncertainty   : 0.048805 [%]
Max Uncertainty   : 0.047047 [kPa]
RSQ   : 1.000000
Calibration points : 15
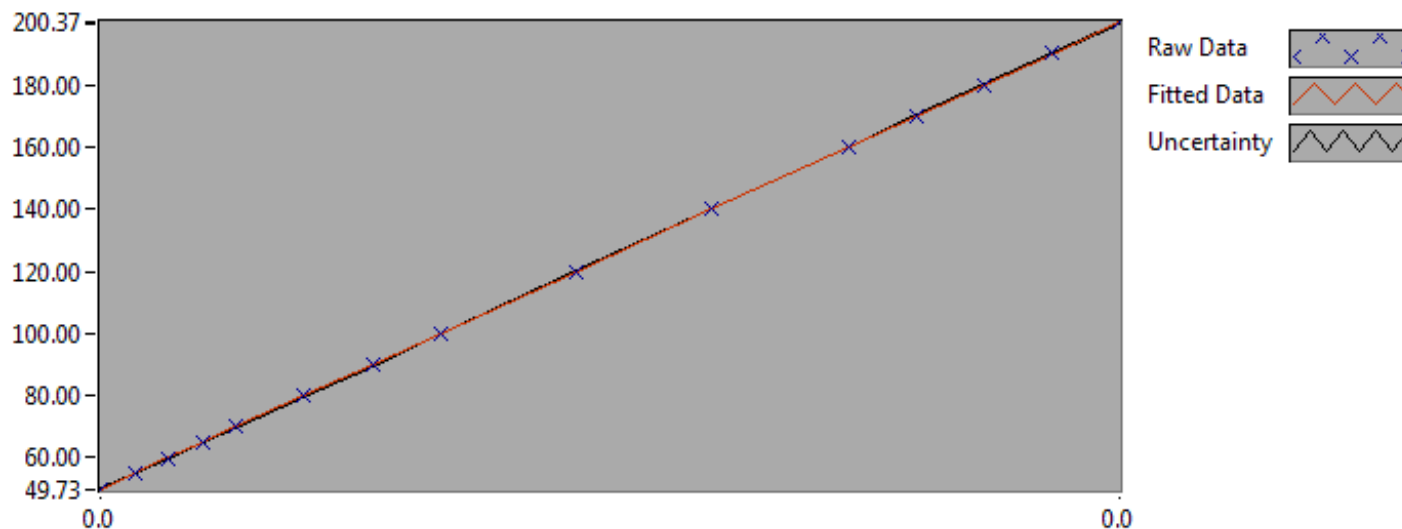
Figure 1 : Calibration chart (The uncertainty band is multiplied by 10)

Katarina Kloster and Ingebjørg Valkvæ

CALIBRATION VALUES

Value [kPa]	Voltage [V]	Best Poly Fit [kPa]	Deviation [kPa]	Uncertainty [%]	Uncertainty [kPa]
49.924465	0.002370	49.923452	0.001012	0.038917	0.019429
54.932018	0.002589	54.927796	0.004222	0.033517	0.018412
59.939572	0.002810	59.978672	-0.039100	0.048805	0.029253
64.947125	0.003027	64.940910	0.006215	0.025936	0.016845
69.954679	0.003245	69.933418	0.021261	0.021804	0.015253
79.969786	0.003683	79.944248	0.025538	0.022136	0.017702
89.984893	0.004122	89.979020	0.005873	0.038883	0.034989
100.000000	0.004560	99.989738	0.010262	0.011933	0.011933
120.030214	0.005437	120.039231	-0.009017	0.009671	0.011608
140.060428	0.006314	140.082665	-0.022237	0.011533	0.016153
160.090643	0.007191	160.120424	-0.029781	0.016164	0.025877
170.105750	0.007628	170.123544	-0.017795	0.027658	0.047047
180.120857	0.008066	180.119551	0.001306	0.024571	0.044258
190.135964	0.008503	190.124050	0.011914	0.012618	0.023991
200.151071	0.008941	200.120744	0.030327	0.012288	0.024594

COMMENTS:

The uncertainty is calculated with 95% confidence. The uncertainty includes the randomness in the calibrated instrument during the calibration, systematic uncertainty in the instrument or property which the instrument under calibration is compared with (dead weight manometer, calibrated weights etc.), and due to regression analysis to fit the calibration points to a linear calibration equation.The calculated uncertainty can be used as the total systematic uncertianty of the calibrated instrument with the given calibration equation.

CALIBRATION REPORT

CALIBRATION PROPERTIES
Calibrated by: Katarina Kloster and Ingebjørg Valkvæ
Type/Producer: Kulite HKM-375M
SN: 8240-4-888
Range: 0-1.7 bar a
Unit: kPa

CALIBRATION SOURCE PROPERTIES
Type/Producer: Pressurements deadweight tester P3023-6-P
SN: 66611
Uncertainty [%]: 0,008

POLY FIT EQUATION:
Y= + 230.02390217E-3X^0 + 22.55034497E+3X^1

CALIBRATION SUMARY:
Max Uncertainty   : 0.194185 [%]
Max Uncertainty   : 0.221837 [kPa]
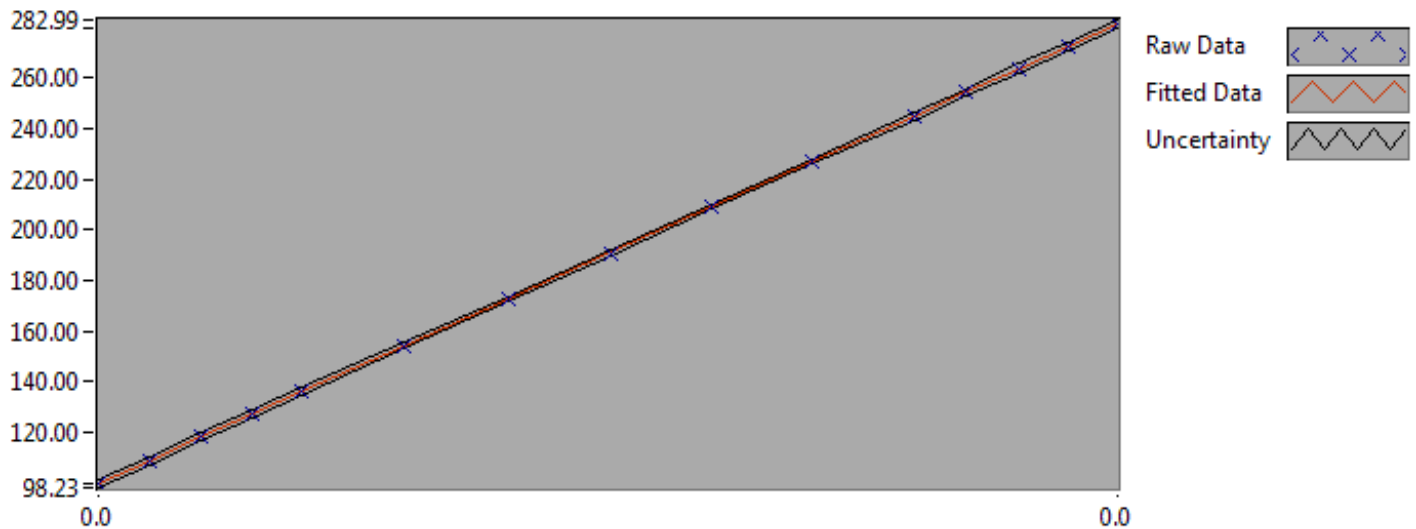RSQ   : 0.999991
Calibration points : 15

Figure 1 : Calibration chart (The uncertainty band is multiplied by 10)

Katarina Kloster and Ingebjørg Valkvæ

CALIBRATION VALUES

Value [kPa]	Voltage [V]	Best Poly Fit [kPa]	Deviation [kPa]	Uncertainty [%]	Uncertainty [kPa]
100.000000	0.004422	99.947240	0.052760	0.194185	0.194185
110.015107	0.004868	110.002871	0.012236	0.164734	0.181233
120.030214	0.005313	120.051003	-0.020789	0.140486	0.168626
130.045321	0.005753	129.962240	0.083081	0.121674	0.158232
140.060428	0.006196	139.948236	0.112193	0.107029	0.149906
160.090643	0.007084	159.966808	0.123835	0.087311	0.139776
180.120857	0.007987	180.332795	-0.211938	0.069897	0.125899
200.151071	0.008875	200.374684	-0.223613	0.060147	0.120385
220.181285	0.009764	220.401110	-0.219825	0.051930	0.114340
240.211499	0.010638	240.128541	0.082958	0.052992	0.127294
260.241714	0.011522	260.050969	0.190744	0.071828	0.186926
270.256821	0.011970	270.157619	0.099202	0.059701	0.161345
280.271928	0.012439	280.722866	-0.450939	0.079151	0.221837
290.287035	0.012864	290.320206	-0.033171	0.070310	0.204100
300.302142	0.013289	299.898876	0.403266	0.064545	0.193829

COMMENTS:

The uncertainty is calculated with 95% confidence. The uncertainty includes the randomness in the calibrated instrument during the calibration, systematic uncertainty in the instrument or property which the instrument under calibration is compared with (dead weight manometer, calibrated weights etc.), and due to regression analysis to fit the calibration points to a linear calibration equation.The calculated uncertainty can be used as the total systematic uncertianty of the calibrated instrument with the given calibration equation.

CALIBRATION REPORT

CALIBRATION PROPERTIES
Calibrated by: Katarina Kloster and Ingebjørg Valkvæ
Type/Producer: Kulite HKM-375M
SN: 8240-4-889
Range: 0-1.7 bar a
Unit: kPa

CALIBRATION SOURCE PROPERTIES
Type/Producer: Pressurements deadweight tester P3023-6-P
SN: 66611
Uncertainty [%]: 0,008

POLY FIT EQUATION:
Y= -353.89720757E-3X^0 + 22.60988576E+3X^1

CALIBRATION SUMARY:
Max Uncertainty   : 0.214530 [%]
Max Uncertainty   : 0.235110 [kPa]
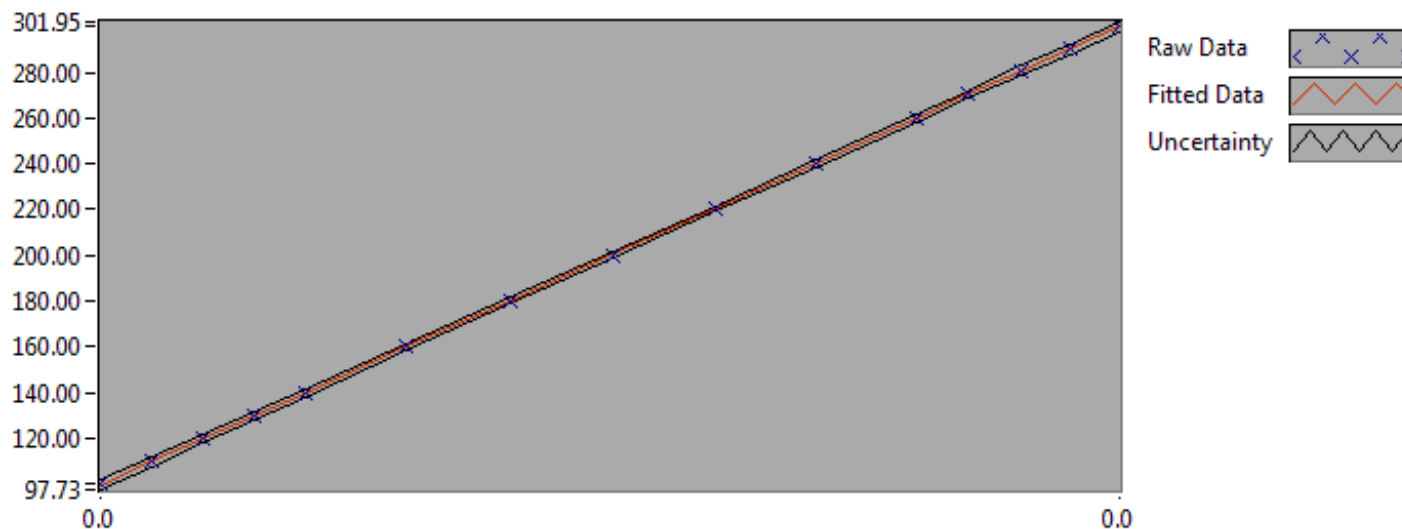RSQ   : 0.999989
Calibration points : 15

Figure 1 : Calibration chart (The uncertainty band is multiplied by 10)

Katarina Kloster and Ingebjørg Valkvæ

CALIBRATION VALUES

Value [kPa]	Voltage [V]	Best Poly Fit [kPa]	Deviation [kPa]	Uncertainty [%]	Uncertainty [kPa]
100.000000	0.004433	99.874824	0.125176	0.214530	0.214530
110.015107	0.004879	109.952849	0.062258	0.181942	0.200164
120.030214	0.005324	120.023979	0.006235	0.155147	0.186223
130.045321	0.005763	129.954830	0.090491	0.134161	0.174470
140.060428	0.006206	139.958848	0.101580	0.117595	0.164704
160.090643	0.007093	160.008765	0.081877	0.094836	0.151824
180.120857	0.007994	180.395812	-0.274955	0.075875	0.136667
200.151071	0.008881	200.445983	-0.294912	0.065345	0.130788
220.181285	0.009767	220.468187	-0.286902	0.057344	0.126261
240.211499	0.010638	240.180414	0.031086	0.058494	0.140510
260.241714	0.011518	260.064219	0.177495	0.076289	0.198535
270.256821	0.011964	270.158684	0.098137	0.065569	0.177204
280.271928	0.012430	280.697295	-0.425367	0.083886	0.235110
290.287035	0.012854	290.266954	0.020081	0.076055	0.220778
300.302142	0.013276	299.814421	0.487721	0.071215	0.213860

COMMENTS:

The uncertainty is calculated with 95% confidence. The uncertainty includes the randomness in the calibrated instrument during the calibration, systematic uncertainty in the instrument or property which the instrument under calibration is compared with (dead weight manometer, calibrated weights etc.), and due to regression analysis to fit the calibration points to a linear calibration equation.The calculated uncertainty can be used as the total systematic uncertianty of the calibrated instrument with the given calibration equation.

CALIBRATION REPORT

CALIBRATION PROPERTIES
Calibrated by: Rakel Ellingsen
Type/Producer: Krohne Optiflux
SN: xxxxxx
Range: 0 - 450 l/s
Unit: l/s

CALIBRATION SOURCE PROPERTIES
Type/Producer: Weighing method
SN: xxxxx
Uncertainty [%]: 0

POLY FIT EQUATION:
$Y = -147.80000000E\text{-}3X^0 + 73.95900000E\text{-}3X^1$

CALIBRATION SUMARY:
Max Uncertainty   : 0.056734 [%]
Max Uncertainty   : 0.000201 [l/s]
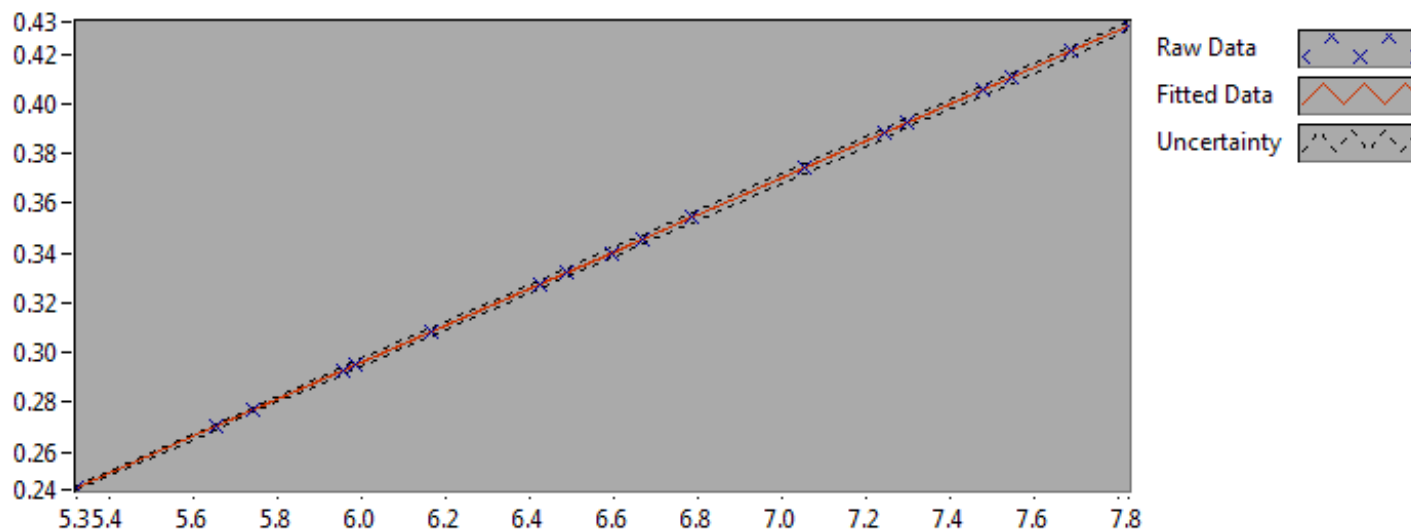RSQ   : 1.000000
Calibration points : 18

Figure 1 : Calibration chart (The uncertainty band is multiplied by 10)

Rakel Ellingsen

CALIBRATION VALUES

Value [l/s]	Voltage [V]	Best Poly Fit [l/s]	Deviation [l/s]	Uncertainty [%]	Uncertainty [l/s]
0.245718	5.320763	0.245718	0.000000	0.033218	0.000082
0.276933	5.742822	0.276933	0.000000	0.040414	0.000112
0.294971	5.986709	0.294971	0.000000	0.050470	0.000149
0.332043	6.487957	0.332043	0.000000	0.048292	0.000160
0.345482	6.669667	0.345482	0.000000	0.055743	0.000193
0.374027	7.055631	0.374027	0.000000	0.050539	0.000189
0.388063	7.245409	0.388063	0.000000	0.048331	0.000188
0.392152	7.300698	0.392152	0.000000	0.043560	0.000171
0.405216	7.477328	0.405216	0.000000	0.046113	0.000187
0.431016	7.826172	0.431016	0.000000	0.041826	0.000180
0.420916	7.689607	0.420916	0.000000	0.041396	0.000174
0.410390	7.547291	0.410390	0.000000	0.046184	0.000190
0.308215	6.165786	0.308215	0.000000	0.049692	0.000153
0.270213	5.651954	0.270213	0.000000	0.040581	0.000110
0.292572	5.954272	0.292572	0.000000	0.047872	0.000140
0.327318	6.424069	0.327318	0.000000	0.047770	0.000156
0.340066	6.596432	0.340066	0.000000	0.051606	0.000175
0.354110	6.786332	0.354110	0.000000	0.056734	0.000201

COMMENTS:

The uncertainty is calculated with 95% confidence. The uncertainty includes the randomness in the calibrated instrument during the calibration, systematic uncertainty in the instrument or property which the instrument under calibration is compared with (dead weight manometer, calibrated weights etc.), and due to regression analysis to fit the calibration points to a linear calibration equation.The calculated uncertainty can be used as the total systematic uncertianty of the calibrated instrument with the given calibration equation.

CALIBRATION REPORT

CALIBRATION PROPERTIES
Calibrated by: Ingebjørg Valkvæ and Rakel Ellingsen
Type/Producer: HBM something
SN: -
Range: -
Unit: Nm

CALIBRATION SOURCE PROPERTIES
Type/Producer: Calibrated Weights
SN: -
Uncertainty [%]: -

POLY FIT EQUATION:
Y= -198.37672571E+0X^0 + 485.75593382E+0X^1

CALIBRATION SUMARY:
Max Uncertainty   : Inf [%]
Max Uncertainty   : 0.637684 [Nm]
RSQ   : 0.999996
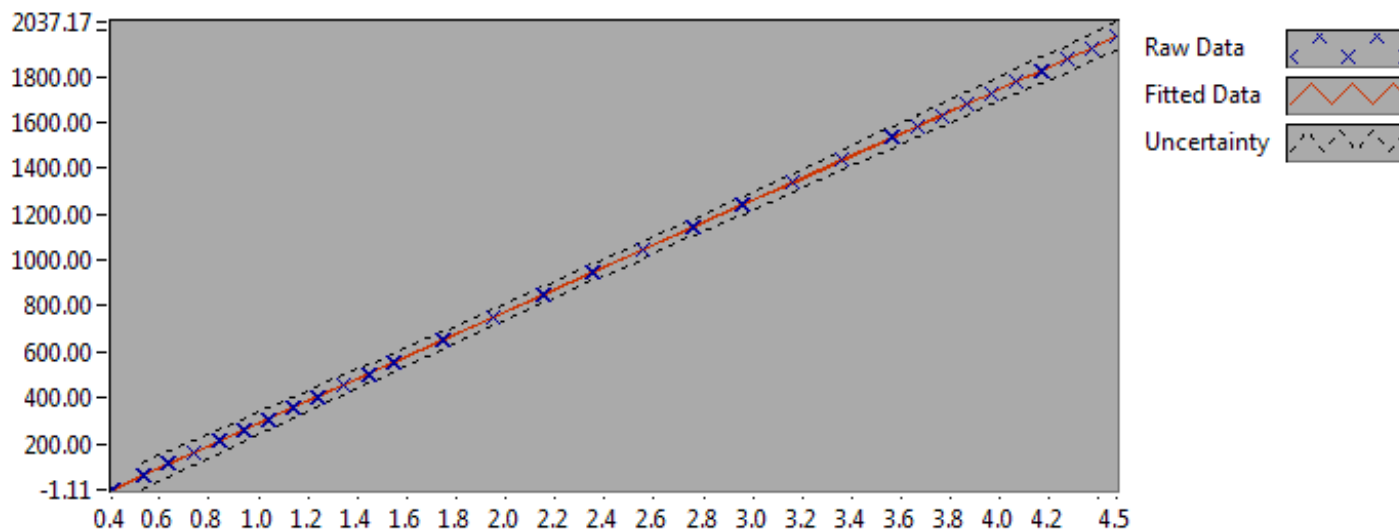Calibration points : 62

Figure 1 : Calibration chart (The uncertainty band is multiplied by 100)

Ingebjørg Valkvæ and Rakel Ellingsen

CALIBRATION VALUES

Value [Nm]	Voltage [V]	Best Poly Fit [Nm]	Deviation [Nm]	Uncertainty [%]	Uncertainty [Nm]
0.000000	0.411103	1.319023	-1.319023	Inf	NaN
62.232086	0.539625	63.749159	-1.517073	0.929771	0.578616
111.240723	0.640597	112.797067	-1.556344	0.501742	0.558142
160.250340	0.741708	161.912364	-1.662024	0.336187	0.538741
209.258194	0.842597	210.919675	-1.661481	0.248674	0.520371
258.261538	0.943763	260.061845	-1.800307	0.194860	0.503247
307.273214	1.044714	309.099399	-1.826185	0.158110	0.485830
356.284694	1.145551	358.081401	-1.796707	0.132369	0.471611
405.299604	1.246641	407.186693	-1.887090	0.112207	0.454773
454.309221	1.347489	456.174269	-1.865048	0.095846	0.435436
503.323837	1.448345	505.165279	-1.841442	0.084157	0.423583
552.336395	1.549544	554.323308	-1.986913	0.073762	0.407414
650.352199	1.751185	652.271704	-1.919505	0.058410	0.379871
748.371532	1.952745	750.180880	-1.809348	0.050309	0.376496
846.387337	2.154160	848.019238	-1.631902	0.041952	0.355073
944.364917	2.355165	945.658887	-1.293971	0.039629	0.374243
1042.362785	2.557232	1043.813654	-1.450869	0.034020	0.354614
1140.346736	2.758217	1141.443401	-1.096665	0.032551	0.371197
1238.333725	2.959519	1239.227173	-0.893447	0.031100	0.385127
1336.313070	3.161170	1337.180384	-0.867314	0.031914	0.426468
1434.288886	3.362508	1434.981264	-0.692378	0.029989	0.430135
1532.265780	3.563903	1532.810460	-0.544680	0.030064	0.460667
1581.255991	3.664348	1581.602213	-0.346222	0.031140	0.492405
1630.244438	3.765170	1630.576824	-0.332386	0.030143	0.491405
1679.242490	3.866613	1679.853679	-0.611189	0.031268	0.525059
1728.229957	3.967118	1728.674297	-0.444340	0.030881	0.533701
1777.218404	4.068064	1777.709732	-0.491328	0.030624	0.544253
1826.214202	4.168683	1826.585763	-0.371561	0.032023	0.584812
1875.209118	4.269352	1875.486411	-0.277293	0.031495	0.590591
1924.201583	4.370276	1924.510718	-0.309135	0.031557	0.607212
1973.202478	4.470917	1973.397523	-0.195045	0.032317	0.637684
1973.202478	4.470766	1973.324330	-0.121852	0.031937	0.630177
1924.201583	4.369343	1924.057608	0.143975	0.031233	0.600980
1875.209118	4.268096	1874.876305	0.332813	0.030948	0.580333
1826.214202	4.167196	1825.863360	0.350842	0.030591	0.558662
1777.218404	4.066122	1776.766192	0.452212	0.030324	0.538930
1728.229957	3.965235	1727.759711	0.470247	0.030017	0.518768
1679.242490	3.864228	1678.695192	0.547298	0.029906	0.502190
1630.244438	3.763146	1629.593776	0.650662	0.029829	0.486286
1581.255991	3.662269	1580.592010	0.663981	0.029979	0.474044
1532.265780	3.561144	1531.469977	0.795803	0.029641	0.454174
1434.288886	3.359278	1433.412434	0.876452	0.029556	0.423914
1336.313070	3.157336	1335.317800	0.995270	0.029309	0.391661

1238.333725	2.955409	1237.230772	1.102953	0.030704	0.380224
1140.346736	2.753641	1139.220844	1.125892	0.031726	0.361786
1042.362785	2.551769	1041.160243	1.202542	0.036705	0.382602
944.364917	2.349533	942.922694	1.442223	0.038492	0.363505
846.387337	2.147558	844.812228	1.575108	0.043139	0.365119
748.371532	1.946166	746.984797	1.386736	0.049893	0.373387
650.352199	1.744142	648.850583	1.501616	0.059170	0.384814
552.336395	1.542244	550.777655	1.558740	0.073122	0.403877
503.323837	1.441143	501.666982	1.656855	0.083338	0.419462
454.309221	1.340170	452.618770	1.690451	0.095829	0.435362
405.299604	1.238995	403.472381	1.827222	0.111528	0.452024
356.284694	1.138218	354.519242	1.765452	0.131296	0.467786
307.273214	1.037151	305.425364	1.847850	0.157712	0.484608
258.261538	0.936187	256.381873	1.879665	0.194413	0.502094
209.258194	0.835114	207.284848	1.973346	0.248944	0.520935
160.250340	0.734295	158.311293	1.939047	0.337082	0.540175
111.240723	0.633552	109.375010	1.865713	0.503007	0.559549
62.232086	0.533018	60.539740	1.692346	0.931124	0.579458
0.000000	0.406109	-1.106755	1.106755	Inf	NaN

COMMENTS:

The uncertainty is calculated with 95% confidence. The uncertainty includes the randomness in the calibrated instrument during the calibration, systematic uncertainty in the instrument or property which the instrument under calibration is compared with (dead weight manometer, calibrated weights etc.), and due to regression analysis to fit the calibration points to a linear calibration equation.The calculated uncertainty can be used as the total systematic uncertianty of the calibrated instrument with the given calibration equation.

CALIBRATION REPORT

CALIBRATION PROPERTIES
Calibrated by: Ingebjørg Valkvæ and Katarina Kloster
Type/Producer: Hottinger Z6FC3
SN: -
Range: 0 - 16
Unit: Nm

CALIBRATION SOURCE PROPERTIES
Type/Producer: Calibrated Weights
SN: -
Uncertainty [%]: -

POLY FIT EQUATION:
Y= -50.08737918E-3X^0 + 3.57294080E+0X^1

CALIBRATION SUMARY:
Max Uncertainty   : 7.311204 [%]
Max Uncertainty   : 0.069267 [Nm]
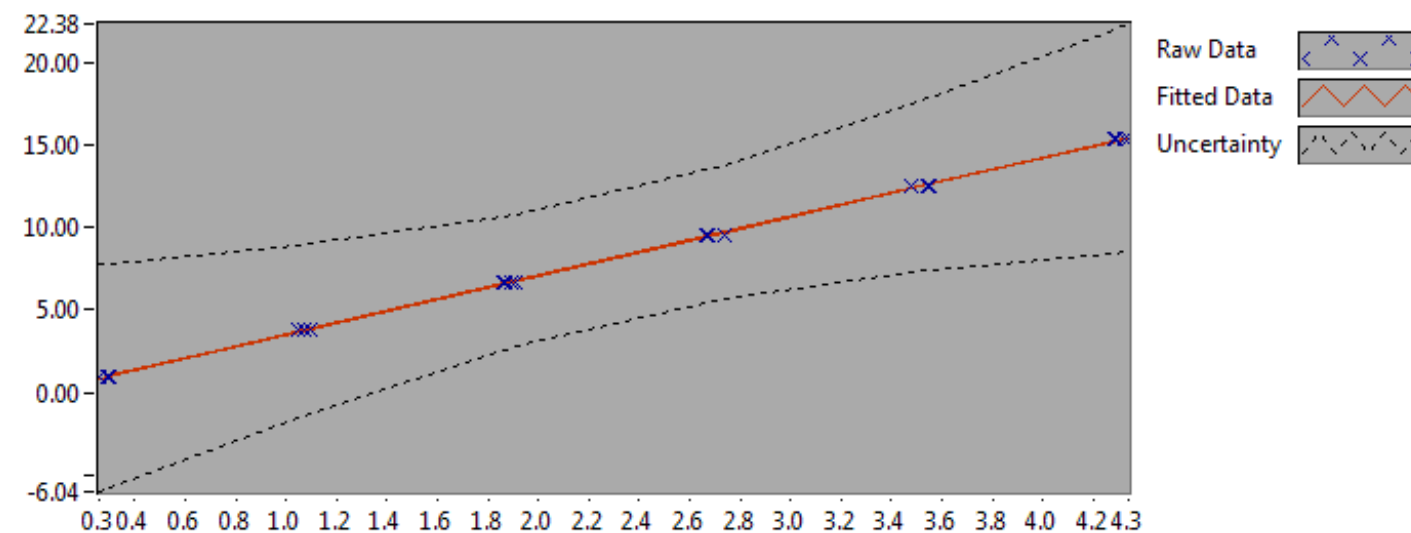RSQ   : 0.999646
Calibration points : 24

Figure 1 : Calibration chart (The uncertainty band is multiplied by 100)

Ingebjørg Valkvæ and Katarina Kloster

CALIBRATION VALUES

Value [Nm]	Voltage [V]	Best Poly Fit [Nm]	Deviation [Nm]	Uncertainty [%]	Uncertainty [Nm]
0.945416	0.259433	0.876851	0.068565	7.311204	0.069121
3.828671	1.050377	3.702849	0.125821	1.364331	0.052236
6.711658	1.863995	6.609857	0.101801	0.606424	0.040701
9.595851	2.667199	9.479656	0.116194	0.418910	0.040198
12.480057	3.478032	12.376715	0.103342	0.409178	0.051066
15.362983	4.293586	15.290642	0.072341	0.444210	0.068244
15.362983	4.325675	15.405293	-0.042310	0.448937	0.068970
12.480057	3.542122	12.605704	-0.125647	0.418699	0.052254
9.595851	2.738004	9.732639	-0.136788	0.424381	0.040723
6.711658	1.912980	6.784877	-0.073218	0.599663	0.040247
3.828671	1.094004	3.858722	-0.030052	1.343533	0.051439
0.945416	0.295461	1.005577	-0.060161	7.223030	0.068288
0.945416	0.288786	0.981728	-0.036312	7.239252	0.068441
3.828671	1.071246	3.777410	0.051261	1.354482	0.051859
6.711658	1.871328	6.636055	0.075603	0.604461	0.040569
9.595851	2.673737	9.503015	0.092835	0.419122	0.040218
12.480057	3.479654	12.382511	0.097547	0.409353	0.051087
15.362983	4.282516	15.251088	0.111895	0.442383	0.067963
15.362983	4.338543	15.451270	-0.088287	0.450868	0.069267
12.480057	3.550343	12.635079	-0.155022	0.419931	0.052408
9.595851	2.736795	9.728318	-0.132467	0.424262	0.040712
6.711658	1.894036	6.717192	-0.005534	0.601678	0.040383
3.828671	1.097132	3.869900	-0.041230	1.342043	0.051382
0.945416	0.303862	1.035594	-0.090178	7.203479	0.068103

COMMENTS:

The uncertainty is calculated with 95% confidence. The uncertainty includes the randomness in the calibrated instrument during the calibration, systematic uncertainty in the instrument or property which the instrument under calibration is compared with (dead weight manometer, calibrated weights etc.), and due to regression analysis to fit the calibration points to a linear calibration equation.The calculated uncertainty can be used as the total systematic uncertianty of the calibrated instrument with the given calibration equation.

E | Risk assessment

NTNU

SINTEF

Risikovurderingsrapport

FRANCIS riggen

Prosjekttittel	Stasjonære og transiente trykkmålinger på Francis riggen
Apparatur	FRANCIS riggen
Enhet	NTNU
Apparaturansvarlig	Bård Brandåstrø
Prosjektleder	Pål-Tore Storli/Ole Gunnar Dahlhaug
HMS-koordinator	Morten Grønli
HMS-ansvarlig (linjeleder)	Olav Bolland
Plassering	Vannkraftlaboratoriet
Romnummer	11
Risikovurdering utført av	Ingebjørg Valkvæ, Rakel Ellingsen, Einar Agnalt og Katarina Kloster

Godkjenning:

	Navn	Dato	Signatur
Prosjektleder	Pål-Tore Storli/ Ole Gunnar Dahlhaug	5/4 -16	
HMS koordinator	Morten Grønli		
HMS ansvarlig (linjeleder)	Olav Bolland		

INNHOLDSFORTEGNELSE

1 INNLEDNING

Stasjonære og transiente trykkmålinger skal gjennomføres flere steder i Francis riggen. Forsøket skal forgå i April 2016.

2 KONKLUSJON

Riggen er bygget til god laboratorium praksis (GLP).

Apparaturkortet får en gyldighet på **4 måneder**
Forsøk pågår kort får en gyldighet på **4 måneder**

3 ORGANISERING

Rolle	NTNU
Prosjektleder	Pål-Tore Storli/ Ole Gunnar Dahlhaug
Apparaturansvarlig	Bård Brandåstrø
Romansvarlig	Halvor Haukvik
HMS koordinator	Morten Grønli
HMS ansvarlig (linjeleder):	Olav Bolland

4 RISIKOSTYRING AV PROSJEKTET

Hovedaktiviteter risikostyring	Nødvendige tiltak, dokumentasjon	DTG
Prosjekt initiering	Prosjekt initiering mal	x
Veiledningsmøte	Skjema for Veiledningsmøte med pre-risikovurdering	x
Innledende risikovurdering	Fareidentifikasjon – HAZID Skjema grovanalyse	x
Vurdering av teknisk sikkerhet	Prosess-HAZOP Tekniske dokumentasjoner	x
Vurdering av operasjonell sikkerhet	Prosedyre-HAZOP Opplæringsplan for operatører	x
Sluttvurdering, kvalitetssikring	Uavhengig kontroll Utstedelse av apparaturkort Utstedelse av forsøk pågår kort	

5 TEGNINGER, FOTO, BESKRIVELSER AV FORSØKSOPPSETT

Vedlegg:
Prosess og Instrumenterings Diagram, (PID) skal inneholde:
- *Alle komponenter i forsøksoppsetningen*
- *Komponentliste med spesifikasjoner*
- *Tegninger og bilder som beskriver forsøksoppsetningen.*

Hvor oppholder operatør seg, hvor er gassflasker, avstegningsventiler for vann/luft.
Annen dokumentasjon som beskriver oppsett og virkemåte.

6   EVAKUERING FRA FORSØKSOPPSETNINGEN

Evakuering skjer på signal fra alarmklokker eller lokale gassalarmstasjon med egen lokal varsling med lyd og lys utenfor aktuelle rom, se 6.2
Evakuering fra rigg området foregår igjennom merkede nødutganger til møteplass, (hjørnet gamle kjemi/kjelhuset eller parkeringsplass 1a-b.)
Aksjon på rigg ved evakuering: Slå av luft og vanntilførsel

7   VARSLING

7.1   Før forsøkskjøring

Varsling per e-post, til **Liste iept-experiments@ivt.ntnu.no**
I e-posten skal det stå::
- Navn på forsøksleder:
- Navn på forsøksrigg:
- Tid for start: (dato og klokkelslett)
- Tid for stop: (dato og klokkelslett)

All forsøkskjøringen skal planlegges og legges inn i aktivitetskalender for lab. Forsøksleder må få bekreftelse på at forsøkene er klarert med øvrig labdrift før forsøk kan iverksettes.

7.2   Ved uønskede hendelser

BRANN
Ved brann en ikke selv er i stand til å slukke med rimelige lokalt tilgjengelige slukkemidler, skal nærmeste brannalarm utløses og arealet evakueres raskest mulig. En skal så være tilgjengelig for brannvesen/bygningsvaktmester for å påvise brannsted.
Om mulig varsles så:

NTNU	SINTEF
Morten Grønli, Mob: 918 97 515	
Olav Bolland: Mob: 918 97 209	
NTNU – SINTEF Beredskapstelefon	800 80 388

GASSALARM
Ved gassalarm skal gassflasker stenges umiddelbart og området ventileres. Klarer man ikke innen rimelig tid å få ned nivået på gasskonsentrasjonen så utløses brannalarm og laben evakueres. Dedikert personell og eller brannvesen sjekker så lekkasjested for å fastslå om det er mulig å tette lekkasje og lufte ut området på en forsvarlig måte.
Varslingsrekkefølge som i overstående punkt.

PERSONSKADE
- Førstehjelpsutstyr i Brann/førstehjelpsstasjoner,
- Rop på hjelp,
- Start livreddende førstehjelp
- **Ring 113** hvis det er eller det er tvil om det er alvorlig skade.

NTNU:
Rapportering av uønskede hendelser, Innsida, avviksmeldinger
https://innsida.ntnu.no/wiki/-/wiki/Norsk/Melde+avvik

SINTEF:
Synergi

8 VURDERING AV TEKNISK SIKKERHET

8.1 Fareidentifikasjon, HAZOP

Se kapittel 13 "Veiledning til rapport mal.
Forsøksoppsetningen deles inn i følgende noder:

Node 1	Rørsystem med pumpe
Node 2	Roterende utstyr (turbin og gir)
Node 3	Hydraulikk

Vedlegg, skjema: Hazop_mal

Vurdering
Node1:
- Overtrykksventil som slår ut dersom trykket i systemet blir for høyt.
- Rørelementer er eksternt levert og godkjent for aktuelt trykk.

Node2:
- Roterende utstyr står utilgjengelig for folk. Dvs det er innkapslet eller man må klatre for å nå opp til det.

Node3:
- Trykk i slanger og rør (olje/vann) Hydraulikkslanger er ikke egenprodusert
- Trykksatt utstyr er sertifisert og kjøpt inn av eksterne leverandører

8.2 Brannfarlig, reaksjonsfarlig og trykksatt stoff og gass

Se kapittel 13 "Veiledning til rapport mal.
Inneholder forsøkene brannfarlig, reaksjonsfarlig og trykksatt stoff

JA	Trykksatt hydraulikkolje, trykksatt vann

Vurdering: Arbeidsmedium er vann. Alle rør er levert av eksternt firma med prøvesertifikat
Hydraulikk til hydrostatisk lager. Hyllevare komponenter, de er dermed ikke egenprodusert

8.3 Trykkpåkjent utstyr

Inneholder forsøksoppsetningen trykkpåkjent utstyr:

JA	Utstyret trykk-testes i henhold til norm og dokumenteres

Vurdering: Prøvesertifikat for trykktesting finnes i labperm.

8.4 Påvirkning av ytre miljø (utslipp til luft/vann, støy, temperatur, rystelser, lukt)

Se kapittel 13 "Veiledning til rapport mal..

NEI	

8.5 Stråling

Se kapittel 13 "Veiledning til rapport mal.

NEI	

Vedlegg:
Vurdering:

8.6 Bruk og behandling av kjemikalier

Se kapittel 13 "Veiledning til rapport mal.

JA	Hydraulikkolje

Vedlegg: Sikkerhetsdatablad
Vurdering: Hydraulikkolje, mineralsk olje. Datablad er vedlagt.

8.7 El sikkerhet (behov for å avvike fra gjeldende forskrifter og normer)

NEI	

9   VURDERING AV OPERASJONELL SIKKERHET

Sikrer at etablerte prosedyrer dekker alle identifiserte risikoforhold som må håndteres gjennom operasjonelle barrierer og at operatører og teknisk utførende har tilstrekkelig kompetanse.

9.1 Prosedyre HAZOP

Se kapittel 13 "Veiledning til rapport mal.
Metoden er en undersøkelse av operasjonsprosedyrer, og identifiserer årsaker og farekilder for operasjonelle problemer.
Vedlegg: HAZOP_MAL_Prosedyre
Vurdering:

9.2 Drifts og nødstopps prosedyre

Se kapittel 13 "Veiledning til rapport mal.
Driftsprosedyren er en sjekkliste som skal fylles ut for hvert forsøk.
Nødstopp prosedyren skal sette forsøksoppsetningen i en harmløs tilstand ved uforutsette hendelser.
Vedlegg: Procedure for running experiments
Nødstopp prosedyre:

9.3 Opplæring av operatører

Dokument som viser Opplæringsplan for operatører utarbeides for alle forøksoppsetninger.
- *Kjøring av pumpesystem*

Vedlegg*: Opplæringsplan for operatører*

9.4 Tekniske modifikasjoner

9.5 Personlig verneutstyr

- *Det er påbudt med vernebriller i sonen anlegget er plassert i.*

9.6 Generelt

9.7 Sikkerhetsutrustning

9.8 Spesielle tiltak

10 TALLFESTING AV RESTRISIKO – RISIKOMATRISE

Se kapittel 13 "Veiledning til rapport mal.
Risikomatrisen vil gi en visualisering og en samlet oversikt over aktivitetens risikoforhold slik at ledelse og brukere får et mest mulig komplett bilde av risikoforhold.

IDnr	Aktivitet-hendelse	Frekv-Sans	Kons	RV
1	Lekkasje i Hydraulikk	1	A	A1
2	Fremmedlegemer i vannet	1	A	A1
3	Rørbrudd	1	A	A1
4	Roterende Aksling	1	B	B1

Vurdering restrisiko: *Det er liten restrisiko ved forsøkene, foruten at trykk-satt vann og olje fordrer bruk av vernebriller. Fremmedlegemer i vannet gir liten risiko for personskade, men kan føre til store skader på maskineri.*

11   LOVER FORSKRIFTER OG PÅLEGG SOM GJELDER

Se http://www.arbeidstilsynet.no/regelverk/index.html
- Lov om tilsyn med elektriske anlegg og elektrisk utstyr (1929)
- Arbeidsmiljøloven
- Forskrift om systematisk helse-, miljø- og sikkerhetsarbeid (HMS Internkontrollforskrift)
- Forskrift om sikkerhet ved arbeid og drift av elektriske anlegg (FSE 2006)
- Forskrift om elektriske forsyningsanlegg (FEF 2006)
- Forskrift om utstyr og sikkerhetssystem til bruk i eksplosjonsfarlig område NEK 420
- Forskrift om håndtering av brannfarlig, reaksjonsfarlig og trykksatt stoff samt utstyr og anlegg som benyttes ved håndteringen
- Forskrift om Håndtering av eksplosjonsfarlig stoff
- Forskrift om bruk av arbeidsutstyr.
- Forskrift om Arbeidsplasser og arbeidslokaler
- Forskrift om Bruk av personlig verneutstyr på arbeidsplassen
- Forskrift om Helse og sikkerhet i eksplosjonsfarlige atmosfærer
- Forskrift om Høytrykksspyling
- Forskrift om Maskiner
- Forskrift om Sikkerhetsskilting og signalgivning på arbeidsplassen
- Forskrift om Stillaser, stiger og arbeid på tak m.m.
- Forskrift om Sveising, termisk skjæring, termisk sprøyting, kullbuemeisling, lodding og sliping (varmt arbeid)
- Forskrift om Tekniske innretninger
- Forskrift om Tungt og ensformig arbeid
- Forskrift om Vern mot eksponering for kjemikalier på arbeidsplassen (Kjemikalieforskriften)
- Forskrift om Vern mot kunstig optisk stråling på arbeidsplassen
- Forskrift om Vern mot mekaniske vibrasjoner
- Forskrift om Vern mot støy på arbeidsplassen

Veiledninger fra arbeidstilsynet
se: http://www.arbeidstilsynet.no/regelverk/veiledninger.html

12   DOKUMENTASJON

- Tegninger, foto, beskrivelser av forsøksoppsetningen
- Hazop_mal
- Sertifikat for trykkpåkjent utstyr
- Håndtering avfall i NTNU
- Sikker bruk av LASERE, retningslinje
- HAZOP_MAL_Prosedyre
- Forsøksprosedyre
- Opplæringsplan for operatører
- Skjema for sikker jobb analyse, (SJA)
- Apparaturkortet
- Forsøk pågår kort

13   VEILEDNING TIL RAPPORTMAL

Kapittel 7 Vurdering av teknisk sikkerhet

Sikre at design av apparatur er optimalisert i forhold til teknisk sikkerhet.
Identifisere risikoforhold knyttet til valgt design, og eventuelt å initiere re-design for å sikre at størst mulig andel av risiko elimineres gjennom teknisk sikkerhet.
Punktene skal beskrive hva forsøksoppsetningen faktisk er i stand til å tåle og aksept for utslipp.

7.1 Fareidentifikasjon, HAZOP

Forsøksoppsetningen deles inn i noder: (eks M*otorenhet, pumpeenhet, kjøleenhet.)*
Ved hjelp av ledeord identifiseres årsak, konsekvens og sikkerhetstiltak. Konkluderes det med at tiltak er nødvendig anbefales disse på bakgrunn av dette. Tiltakene lukkes når de er utført og Hazop sluttføres.
(eks "No flow", årsak: rør er deformert, konsekvens: pumpe går varm, sikkerhetsforanstaltning: måling av flow med kobling opp mot nødstopp eller hvis konsekvensen ikke er kritisk benyttes manuell overvåkning og punktet legges inn i den operasjonelle prosedyren.)

7.2 Brannfarlig, reaksjonsfarlig og trykksatt stoff.

I henhold til Forskrift om håndtering av brannfarlig, reaksjonsfarlig og trykksatt stoff samt utstyr og anlegg som benyttes ved håndteringen

Brannfarlig stoff: Fast, flytende eller gassformig stoff, stoffblanding, samt stoff som forekommer i kombinasjoner av slike tilstander, som i kraft av sitt flammepunkt, kontakt med andre stoffer, trykk, temperatur eller andre kjemiske egenskaper representerer en fare for brann.

Reaksjonsfarlig stoff: Fast, flytende, eller gassformig stoff, stoffblanding, samt stoff som forekommer i kombinasjoner av slike tilstander, som ved kontakt med vann, ved sitt trykk, temperatur eller andre kjemiske forhold, representerer en fare for farlig reaksjon, eksplosjon eller utslipp av farlig gass, damp, støv eller tåke.

Trykksatt stoff: Annet fast, flytende eller gassformig stoff eller stoffblanding enn brann- eller reaksjonsfarlig stoff, som er under trykk, og som derved kan representere en fare ved ukontrollert utslipp.

Nærmere kriterier for klassifisering av brannfarlig, reaksjonsfarlig og trykksatt stoff er fastsatt i vedlegg 1 i veiledningen til forskriften "Brannfarlig, reaksjonsfarlig og trykksatt stoff"
http://www.dsb.no/Global/Publikasjoner/2009/Veiledning/Generell%20veiledning.pdf
http://www.dsb.no/Global/Publikasjoner/2010/Tema/Temaveiledning_bruk_av_farlig_stoff_Del_1.pdf
Rigg og areal skal gjennomgås med hensyn på vurdering av Ex sone
- Sone 0: Alltid eksplosiv atmosfære, for eksempel inne i tanker med gass, brennbar væske.
- Sone 1: Primær sone, tidvis eksplosiv atmosfære for eksempel et fylle tappe punkt

- Sone 2: Sekundert utslippssted, kan få eksplosiv atmosfære ved uhell, for eksempel ved flenser, ventiler og koblingspunkt

7.4 Påvirkning av ytre miljø

Med forurensning forstås: tilførsel av fast stoff, væske eller gass til luft, vann eller i grunnen støy og rystelser påvirkning av temperaturen som er eller kan være til skade eller ulempe for miljøet.
Regelverk: http://www.lovdata.no/all/hl-19810313-006.html#6
NTNU retningslinjer for avfall se: http://www.ntnu.no/hms/retningslinjer/HMSR18B.pdf

7.5 Stråling

Stråling defineres som

Ioniserende stråling: Elektromagnetisk stråling (i strålevernsammenheng med bølgelengde <100 nm) eller hurtige atomære partikler (f.eks alfa- og beta-partikler) som har evne til å ionisere atomer eller molekyler
Ikke-ioniserende stråling: Elektromagnetisk stråling (bølgelengde >100 nm), og ultralyd$_1$, som har liten eller ingen evne til å ionisere.
Strålekilder: Alle ioniserende og sterke ikke-ioniserende strålekilder.
Ioniserende strålekilder: Kilder som avgir ioniserende stråling, f.eks alle typer radioaktive kilder, røntgenapparater, elektronmikroskop
Sterke ikke-ioniserende strålekilder: Kilder som avgir sterk ikke-ioniserende stråling som kan skade helse og/eller ytre miljø, f.eks laser klasse 3B og 4, MR$_2$-systemer, UVC$_3$-kilder, kraftige IR-kilder$_4$
$_1$ Ultralyd er akustisk stråling ("lyd") over det hørbare frekvensområdet (>20 kHz). I strålevernforskriften er ultralyd omtalt sammen med elektromagnetisk ikke-ioniserende stråling. $_2$ MR (eg. NMR) - kjernemagnetisk resonans, metode som nyttes til å «avbilde» indre strukturer i ulike materialer. $_3$ UVC er elektromagnetisk stråling i bølgelengdeområdet 100-280 nm. $_4$ IR er elektromagnetisk stråling i bølgelengdeområdet 700 nm – 1 mm.

For hver laser skal det finnes en informasjonsperm(HMSRV3404B) som skal inneholde:
- Generell informasjon
- Navn på instrumentansvarlig og stedfortreder, og lokal strålevernskoordinator
- Sentrale data om apparaturen
- Instrumentspesifikk dokumentasjon
- Referanser til (evt kopier av) datablader, strålevernbestemmelser, o.l.
- Vurderinger av risikomomenter
- Instruks for brukere
- Instruks for praktisk bruk; oppstart, drift, avstenging, sikkerhetsforholdsregler, loggføring, avlåsing, evt. bruk av strålingsmåler, osv.
- Nødprosedyrer

Se ellers retningslinjen til NTNU for laser: http://www.ntnu.no/hms/retningslinjer/HMSR34B.pdf

7.6 Bruk og behandling av kjemikalier.

Her forstås kjemikalier som grunnstoff som kan utgjøre en fare for arbeidstakers sikkerhet og helse.
Se ellers: http://www.lovdata.no/cgi-wift/ldles?doc=/sf/sf/sf-20010430-0443.html
Sikkerhetsdatablar skal være i forøkenes HMS perm og kjemikaliene registrert i Stoffkartoteket.

Kapittel 8 Vurdering av operasjonell sikkerhet

Sikrer at etablerte prosedyrer dekker alle identifiserte risikoforhold som må håndteres gjennom operasjonelle barrierer og at operatører og teknisk utførende har tilstrekkelig kompetanse.

8.1 Prosedyre Hazop

Prosedyre-HAZOP gjennomføres som en systematisk gjennomgang av den aktuelle prosedyren ved hjelp av fastlagt HAZOP-metodikk og definerte ledeord. Prosedyren brytes ned i enkeltstående arbeidsoperasjoner (noder) og analyseres ved hjelp av ledeordene for å avdekke mulige avvik, uklarheter eller kilder til mangelfull gjennomføring og feil.

8.2 Drifts og nødstopp prosedyrer

Utarbeides for alle forsøksoppsetninger.

Driftsprosedyren skal stegvis beskrive gjennomføringen av et forsøk, inndelt i oppstart, under drift og avslutning. Prosedyren skal beskrive forutsetninger og tilstand for start, driftsparametere med hvor store avvik som tillates før forsøket avbrytes og hvilken tilstand riggen skal forlates.

Nødstopp-prosedyre beskriver hvordan en nødstopp skal skje, (utført av uinnvidde),
hva som skjer, (strøm/gass tilførsel) og
hvilke hendelser som skal aktivere nødstopp, (brannalarm, lekkasje).

Kapittel 9 Risikomatrise Tallfesting av restrisiko

For å synliggjøre samlet risiko, jevnfør skjema for risikovurdering, plottes hver enkelt aktivitets verdi for sannsynlighet og konsekvens inn i risikomatrisen. Bruk aktivitetens IDnr. Eksempel: Hvis aktivitet med IDnr. 1 har fått en risikoverdi D3 (sannsynlighet 3 x konsekvens D) settes aktivitetens IDnr i risikomatrisens felt for 3D. Slik settes alle aktivitetenes risikoverdier (IDnr) inn i risikomatrisen.

I risikomatrisen er ulike grader av risiko merket med rød, gul eller grønn. Når en aktivitets risiko havner på rød (= uakseptabel risiko), skal risikoreduserende tiltak gjennomføres. Ny vurdering gjennomføres etter at tiltak er iverksatt for å se om risikoverdien er kommet ned på akseptabelt nivå.

KONSEKVENS	Svært alvorlig	E1	E2	E3	E4	E5
	Alvorlig	D1	D2	D3	D4	D5
	Moderat	C1	C2	C3	C4	C5
	Liten	B1	B2	B3	B4	B5
	Svært liten	A1	A2	A3	A4	A5
		Svært liten	Liten	Middels	Stor	Svært Stor
		SANSYNLIGHET				

Prinsipp over akseptkriterium. Forklaring av fargene som er brukt i risikomatrisen.

Farge		Beskrivelse
Rød	🟥	Uakseptabel risiko. Tiltak skal gjennomføres for å redusere risikoen.
Gul	🟨	Vurderingsområde. Tiltak skal vurderes.
Grønn	🟩	Akseptabel risiko. Tiltak kan vurderes ut fra andre hensyn.